

Minimum Detectable Concentrations With Typical Radiation Survey Instruments for Various Contaminants and Field Conditions

U.S. Nuclear Regulatory Commission

Office of Nuclear Regulatory Research

E.W. Abelquist, W.S. Brown, G.E. Powers,
A.M. Huffert



AVAILABILITY NOTICE

Availability of Reference Materials Cited in NRC Publications

Most documents cited in NRC publications will be available from one of the following sources:

1. The NRC Public Document Room, 2120 L Street, NW., Lower Level, Washington, DC 20555-0001
2. The Superintendent of Documents, U.S. Government Printing Office, P. O. Box 37082, Washington, DC 20402-9328
3. The National Technical Information Service, Springfield, VA 22161-0002

Although the listing that follows represents the majority of documents cited in NRC publications, it is not intended to be exhaustive.

Referenced documents available for inspection and copying for a fee from the NRC Public Document Room include NRC correspondence and internal NRC memoranda; NRC bulletins, circulars, information notices, inspection and investigation notices; licensee event reports; vendor reports and correspondence; Commission papers; and applicant and licensee documents and correspondence.

The following documents in the NUREG series are available for purchase from the Government Printing Office: formal NRC staff and contractor reports, NRC-sponsored conference proceedings, international agreement reports, grantee reports, and NRC booklets and brochures. Also available are regulatory guides, NRC regulations in the *Code of Federal Regulations*, and *Nuclear Regulatory Commission Issuances*.

Documents available from the National Technical Information Service include NUREG-series reports and technical reports prepared by other Federal agencies and reports prepared by the Atomic Energy Commission, forerunner agency to the Nuclear Regulatory Commission.

Documents available from public and special technical libraries include all open literature items, such as books, journal articles, and transactions. *Federal Register* notices, Federal and State legislation, and congressional reports can usually be obtained from these libraries.

Documents such as theses, dissertations, foreign reports and translations, and non-NRC conference proceedings are available for purchase from the organization sponsoring the publication cited.

Single copies of NRC draft reports are available free, to the extent of supply, upon written request to the Office of Administration, Distribution and Mail Services Section, U.S. Nuclear Regulatory Commission, Washington DC 20555-0001.

Copies of industry codes and standards used in a substantive manner in the NRC regulatory process are maintained at the NRC Library, Two White Flint North, 11545 Rockville Pike, Rockville, MD 20852-2738, for use by the public. Codes and standards are usually copyrighted and may be purchased from the originating organization or, if they are American National Standards, from the American National Standards Institute, 1430 Broadway, New York, NY 10018-3308.

Minimum Detectable Concentrations With Typical Radiation Survey Instruments for Various Contaminants and Field Conditions

Manuscript Completed: January 1998

Date Published: June 1998

Prepared by

E.W. Abelquist¹, W.S. Brown², G.E. Powers,
A.M. Huffert

**Division of Regulatory Applications
Office of Nuclear Regulatory Research
U.S. Nuclear Regulatory Commission
Washington, DC 20555-0001**



¹Environmental Survey and Site Assessment Program, Environmental and Health Sciences Division,
Oak Ridge Institute for Science and Education, Oak Ridge, TN 37831-0117

²Human Factors and Performance Analysis Group, Brookhaven National Laboratory, Upton, NY 11973-5000

ABSTRACT

This document describes and quantitatively evaluates the effects of various factors on the detection sensitivity of commercially available portable field instruments being used to conduct radiological surveys in support of decommissioning. The U.S. Nuclear Regulatory Commission (NRC) has amended its regulations to establish residual radioactivity criteria for decommissioning of licensed nuclear facilities. In support of that rulemaking, the Commission has prepared a Generic Environmental Impact Statement (GEIS), consistent with the National Environmental Policy Act (NEPA). The effects of this new rulemaking on the overall cost of decommissioning are among the many factors considered in the GEIS. The overall cost includes the costs of decontamination, waste disposal, and radiological surveys to demonstrate compliance with the applicable guidelines. An important factor affecting the costs of such radiological surveys is the minimum detectable concentration (MDC) of field survey instruments in relation to the residual radioactivity criteria. The purpose of this study was two-fold. First, the data were used to determine the validity of the theoretical minimum detectable concentrations (MDCs) used in the GEIS. Second, the results of the study, published herein, provide guidance to licensees for (a) selection and proper use of portable survey instruments and (b) understanding the field conditions and the extent to which the capabilities of those instruments can be limited. The types of instruments commonly used in field radiological surveys that were evaluated included, in part, gas proportional, Geiger-Mueller (GM), zinc sulfide (ZnS) scintillation, and sodium iodide (NaI) scintillation detectors.

CONTENTS

<u>Section</u>	<u>Page</u>
ABSTRACT	iii
ABBREVIATIONS	xii
ACKNOWLEDGMENTS	xiii
FOREWORD	xv
1 INTRODUCTION	1-1
1.1 Background	1-1
1.2 Need for This Report	1-1
1.3 Scope	1-2
1.4 Methodology	1-3
2 INSTRUMENTATION	2-1
2.1 Gas Proportional Detectors	2-1
2.2 Geiger-Mueller Detectors	2-1
2.3 Zinc Sulfide Scintillation Detectors	2-1
2.4 Sodium Iodide Scintillation Detectors	2-2
2.5 Ratemeter-Scalers	2-2
2.6 Pressurized Ionization Chamber	2-2
2.7 Portable Gamma Spectrometer	2-2
2.8 Laboratory Instrumentation	2-2
2.9 Additional Instrumentation	2-3
3 STATISTICAL INTERPRETATIONS OF MINIMUM DETECTABLE CONCENTRATIONS	3-1
3.1 MDC Fundamental Concepts	3-1
3.2 Review of MDC Expressions	3-6
4 VARIABLES AFFECTING INSTRUMENT MINIMUM DETECTABLE CONCENTRATIONS	4-1
4.1 Radionuclide Sources for Calibration	4-2
4.2 Source-to-Detector Distance	4-3
4.3 Window Density Thickness	4-5
4.4 Source Geometry Factors	4-6
4.5 Ambient Background Count Rate	4-7
5 VARIABLES AFFECTING MINIMUM DETECTABLE CONCENTRATIONS IN THE FIELD	5-1
5.1 Background Count Rates for Various Materials	5-1
5.2 Backscatter Effects	5-2

CONTENTS

<u>Section</u>	<u>Page</u>
5.3 Effects of Surface Condition on Detection Sensitivity	5-3
5.3.1 Surface Preparation	5-3
5.3.2 Measurement Results for Various Surface Types	5-4
5.4 Attenuation Effects of Overlaying Material (Self-Absorption)	5-7
5.4.1 Methodology	5-7
5.4.2 Measurement of Various Surface Coatings	5-9
5.5 Use of Alpha and/or Beta Measurements to Assess Surface Activity	5-11
6 HUMAN PERFORMANCE AND SCANNING SENSITIVITY	6-1
6.1 Introduction	6-1
6.2 Review of Scanning Sensitivity Expressions and Results	6-2
6.3 Signal Detection Theory	6-4
6.4 Human Factors and Two Stages of Scanning	6-5
6.5 The Ideal Observer Paradigm	6-7
6.6 Actual Surveyor Performance - Field Tests and Computer Simulations	6-7
6.6.1 Field Tests of Surveyor Performance	6-8
6.6.1.1 General Methodology of Field Tests	6-8
6.6.1.2 Field Test Results	6-9
6.6.2 Computer Simulation Tests of Surveyor Performance	6-10
6.6.2.1 Adaptive Procedure	6-10
6.6.2.2 Confidence Ratings Procedure	6-11
6.6.2.3 Continuous Monitoring Procedure	6-11
6.6.2.4 General Discussion	6-12
6.7 Estimation of Scan Minimum Detectable Count Rates (MDCRs)	6-12
6.7.1 Determination of MDCR and Use of Surveyor Efficiency	6-13
6.7.2 Review of Assumptions and Results	6-15
6.8 Scan MDCs for Structure Surfaces and Land Areas	6-16
6.8.1 Scan MDCs for Building/Structure Surfaces	6-17
6.8.2 Scan MDCs for Land Areas	6-19
7 IN SITU GAMMA SPECTROMETRY AND EXPOSURE RATE MEASUREMENTS . . .	7-1
7.1 <i>In Situ</i> Gamma Spectrometry Measurements in Outdoor Test Area	7-1
7.2 Exposure Rate Measurements in Outdoor Test Area	7-3
8 LABORATORY INSTRUMENTATION DETECTION LIMITS	8-1
8.1 Review of Analytical Minimum Detectable Concentrations	8-1
8.2 Background Activities for Various Soil Types	8-1
8.3 Effects of Soil Condition on MDC	8-2
8.3.1 Effects of Soil Moisture on MDC	8-3

<u>Section</u>	<u>Page</u>
8.3.2 Effects of Soil Density on MDC	8-4
8.3.3 Effects of High-Z Materials on MDC	8-4
9 REFERENCES	9-1

TABLES

<u>Table</u>	<u>Page</u>
3.1 MDC Results for Data Obtained From Gas Proportional Detector Using Various MDC Expressions	3-8
4.1 Characteristics of Radionuclide Sources Used for Calibration and Static Measurements	4-8
4.2 Average Total Efficiencies for Various Detectors and Radionuclides	4-9
4.3 Minimum Detectable Concentrations for Various Detectors and Radionuclides	4-10
4.4 Instrument Efficiencies	4-11
4.5 Source-to-Detector Distance Effects for β Emitters	4-12
4.6 Source-to-Detector Distance Effects for α Emitters	4-12
4.7 Minimum Detectable Concentrations for Various Source-to-Detector Distances for β Emitters	4-13
4.8 Minimum Detectable Concentrations for Various Source-to-Detector Distances for α Emitters	4-14
4.9 Window Density Thickness Effects for β Emitters	4-15
4.10 Minimum Detectable Concentrations for Various Window Density Thicknesses ...	4-16
4.11 Source Geometry Effects on Instrument Efficiency	4-17
4.12 Ambient Background Effects	4-18
5.1 Background Count Rate for Various Materials	5-16
5.2 Minimum Detectable Concentrations for Various Materials	5-17
5.3 Efficiencies and Backscatter Factors for SrY-90	5-18
5.4 Surface Material Effects on Source Efficiency for Tc-99 Distributed on Various Surfaces	5-19
5.5 Surface Material Effects on Source Efficiency for Th-230 Distributed on Various Surfaces	5-20
5.6 Surface Material Effects on MDC for Tc-99 and Th-230 Distributed on Various Surfaces	5-21
5.7 Effects of Oil Density Thickness on Source Efficiency and MDC (Gas Proportional— $\alpha + \beta$)	5-22
5.8 Effects of Paint Density Thickness on Source Efficiency and MDC (Gas Proportional— $\alpha + \beta$)	5-23

CONTENTS

<u>Table</u>	<u>Page</u>
5.9 Effects of Paint Density Thickness on Source Efficiency and MDC (Gas Proportional— α -only)	5-24
5.10 Effects of Paint Density Thickness on Source Efficiency and MDC (Gas Proportional— β -only)	5-25
5.11 Effects of Paint Density Thickness on Source Efficiency and MDC (GM Detector)	5-26
5.12 Effects of Paint Density Thickness on Source Efficiency and MDC (ZnS Scintillation Detector)	5-27
5.13 Effects of Dust Density Thickness on Source Efficiency and MDC (Gas Proportional— $\alpha + \beta$)	5-28
5.14 Effects of Dust Density Thickness on Source Efficiency and MDC (Gas Proportional— α only)	5-29
5.15 Effects of Dust Density Thickness on Source Efficiency and MDC (Gas Proportional— β only)	5-30
5.16 Effects of Dust Density Thickness on Source Efficiency and MDC (GM Detector)	5-31
5.17 Effects of Dust Density Thickness on Source Efficiency and MDC (ZnS Scintillation Detector)	5-32
5.18 Effects of Water Density Thickness on Source Efficiency and MDC (Gas Proportional— $\alpha+\beta/C-14$)	5-33
5.19 Effects of Water Density Thickness on Source Efficiency and MDC (Gas Proportional— $\alpha+\beta/Tc-99$)	5-34
5.20 Effects of Water Density Thickness on Source Efficiency and MDC (Gas Proportional— $\alpha+\beta/SrY-90$)	5-35
5.21 Effects of Water Density Thickness on Source Efficiency and MDC (Gas Proportional— α -only)	5-36
5.22 Effects of Water Density Thickness on Source Efficiency and MDC (Gas Proportional— β -only/C-14)	5-37
5.23 Effects of Water Density Thickness on Source Efficiency and MDC (Gas Proportional— β -only/Tc-99)	5-38
5.24 Effects of Water Density Thickness on Source Efficiency and MDC (Gas Proportional— β -only/SrY-90)	5-39
5.25 Effects of Water Density Thickness on Source Efficiency and MDC (GM Detector/C-14)	5-40
5.26 Effects of Water Density Thickness on Source Efficiency and MDC (GM Detector/Tc-99)	5-41
5.27 Effects of Water Density Thickness on Source Efficiency and MDC (GM Detector/SrY-90)	5-42

<u>Table</u>	<u>Page</u>
5.28 Effects of Water Density Thickness on Source Efficiency and MDC (ZnS Scintillation Detector)	5-43
5.29 Total Efficiencies for Detectors Used To Assess Uranium Surface Activity	5-44
5.30 Normalized Total Efficiencies for Processed Uranium With Various Absorber Thicknesses	5-45
5.31 Detector Efficiency for Low Enriched Uranium (3%) Using a 126-cm ² Proportional Detector with a 0.4 mg cm ⁻² Window (Gas Proportional— $\alpha + \beta$)	5-45
5.32 Detector Efficiency for Low Enriched Uranium (3%) Using a 126-cm ² Proportional Detector with a 3.8 mg cm ⁻² Window (Gas Proportional— β -only)	5-46
6.1 Values of d' for Selected True Positive and False Positive Proportions	6-26
6.2 Scanning Sensitivity (MDCR) of the Ideal Observer for Various Background Levels	6-26
6.3 NaI Scintillation Detector Count Rate Versus Exposure Rate (cpm per μ R/h)	6-27
6.4 NaI Scintillation Detector Scan MDCs for Common Radiological Contaminants	6-28
7.1 <i>In Situ</i> Gamma Spectrometry Data From Outdoor Test Area	7-4
7.2 Exposure Rate Measurements From Outdoor Test Area	7-5
8.1 Typical Radionuclide Concentrations Found in Background Soil Samples in the United States	8-5
8.2 Effects of Moisture Content on Gamma Spectrometry Analyses	8-6
8.3 Effects of High-Z Content on Gamma Spectrometry Analyses	8-7

FIGURES

<u>Figure</u>	
3.1 Critical Level, L_C	3-9
3.2 Detection Limit, L_D	3-9
4.1 MDCs for Gas Proportional Detector ($\alpha + \beta$ Mode) for Various Radionuclides	4-19
4.2 MDCs for GM Detector for Various Radionuclides	4-19
4.3 Source-to-Detector Distance Effects on MDC for Higher Energy β Emitters	4-20
4.4 Source-to-Detector Distance Effects on MDC for Lower Energy β Emitters	4-20
4.5 Source-to-Detector Distance Effects on MDC for α Emitters	4-21
4.6 Effects of Window Density Thickness on Total Efficiency for Higher Energy β Emitters	4-21
4.7 Effects of Window Density Thickness on Total Efficiency for Lower Energy β Emitters	4-22
4.8 Effects of Window Density Thickness on MDC for Higher Energy β Emitters	4-22
4.9 Effects of Window Density Thickness on MDC for Lower Energy β Emitters	4-23

CONTENTS

<u>Figure</u>	<u>Page</u>
4.10 Effects of Ambient Background on MDC Calculation	4-23
5.1 Effect of Surface Material on Gas Proportional Detector (α only) MDC	5-47
5.2 Effect of Surface Material on Gas Proportional Detector (β -only) MDC	5-47
5.3 Effects of Oil Density Thickness on Source Efficiency for Various Sources	5-48
5.4 Effects of Oil Density Thickness on MDC	5-48
5.5 Effects of Paint Density Thickness on Source Efficiency (Gas Proportional - $\alpha + \beta$)	5-49
5.6 Effects of Paint Density Thickness on Source Efficiency (Gas Proportional - α -Only)	5-49
5.7 Effects of Paint Density Thickness on Source Efficiency (Gas Proportional - β -Only)	5-50
5.8 Effects of Paint Density Thickness on Source Efficiency (GM Detector)	5-50
5.9 Effects of Paint Density Thickness on Source Efficiency (ZnS Scintillation Detector)	5-51
5.10 Effects of Dust Density Thickness on Source Efficiency (Gas Proportional - $\alpha + \beta$)	5-51
5.11 Effects of Dust Density Thickness on Source Efficiency (Gas Proportional - α -Only)	5-52
5.12 Effects of Dust Density Thickness on Source Efficiency (Gas Proportional - β -Only)	5-52
5.13 Effects of Dust Density Thickness on Source Efficiency (GM Detector)	5-53
5.14 Effects of Dust Density Thickness on Source Efficiency (ZnS Scintillation Detector)	5-53
5.15 Effects of Water Density Thickness on Source Efficiency (Gas Proportional - $\alpha + \beta$)	5-54
5.16 Effects of Water Density Thickness on Source Efficiency (Gas Proportional - α -Only)	5-54
5.17 Effects of Water Density Thickness on Source Efficiency (Gas Proportional - β -Only)	5-55
5.18 Effects of Water Density Thickness on Source Efficiency (GM Detector)	5-55
5.19 Effects of Water Density Thickness on Source Efficiency (ZnS Scintillation Detector)	5-56
5.20 Effects of Dust Density Thickness on MDC for Various Sources Using the Gas Proportional Detector in $\alpha + \beta$ and α -only modes	5-56

<u>Figure</u>	<u>Page</u>
5.21 Effects of Dust Density Thickness on MDC for Various Sources Using the Gas Proportional Detector in β -Only mode	5-57
5.22 Effects of Dust Density Thickness on MDC for Various Sources Using the GM Detector	5-57
5.23 Effects of Dust Density Thickness on MDC for an Alpha Source Using the ZnS Scintillation Detector	5-58
5.24 Overall Effects of Paint, Dust, and Water Density Thickness on Source Efficiency for Various Sources Using the Gas Proportional Detector in β -only mode	5-58
6.1 Signal Detection Theory Measures of Sensitivity (d') and Criterion Shown Relative to Assumed Underlying Distributions	6-29
6.2 Relative Operating Characteristic (Ideal Observer) for Detection of 120 cpm (Net) in a Background of 60 cpm; Observation Intervals of 1 Second and 4 Seconds	6-29
6.3 Instructions Provided to Field Survey Test Participants for Indoor GM Scans	6-30
6.4 Scale Map of the Wall Showing Location, Extent, and Radiation Levels of Hidden Sources for GM Scans	6-31
6.5 Scale Map of the Wall Showing Location, Extent, and Radiation Levels of Hidden Sources for Gas Proportional Scans	6-31
6.6 Scale Map of the Outdoor Scan Test Area Showing Location, Extent, and Radiation Levels of Hidden Sources for NaI Scans	6-32
7.1 Co-60 <i>In Situ</i> Gamma Spectrometry Results in Outdoor Test Area	7-6
7.2 Exposure Rate Measurements in the Outdoor Test Area	7-7
8.1 Efficiency vs. Energy for Various Densities	8-8

ABBREVIATIONS

ANL	Argonne National Laboratory
ANSI	American National Standards Institute, Inc.
BNL	Brookhaven National Laboratory
DCGL	derived concentration guideline level
dpm	disintegrations per minute
EML	Environmental Measurements Laboratory (U.S. Dept. of Energy)
EPA	Environmental Protection Agency
ESSAP	Environmental Survey and Site Assessment Program
FIDLER	Field Instrument for the Detection of Low Energy Radiation
GEIS	Generic Environmental Impact Statement
GM	Geiger-Mueller
LARADS	laser assisted ranging and data system
MDC	minimum detectable concentration
MDCR	minimum detectable count rate
NaI	sodium iodide
NCRP	National Council on Radiation Protection and Measurements
NEPA	National Environmental Policy Act
NIST	National Institute of Standards and Technology
NRC	Nuclear Regulatory Commission
ORISE	Oak Ridge Institute for Science and Education
ORNL	Oak Ridge National Laboratory
PNNL	Pacific Northwest National Laboratory
PIC	pressurized ionization chamber
ROC	relative operating characteristic
TEDE	total effective dose equivalent
USRADS	ultrasonic ranging and data system
ZnS	zinc sulfide

ACKNOWLEDGMENTS

This report was a collaborative effort by the staff of the Environmental Survey and Site Assessment Program (ESSAP) of the Oak Ridge Institute for Science and Education, Brookhaven National Laboratory, and the Nuclear Regulatory Commission. In addition to writing certain sections, Eric Abelquist, working closely with Tony Huffert and George Powers of the NRC, was responsible for the overall planning and management of this project. Dr. William Brown, Brookhaven National Laboratory, provided input on the human factors associated with scanning and wrote the bulk of Section 6. Many of the detection sensitivity experiments conducted in this report were designed and performed by Elmer Bjelland and Lea Mashburn, while Jim Payne and Scott Potter performed many measurements during development of the feasibility study. Other technical contributors included Wade Adams, Armin Ansari, William L. (Jack) Beck, Dale Condra, Ray Morton, Ann Payne, Steven King, Tim Vitkus, and Duane Quayle. Elaine Waters, Robyn Ellis, Debi Herrera, Tabatha Fox, and Debbie Adams provided much of the word processing support, while Teresa Bright and Dean Herrera produced all of the graphics.

Special thanks to Jim Berger, George Chabot, Bobby Coleman, Ken Swinth, and Ed Walker who performed valuable reviews of the report and provided thoughtful comments, and to all the computer simulation and field survey test participants.

FOREWORD

The NRC has amended its regulations to establish residual radioactivity criteria for decommissioning of licensed nuclear facilities. In support of that rulemaking, the Commission has prepared a Generic Environmental Impact Statement (GEIS), consistent with the National Environmental Policy Act (NEPA). The effects of this new rulemaking on the overall cost of decommissioning are among the many factors considered in the GEIS. The overall cost includes the costs of decontamination, waste disposal, and radiological surveys to demonstrate compliance with the applicable guidelines.

An important factor affecting the costs of such radiological surveys is the minimum detectable concentration (MDC) of field survey instruments in relation to the residual contamination guidelines. This study provides guidance to licensees for (a) selection and proper use of portable survey instruments and (b) understanding the field conditions and the extent to which the capabilities of those instruments can be limited. The types of instruments commonly used in field radiological surveys that were evaluated include, in part, gas proportional, Geiger-Mueller (GM), zinc sulfide (ZnS) scintillation, and sodium iodide (NaI) scintillation detectors. This report describes and quantitatively evaluates the effects of various factors on the detection sensitivity of commercially available portable field instruments being used to conduct radiological surveys in support of decommissioning.

The initial draft of this report was published in August 1995. In response to the comments received, substantial revisions were made to include modifications to the scan MDC approach and the determination of instrument sensitivity for uranium and thorium decay series. The results, approaches and methods described herein are provided for information only and should not be considered a substitute for NRC requirements.



John W Craig, Director
Division of Regulatory Applications
Office of Nuclear Regulatory Research

1 INTRODUCTION

1.1 Background

Facilities licensed by the U.S. Nuclear Regulatory Commission (NRC) are required to demonstrate that residual radioactivity at their site meets the applicable guidelines before the associated license can be terminated. NRC has completed a decommissioning rulemaking effort, that culminated in a *Federal Register* notice on July 21, 1997, to establish residual contamination criteria for release of facilities for restricted or unrestricted use. In support of that rulemaking, the Commission has prepared a Generic Environmental Impact Statement (GEIS), consistent with the National Environmental Policy Act (NEPA).

The effects of this new rulemaking on the overall cost of decommissioning are among the many factors considered in the GEIS. The overall cost includes the costs of decontamination, waste disposal, and radiological surveys to demonstrate compliance with the applicable release criteria. An important factor affecting the costs of such radiological surveys is the minimum detectable concentration (MDC) of field survey instruments in relation to the derived concentration guideline levels (DCGLs)—radionuclide specific levels corresponding to the release criterion. The MDC may apply to either the concentration of radioactivity present on a material surface or within a volume of material. If the DCGLs are lower than the MDC of field survey instruments, extensive laboratory analysis would become necessary, significantly increasing the overall cost of decommissioning projects.

1.2 Need for This Report

Currently, comprehensive and well-controlled data on detection sensitivity of field survey instruments, under conditions typically encountered by licensees during decommissioning, are not available. A literature search was performed on the detection sensitivity capabilities of portable survey instruments. In general, the MDC information contained in the literature is for optimum capabilities under conditions of low background, smooth clean surfaces, and experienced survey personnel. Additional studies were determined to be necessary to develop comprehensive information, relative to instrument performance, under actual field conditions. In the determination of scan MDCs, many studies do not identify the method by which detector sensitivities were determined or defined (e.g., detection sensitivities may be calculated for various confidence levels, using ratemeter output as opposed to integrated counts or audible signal change), and as such, comparison of detection sensitivities reported in the literature may not be appropriate. A few notable studies that do specify the methodology to determine scanning sensitivities are summarized in Section 6.

The purpose of this study was two-fold. First, the results of the study, published herein, will provide guidance to licensees for selection and proper use of portable survey instruments, and an understanding of the field conditions under which, and the extent to which, the capabilities of

INTRODUCTION

those instruments can be limited. Second, the data were used to determine the validity of the theoretical MDCs used in the GEIS.

1.3 Scope

The major emphasis of this study was the measure of detection sensitivity for field survey instruments in both the static and scanning modes of operation. The parameters that were studied for their effects on the detection sensitivity of field instruments included variables that determine the instrument MDC (e.g., probe surface area, radionuclide energy, window density thickness, source-to-detector geometry) and variables that can affect the detection sensitivity of the instrument in the field (e.g., various surface types and coatings, including painted, scabbled, or wet surfaces). It was not anticipated that empirical data would be obtained for every possible combination of variables; rather, the emphasis was on establishing the necessary baseline data, so that accurate predictions could be made regarding an instrument's response under a variety of possible field conditions.

Scan MDCs were evaluated for both building surfaces and land areas. The innovative approach used to determine scan MDCs coupled the detector and contamination characteristics with human factors.

The types of instruments commonly used in field radiological surveys that were evaluated in this study included gas proportional, Geiger-Mueller (GM), zinc sulfide (ZnS) scintillation, and sodium iodide (NaI) scintillation detectors. Comparison of field survey instruments by different manufacturers (Ludlum, Eberline, Bicon, etc.) was not the intended purpose of this study. The specific instruments that were used for these measurements are, in general, representative; one notable exception is the pressurized ionization chamber described in Section 2. All instrumentation used in this study is described in Section 2.

The detection sensitivity of a number of commonly used laboratory procedures was also addressed in this study. Because most of the information on laboratory procedures and thermoluminescence dosimeters is already available, this information was provided in the form of a literature review. However, it was anticipated that some laboratory measurements would have to be made to address specific objectives of the study.

Finally, this report was not intended to be a complete evaluation of the performance of portable survey instrumentation. Several references are available that provide comprehensive information on the performance of health physics instrumentation. One such study involves the evaluation of ionization chambers, GM detectors, alpha survey meters, and neutron dose equivalent survey meters according to the draft ANSI standard N42.17 (Swinth & Kenoyer 1984). These instruments were subjected to a broad array of testing, including general characteristics, electronic and mechanical requirements, radiation response, interfering responses, and environmental factors. An important result of the cited study was highlighting the susceptibility of air and gas-

flow proportional counters to environmental factors such as humidity, elevations, and temperature. The study also concluded that the alpha scintillation detector is relatively stable under variable environmental conditions. Another study summarized the regulatory requirements and practices of NRC licensees regarding the use of accredited calibration laboratories. That report concluded that more definitive guidance was needed to describe how to perform and document calibration to demonstrate compliance with the regulatory requirements (NUREG/CR-6062).

1.4 Methodology

During radiological surveys in support of decommissioning, field instruments are generally used to scan the surface areas for elevated direct radiation, and to make direct measurements of total surface activity at particular locations. Although the surface scans and direct measurements can be performed with the same instruments, the two procedures have very different MDCs. Scanning can have a much higher MDC than a static count, depending on scanning speed, distance of the probe to the surface, and other instrument factors. The scanning MDC is also affected by the "human factor," described in Section 6. Therefore, when applicable, the MDC of each instrument was determined for both the scanning and static modes of operation.

There are several statistical interpretations of the MDC concept that can result in different MDC values for an instrument, using the same set of data. The specific approach for statistical interpretation of the data, in this study, was selected after a thorough review of the relevant literature. A sensitivity study, evaluating the quantitative effects of various statistical treatments on the MDC, was also performed (Section 3).

Studies were performed primarily at Oak Ridge Institute for Science and Education (ORISE) facilities in Oak Ridge, Tennessee. A measurement hood, constructed of Plexiglas, provided a controlled environment in which to obtain measurements with minimal disturbances from ambient airflow. The Plexiglas measurement hood measured 93 cm in length, 60 cm in height, and 47 cm in depth, and was equipped with a barometer and thermometer to measure ambient pressure and temperature within the chamber. Measurements were performed within the measurement hood using a detector-source jig to ensure that the detector-to-source geometry was reproducible for all parameters studied. Various field conditions were simulated, under well-controlled and reproducible conditions. Special sources were constructed and characterized in ORISE laboratories to meet specific objectives of this study. On the basis of the empirical results obtained from these studies, sets of normalized curves were constructed that would indicate instrument response as a function of source energy, geometry, background radiation level, and other parameters, including source-to-detector distance, window density thickness, and density thickness of overlaying material.

The quantitative data were treated and reported in accordance with Environmental Protection Agency guidance (HPSR 1980). Data were reported with an unambiguous statement of the

INTRODUCTION

uncertainty. The assessment of the uncertainty included an estimate of the combined overall uncertainty. Random uncertainties associated with measurement parameters (e.g., number of counts, weight, volume) were propagated to determine an overall uncertainty. It was generally assumed that measurement parameters were statistically independent; therefore, the propagation of errors did not consider any covariance terms. Uncertainties were also propagated in the MDC determination to provide a measure of the overall uncertainty in the MDC from both counting errors and other sources of error (e.g., detector efficiency, source efficiency, calibration source activity).

Experts at several other facilities were contacted to discuss various aspects of this study, such as the statistical approaches to MDC measurements, methods for construction of calibration sources, and to obtain calibration sources, already constructed, that could be used in this study. These institutions included the National Institute of Standards and Technology (NIST), the Department of Energy's Environmental Measurement Laboratory (EML), Argonne National Laboratory (ANL), Pacific Northwest National Laboratory (PNNL), and Oak Ridge National Laboratory (ORNL). ORISE also collaborated with Brookhaven National Laboratory (BNL) to address the "human factor" in performing radiological scan surveys (Section 6).

2 INSTRUMENTATION

The types of instruments commonly used in field radiological surveys are briefly described in this section. The instrumentation that was used in this study is specified by make and model. This was necessary in the event that the data generated in this study are reviewed and/or compared to the results obtained by other investigators. However, the use of these instruments does not, in any way, represent an endorsement of a particular product, or a particular manufacturer, on the part of the Oak Ridge Institute for Science and Education (ORISE) or the NRC.

2.1 Gas Proportional Detectors

Gas proportional detectors are used for detecting both alpha and beta radiation. Ludlum 43-68 detectors, with a physical probe area of 126 cm² (effective probe area is 100 cm², which accounts for the fraction of the probe area covered by the protective screen), were used in this study. Gas proportional detectors with larger probe surfaces, such as the Ludlum Model 43-37 detectors with a physical probe area of 573 cm², are suitable for scanning surface areas. The detector cavity in these instruments is filled with P-10 gas (90% argon, 10% methane). Alpha or beta particles, or both, enter this cavity through an aluminized Mylar window. The density thickness of this window is one factor that can affect the detector efficiency, hence the MDC of the instrument. The instrument can be used to detect (a) only alpha radiation by using a low operating voltage, (b) alpha and beta radiation by using a higher operating voltage, or (c) only beta radiation by using a Mylar shield to block the alpha particles in a mixed alpha/beta field. Instrument response was evaluated using all three modes of operation.

2.2 Geiger-Mueller Detectors

“Pancake” detectors are used for detecting beta and gamma radiation (these detectors can also respond to alpha radiation to varying degrees). Eberline Model HP-260 detectors were used in this study. This instrument has a physical probe area of approximately 20 cm² (15.5-cm² effective probe area). The detector tube is filled with readily ionizable inert gas, which is a mixture of argon, helium, neon, and a halogen-quenching gas. Incident radiation enters this cavity through a mica window. The density thickness of the window can vary between 1.4 and 2.0 mg/cm², affecting detection sensitivity. The output pulses are registered on a digital scaler/ratemeter with a set threshold value.

2.3 Zinc Sulfide Scintillation Detectors

Alpha scintillation detectors use scintillators as detection media, instead of gas. A commonly used detector is the zinc sulfide scintillation detector, which uses silver-activated zinc sulfide, ZnS(Ag). The Eberline Model AC-3-7, with a physical probe area of 74 cm² (59 cm² effective probe area), was used in this study. Alpha particles enter the scintillator through an aluminized Mylar window. The Mylar window prevents ambient light from activating the photomultiplier, but is still thin enough to allow penetration by alpha radiation without significant energy degradation. The light

INSTRUMENTATION

pulses are amplified by a photomultiplier, converted to voltage pulses, and counted on a digital scaler/ratemeter with a set threshold value.

2.4 Sodium Iodide Scintillation Detectors

For detection of gamma radiation, thallium-activated sodium iodide scintillation detectors are widely used. Primarily, these detectors are useful for scanning surface areas for elevated gamma radiation. In this study, the Victoreen Model 489-55 with a 3.2-cm × 3.8-cm (1.25" × 1.5") NaI(Tl) crystal and the Ludlum model 44-10 with a 5.1-cm × 5.1-cm (2" × 2") NaI(Tl) crystal were used. The output voltage pulse is recorded on a ratemeter.

2.5 Ratemeter-Scalers

The detectors that were described above are used in conjunction with ratemeter-scalers. The detector response is recorded as an integrated count or it is noted as a count rate, or both. Both modes of operation were evaluated in the study. The following instrument combinations were used: Ludlum Model 2221 ratemeter-scaler was used with Ludlum 43-68, Eberline HP-260, and Eberline AC-3-7 detectors; and Ludlum Model 12 ratemeter-scaler was used with the Victoreen 489-55 and Ludlum 44-10 detectors.

2.6 Pressurized Ionization Chamber

The pressurized ionization chamber (PIC) can be used to monitor "real time" direct gamma-ray levels and record exposure rates. Ionization chambers operate by collecting ions within a cavity chamber filled with pressurized argon gas. The current generated is proportional to the amount of ionization produced in the chamber. Quantitative measurements of exposure rate are made and recorded in microrentgen per hour. In this study, Reuter-Stokes Model RSS-112 was used.

2.7 Portable Gamma Spectrometer

Portable gamma spectrometers can be used to identify and quantitate gamma-emitting radionuclides in the field. The Environmental Survey and Site Assessment Program (ESSAP) at ORISE has used the portable gamma-spectrometry capability, mainly for qualitative analysis of contaminants in the field, but not to obtain data for direct comparison with the guidelines. The system used by ESSAP for this study was manufactured by EG&G ORTEC, and includes a 13% relative efficiency, p-type germanium detector.

2.8 Laboratory Instrumentation

The study of field survey instruments was extended to include a limited number of measurements using laboratory instrumentation. The following laboratory instrumentation was used:

- Canberra 3100 VAX workstation connected to intrinsic germanium detectors (Oxford instruments and EG&G ORTEC) with extended range capability for low-energy x-rays
- Canberra 3100 VAX workstation connected to solid-state alpha detectors (Canberra and Oxford instruments)
- low background alpha/beta gas flow proportional counters (Oxford instruments)
- liquid scintillation counter (Packard instruments)

2.9 Additional Instrumentation

Additional survey instrumentation commonly used for decommissioning surveys that were not evaluated in this report, includes in part:

- The FIDLER (Field Instrument for the Detection of Low Energy Radiation)—consists of a thin NaI crystal and used to detect gamma and x-radiation below 100 keV.
- The dual phosphor alpha and beta detector—consists of ZnS(Ag) adhered to a plastic scintillation material. This detector allows for the simultaneous assessment of alpha and beta radiation at each survey location. Cross talk between the alpha and beta channels should be carefully considered when evaluating the data.

Other instrumentation of emerging importance, but not studied in this report includes, in part:

- devices that track both the position and output of radiation detectors, such as the ultrasonic ranging and data system (USRADS). USRADS (from ChemRad) provides a documented survey by correlating the location and magnitude of the instrument response at one-second intervals. Similarly, the Thermo Nutech laser assisted ranging and data system (LARADS) combines radiological data acquisition and spatial identification in to produce a documented radiological survey. Both systems eliminate subjective interpretation of the data by the surveyor and provide verification of the survey are coverage.
- a floor monitor developed by Shonka Research Associates, Inc. that uses position sensitive proportional counter-based radiation detectors. The position-sensitive proportional counter allows one detector to act as the equivalent of hundreds of individual detectors—which results in the collection of vast amounts of data. Process software saves the survey data at very high rates and correlates the data as a function of survey location. The system provides completely documented radiation surveys and allows visualization of the survey results in a real-time mode:

3 STATISTICAL INTERPRETATIONS OF MINIMUM DETECTABLE CONCENTRATIONS

Detection limits for field survey instrumentation are an important criterion in the selection of appropriate instrumentation and measurement procedures. For the most part, detection limits need to be determined in order to evaluate whether a particular instrument and measurement procedure is capable of detecting residual activity at the regulatory release criteria (DCGLs). One may demonstrate compliance with decommissioning criteria by performing surface activity measurements and directly comparing the results to the surface activity DCGLs. However, before any measurements are performed, the survey instrument and measurement procedures to be used must be shown to possess sufficient detection capabilities relative to the surface activity DCGLs; i.e., the detection limit of the survey instrument must be less than the appropriate surface activity DCGL.

The measurement of residual radioactivity during surveys in support of decommissioning often involves measurement of residual radioactivity at near-background levels. Thus, the minimum amount of radioactivity that may be detected by a given survey instrument and measurement procedure must be determined. In general, the minimum detectable concentration (MDC) is the minimum activity concentration on a surface or within a material volume, that an instrument is expected to detect (e.g., activity expected to be detected with 95% confidence). It is important to note, however, that this activity concentration, or the MDC, is determined *a priori*, that is, before survey measurements are conducted.

As generally defined, the detection limit, which may be a count or count rate, is independent of field conditions such as scabbled, wet, or dusty surfaces. That is, the detection limit is based on the number of counts and does not necessarily equate to measured activity under field conditions. These field conditions do, however, affect the instrument's "detection sensitivity" or MDC. Therefore, the terms MDC and detection limit should not be used interchangeably.

For this study, the MDC corresponds to the smallest activity concentration measurement that is practically achievable with a given instrument and type of measurement procedure. That is, the MDC depends not only on the particular instrument characteristics (instrument efficiency, background, integration time, etc.), but also on the factors involved in the survey measurement process (HPSR 1980), which include surface type, source-to-detector geometry, and source efficiency (backscatter and self-absorption).

3.1 MDC Fundamental Concepts

The scope of this report precludes a rigorous derivation of MDC concepts, yet sufficient theory is presented to acquaint the user of this manual with the fundamental concepts. The detection limits discussed in this report are based on counting statistics alone and do not include other sources of error (systematic uncertainties in the measurement process are addressed in NUREG/CR-4007 and ANSI N13.30). Although the following statistical formulation assumes a normal distribution

STATISTICAL INTERPRETATIONS OF MDCs

of net counts, between sample and blank, it should be recognized that this may not be the case for low blank total counts. However, in consideration of the advantage of having a single, simple MDC expression, and the fact that deviations from the normality assumption do not affect the MDC expression contained herein as severely as had been expected (Brodsky 1992), it was decided that the normality assumption was proper for purposes of this report. That is, the MDC concepts discussed below should be considered as providing information on the general detection capability of the measurement system, and not as absolute levels of activity that can or cannot be detected (NCRP 58).

The MDC concepts discussed in this document derive from statistical hypothesis testing, in which a decision is made on the presence of activity. Specifically, a choice is made between the null hypothesis (H_0) and the alternative hypothesis (H_a). The null hypothesis is generally stated as "no net activity is present in the sample" (i.e., observed counts are not greater than background), while the alternative hypothesis states that the observed counts are greater than background, and thus, that net activity is present. These statements are written:

H_0 : No net activity is present in the sample, and
 H_a : Net activity is present in the sample.

It should be noted that the term "sample" has a general meaning in this context, it may apply to direct measurements of surface activity, laboratory analyses of samples, etc.

A first step in the understanding of the MDC concepts is to consider an appropriate blank (background) distribution for the medium to be evaluated. Currie (1968) defines the blank as the signal resulting from a sample which is identical, in principle, to the sample of interest, except that the residual activity is absent. This determination must be made under the same geometry and counting conditions as used for the sample (Brodsky & Gallagher 1991). In the context of this report, an example of this medium may be an unaffected concrete surface that is considered representative of the surfaces to be measured in the remediated area. It should be noted that the terms blank and background are used interchangeably in this report.

In this statistical framework, one must consider the distribution of counts obtained from measurements of the blank, which may be characterized by a population mean (μ_B) and standard deviation (σ_B). Now consider the measurement of a sample that is known to be free of residual activity. This zero-activity (background) sample has a mean count (C_B) and standard deviation (s_B). The net count (and, subsequently, residual activity) may be determined by subtracting the blank counts from the sample counts. This results in a zero-mean count frequency distribution that is approximately normally distributed (Figure 3.1). The standard deviation of this distribution, σ_0 , is obtained by propagating the individual errors (standard deviations) associated

with both the blank (σ_B) and the zero-activity samples (s_B). That is,

$$\sigma_0 = \sqrt{\sigma_B^2 + s_B^2} \quad (3-1)$$

A critical level may then be determined from this distribution and used as a decision tool to decide when activity is present. The critical level, L_C , is that net count in a zero-mean count distribution having a probability, denoted by α , of being exceeded (Figure 3.1). It is a common practice to set α equal to 0.05 and to accept a 5% probability of incorrectly concluding that activity is present when it is not. That is, if the observed net count is less than the critical level, the surveyor correctly concludes that no net activity is present. When the net count exceeds L_C , the null hypothesis is rejected in favor of its alternative, and the surveyor falsely concludes that net activity is present in the blank sample. It should also be noted that the critical level, L_C , is equivalent to a given probability (e.g., 5%) of committing a Type I error (false positive detection). The expression for L_C is generally given as:

$$L_C = k_\alpha \sigma_0 \quad (3-2)$$

where k_α is the value of the standard normal deviate corresponding to a one-tailed probability level of $1-\alpha$. As stated previously, the usual choice for α is 0.05, and the corresponding value for k_α is 1.645. For an appropriate blank counted under the same conditions as the sample, the assumption may be made that the standard deviations of the blank and zero-activity sample are equal (i.e., σ_B equals s_B). Thus, the critical level may be expressed as:

$$L_C = 1.645 \sqrt{2 s_B^2} = 2.33 s_B \quad (3-3)$$

The L_C value determined above is in terms of net counts, and as such, the L_C value should be added to the background count if comparisons are to be made to the directly observable instrument gross count.

The detection limit, L_D , is defined to be the number of mean net counts obtained from samples for which the observed net counts are almost always certain to exceed the critical level (Figure 3.2). It is important to recognize that L_D is the mean of a net count distribution. The detection limit is positioned far enough above zero so that there is a probability, denoted by β , that the L_D will result in a signal less than L_C . It is common practice to set β equal to 0.05 and to accept a 5% probability of incorrectly concluding that no activity is present, when it is indeed present (Type II error). That is, the surveyor has already agreed to conclude that no net activity is present for an observed net count that is less than the critical level, however, an amount of residual activity that

STATISTICAL INTERPRETATIONS OF MDCs

would yield a mean net count of L_D is expected to produce a net count less than the critical level 5 % of the time. This is equivalent to missing residual activity when it was present.

The expression for L_D is generally given as:

$$L_D = L_C + k_\beta \sigma_D \quad (3-4)$$

where k_β is the value of the standard normal deviate corresponding to a one-tailed probability level of $1-\beta$ for detecting the presence of net activity, and σ_D is the standard deviation of the net sample count (C_S) when C_S equals L_D . For clarification, consider the measurement of a sample that provides a gross count given by C_{S+B} , at the detection level. The net sample count, C_S , is calculated by subtracting the mean blank count (μ_B) from the gross count. The detection limit may be written as follows, recognizing that C_S equals L_D :

$$L_D = C_S + (C_B - \mu_B) \quad (3-5)$$

The standard deviation of the net sample, σ_D , is obtained by propagating the error in the gross count and from the background when the two are subtracted to obtain L_D . As previously noted, the standard deviation of this distribution, σ_o , is obtained by propagating the uncertainties associated with both the blank (C_B) and the zero-activity samples (μ_B), therefore,

$$\sigma_D = \sqrt{(C_S + \sigma_o^2)} = \sqrt{(L_D + \sigma_o^2)} \quad (3-6)$$

This expression for σ_D may be substituted into Equation 3-4 and the equation solved for L_D .

As stated previously, the usual choice for β is 0.05, and the corresponding value for k_β is 1.645. If the assumption is made that σ_D is approximately equal to the standard deviation of the background, then for the case of paired observations of the background and sample σ_o^2 equals $2s_B^2$. Following considerable algebraic manipulation, the detection limit may be expressed as:

$$L_D = 2.71 + 4.65 s_B \quad (3-7)$$

The assumption that the standard deviation of the count (σ_D) is approximately equal to that of the background greatly simplifies the expression for L_D , and is usually valid for total counts greater than 70 for each sample and blank count (Brodsky 1992). Brodsky has also examined this expression and determined that in the limit of very low background counts, s_B would be zero and the constant 2.71 should be 3, based on a Poisson count distribution (Brodsky & Gallagher 1991). Thus, the expression for the detection limit becomes:

$$L_D = 3 + 4.65 s_B \quad (3-8)$$

The detection limit calculated above may be stated as the net count having a 95% probability of being detected when a sample contains activity at L_D , and with a maximum 5% probability of falsely interpreting sample activity as activity due to background (false negative or Type II error).

The MDC of a sample follows directly from the detection limit concepts. It is a level of radioactivity, either on a surface or within a volume of material, that is practically achievable by an overall measurement process (HPSR 1980). The expression for MDC may be given as:

$$MDC = \frac{(3 + 4.65 s_B)}{KT} \quad (3-9)$$

where K is a proportionality constant that relates the detector response to the activity level in a sample for a given set of measurement conditions and T is the counting time. This factor typically encompasses the detector efficiency, self-absorption factors, and probe area corrections.

This expression of the MDC equation was derived assuming equivalent (paired) observations of the sample and blank (i.e., equal counting intervals for the sample and background), in contrast to the MDC expression that results when taking credit for repetitive observations of the blank (well-known blank). There is some debate concerning the appropriateness of taking credit for repetitive observations of the blank, considering the uncertainties associated with using a well-known blank for many samples when there can be instrument instabilities or changes in the measurement process that may be undetected by the surveyor (Brodsky & Gallagher 1991). Therefore, it is desirable to obtain repetitive measurements of background, simply to provide a better estimate of the background value that must be subtracted from each gross count in the determination of surface activity. Thus, the background is typically well known for purposes other than reducing the corresponding MDC, such as to improve the accuracy of the background value. The expression for MDC that will be used throughout this report is given as:

$$MDC = \frac{3 + 4.65 \sqrt{C_B}}{KT} \quad (3-10)$$

where C_B is the background count in time, T , for paired observations of the sample and blank. For example, if ten 1-minute repetitive observations of background were performed, C_B would be equal to the average of the ten observations and T is equal to 1 minute. The quantities encompassed by the proportionality constant, K , such as the detection efficiency and probe geometry, should also be average, "well-known" values for the instrument. For making

STATISTICAL INTERPRETATIONS OF MDCs

assessments of MDC for surface activity measurements, the MDC is given in units of disintegrations per minute per 100 square centimeters (dpm/100 cm²).

For cases in which the background and sample are counted for different time intervals, the MDC becomes (Strom & Stansbury 1992)

$$MDC = \frac{3 + 3.29 \sqrt{R_B T_{S+B} \left(1 + \frac{T_{S+B}}{T_B}\right)}}{KT_{S+B}} \quad (3-11)$$

where R_B is the background counting rate, and T_{S+B} and T_B are the sample and background counting times, respectively.

One difficulty with the MDC expression in Equation 3-10 is that all uncertainty is attributed to Poisson counting errors, which can result in an overestimate of the detection capabilities of a measurement process. The proportionality constant, K , embodies measurement parameters that have associated uncertainties that may be significant as compared to the Poisson counting errors. A conservative solution to this problem has been to replace the parameter values (specifically the mean parameter values) that determine K with lower bound values that represent a 95% probability that the parameter values are higher than that bound (NUREG/CR-4007; ANSI N13.30). In this case, the MDC equation becomes

$$MDC = \frac{3 + 4.65 \sqrt{C_B}}{K_{0.05} T} \quad (3-12)$$

where $K_{0.05}$ is the lower bound value that represents a 95% probability that values of K are higher than that bound (ANSI N13.30). For example, if the detector efficiency in a specified measurement process was experimentally determined to be 0.20 ± 0.08 (2σ error), the value of the detector efficiency that would be used in Equation 3-10 is 0.12. This would have the effect of increasing the MDC by a factor of 1.7 (using 0.12 instead of 0.20). Therefore, it is important to have an understanding of the magnitude of the uncertainty associated with each of the parameters used in the MDC determination. In this context, errors associated with each measurement parameter were propagated in the MDC determination. The magnitude of the uncertainty in the MDC may then be used as a decision tool, allowing for determination of the need to implement some methodology for adjusting the MDC for uncertainties in K .

3.2 Review of MDC Expressions

A significant aspect of this study involved the review of the relevant literature on statistical

interpretations of MDC. One approach, suited for this application of the MDC concept, was selected and used throughout the entire study, for consistency. However, other statistical approaches were considered in a sensitivity study. That is, the same set of measurement results were used to calculate the MDC, using several statistical treatments of the data. The tabulated results provided the range of MDC values, calculated using the various approaches.

The data used to perform the MDC sensitivity analysis were obtained by performing static measurements under ideal laboratory conditions with a gas proportional detector, operated in the beta-only mode, on a SrY-90 source (the expressions for scanning sensitivity were not evaluated in this part). For purposes of comparison, both the background and sample counting times were one minute long, i.e., paired observations. Ten repetitive measurements of background were obtained and the mean and standard deviation were calculated to be 354 and 18 counts, respectively. The total efficiency of the detector was determined to be 0.34 count per disintegration and probe area correction for 126-cm² detector was made.

Several expressions of MDC (or the various terms used to convey detection limit) were reviewed in the literature. The measurement results determined above were used to determine the values for the various expressions of MDC. The average background from the repetitive observations was used in the MDC equations that required a background value, while the standard deviation of the background distribution was used for others. Table 3.1 illustrates the variations in MDC that may be calculated from the same set of measurement results. The MDC values ranged from 146 to 211 dpm/100 cm², for the gas proportional detectors calibrated to SrY-90.

This limited MDC sensitivity study demonstrates that the MDC expressions widely referenced in the literature produce very consistent MDC results. The smallest value of MDC results from the expression that allows credit to be taken for the "well-known" blank (Currie 1968). There would likely be no difference in the conclusion that would be reached concerning the demonstration that the instrumentation possesses sufficient detection capabilities relative to the surface activity DCGLs.

STATISTICAL INTERPRETATIONS OF MDCS

Table 3.1 MDC Results for Data Obtained From Gas Proportional Detector Using Various MDC Expressions

MDC Expression ^{a,b}	MDC Result ^c (dpm/100 cm ²)	Reference
$2.71 + 4.65 \sqrt{B}$	210	NCRP 58 HPSR 1980
$2.71 + 4.65 \sigma_B$	204	Currie 1968
$2.71 + 3.29 \sigma_B$	146	Currie 1968
$3 + 4.65 \sqrt{B}$	211	Brodsky & Gallagher 1991
$\frac{3 + 3.29 \sqrt{R_b t_g (1 + \frac{t_g}{t_b})^d}}{(Efficiency)(t_g)}$	211	Strom & Stansbury 1992

^aThe data used in each MDC expression were obtained from a 43-68 gas proportional detector and SrY-90 source. Average background counts (*B*) of 354 in 1 minute, standard deviation of 18, probe area correction for 126-cm² detector, and detector efficiency of 0.34 count per disintegration were obtained.

^bEach MDC expression is written using symbols that may be different from the ones that were presented in their respective references. However, the meaning of each has been preserved.

^cEach MDC result was presented in terms of dpm/100 cm² to facilitate comparison of the different MDC expressions. This involved correcting the MDC expression for probe area and detector efficiency.

^dThe terms *R_b*, *t_g*, and *t_b* refer to the background counting rate, gross count time, and background counting time, respectively. Using *t_g* equal to *t_b* (1 minute), resulted in the same expression as that of Brodsky and Gallagher (1991).

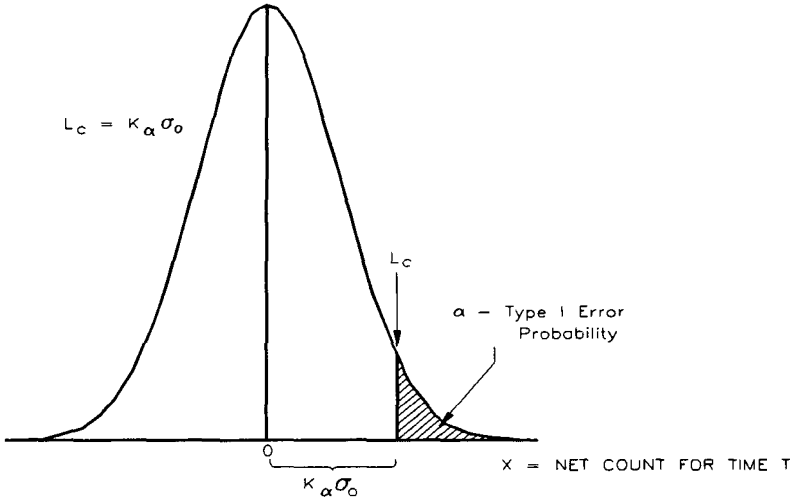


Figure 3.1: Critical Level, L_c

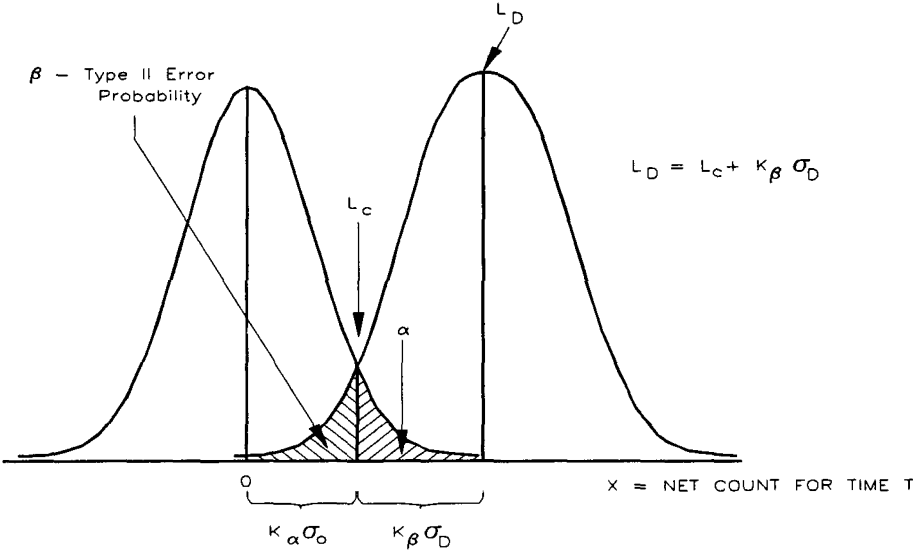


Figure 3.2: Detection Limit, L_D

4 VARIABLES AFFECTING INSTRUMENT MINIMUM DETECTABLE CONCENTRATIONS

Before the MDC for a particular instrument and survey procedure can be determined, it is necessary to introduce the expression for total alpha or beta surface activity per unit area. The International Standard ISO 7503-1, "Evaluation of Surface Contamination," recommends that the total surface activity, A_s , be calculated similarly to the following expression:

$$A_s = \frac{R_{S+B} - R_B}{(\epsilon_i)(W)(\epsilon_s)} \quad (4-1)$$

where,

- R_{S+B} = the gross count rate of the measurement in cpm,
- R_B = the background count rate in cpm,
- ϵ_i = the instrument or detector efficiency (unitless),
- ϵ_s = the efficiency of the contamination source (unitless), and
- W = the area of the detector window (cm^2).

(For instances in which W does not equal 100 cm^2 , probe area corrections are necessary to convert the detector response to units of dpm per 100 cm^2 .)

This expression clearly distinguishes between instrument (detector) efficiency and source efficiency. The product of the instrument and source efficiency yields the total efficiency ϵ_{tot} . Currently, surface contamination is assessed by converting the instrument response to surface activity using one overall total efficiency. This is not a problem provided that the calibration source exhibits characteristics similar to the surface contamination—including radiation energy, backscatter effects, source geometry, self-absorption, etc. In practice this is hardly the case; more likely, total efficiencies are determined with a clean, stainless steel source, and then those efficiencies are used to measure contamination on a dust-covered concrete surface. By separating the efficiency into two components, the surveyor has a greater ability to consider the actual characteristics of the surface contamination.

The instrument efficiency is defined as the ratio between the net count rate of the instrument and the surface emission rate of a source for a specified geometry. The surface emission rate, $q_{2\pi}$, is defined as the "number of particles of a given type above a given energy emerging from the front face of the source per unit time" (ISO 7503-1). The surface emission rate is the 2π particle fluence that embodies both the absorption and scattering processes that affect the radiation emitted from the source. Thus, the instrument efficiency is determined by

$$\epsilon_i = \frac{R_{S+B} - R_B}{q_{2\pi}} \quad (4-2)$$

VARIABLES AFFECTING INSTRUMENT MDCs

The instrument efficiency is determined during calibration by obtaining a static count with the detector over a calibration source that has a traceable activity or surface emission rate or both. In many cases, it is the source surface emission rate that is measured by the manufacturer and certified as National Institute of Standards and Technology (NIST) traceable. The source activity is then calculated from the surface emission rate based on assumed backscatter and self-absorption properties of the source. The theoretical maximum value of instrument efficiency is 1.

The source efficiency, ϵ_s , is defined as the ratio between the number of particles of a given type emerging from the front face of a source and the number of particles of the same type created or released within the source per unit time (ISO 7503-1). The source (or surface) efficiency takes into account the increased particle emission due to backscatter effects, as well as the decreased particle emission due to self-absorption losses. For an ideal source (no backscatter or self-absorption), the value of ϵ_s is 0.5. Many real sources will exhibit values of ϵ_s less than 0.5, although values greater than 0.5 are possible, depending on the relative importance of the absorption and backscatter processes. Source efficiencies may either be determined experimentally or simply selected from the guidance contained in ISO 7503-1 (refer to Section 5.3.2).

This current section considers some of the factors that affect the instrument efficiency ϵ_i . These detector-related factors include detector size (probe surface area), window density thickness, geotropism, instrument response time, and ambient conditions such as temperature, pressure, and humidity. The instrument efficiency also depends on the radionuclide source used for calibration and the solid angle effects, which include source-to-detector distance and source geometry.

Section 5 covers some of the factors that affect the source efficiency ϵ_s . Among these source-related factors are the type of radiation and its energy, source uniformity, surface roughness and coverings, and surface composition (e.g., wood, metal, concrete).

4.1 Radionuclide Sources for Calibration

For accurate measurements of total surface activity, it is essential that field instruments be calibrated appropriately. The MDC of an instrument depends on a variety of parameters, one of which involves the selection of calibration sources. Calibration sources should be selected that emit alpha or beta radiation with energies similar to those expected of the contaminant in the field. ISO 8769, "Reference Sources for the Calibration of Surface Contamination Monitors," provides recommendations on calibration source characteristics. As discussed in Section 5.5, the most representative calibration source would be one prepared from the radioactive material being assessed in the field. For example, both the uranium and thorium series emit a complex decay

scheme of alpha, beta and gamma radiations—calibration to a single radionuclide must carefully be assessed to ensure that it is representative of the detector's response to these decay series.

An instrument's MDC depends on the type and energy of radiation. The radionuclides selected for this study were chosen so that they represent the types or the range, or both, of energies commonly encountered in decommissioned facilities. These radionuclides are C-14, Ni-63, SrY-90, Tc-99, and Tl-204 for beta measurements, and Th-230 and Pu-239 for alpha measurements. The calibration sources, available at ESSAP facilities, are traceable to NIST standards. Generally, the sources are of three geometric shapes: "button" sources (simulating a point source, approximately 5 cm²), disc sources that cover a standard area of approximately 15 cm², or distributed sources that typically range from 126 to 150 cm². Table 4.1 summarizes the calibration sources used in this study.

The efficiencies determined in this section are for ideal laboratory conditions, which include the use of smooth, clean calibration source surfaces. Table 4.2 presents the average total efficiencies for the gas proportional, GM, and ZnS detectors compiled from historical calibration data at ESSAP. Table 4.3 provides MDCs that were calculated for the gas proportional detector ($\alpha + \beta$ mode) and the GM detector using the ambient background count rates provided in Table 5.1 and the total efficiencies in Table 4.2. As expected, the MDCs decrease with increasing beta energy. This is shown graphically in Figures 4.1 and 4.2 for the gas proportional and GM detectors, respectively. For beta energies (beta endpoint energies are used here) ranging from 300 to 1400 keV, the calculated MDCs are generally constant. However, the MDCs increase rapidly with decreasing beta energies below 300 keV.

The determination of source efficiencies in Section 5 required the assessment of instrument efficiencies under specific experimental conditions. These conditions included active area of source, detector specifications, and a source-to-detector geometry that included two sheets of Mylar. Table 4.4 shows results of instrument efficiencies determined under these conditions.

4.2 Source-to-Detector Distance

The distance between a source and the detector is another factor that may affect the instrument efficiency and, thus, the MDC. In this study, instrument MDC was evaluated as a function of distance from the source. The range of distances was selected to be appropriate for the type of radiation being measured, and in consideration of the typical detector-to-surface distances encountered in the course of performing surveys in support of decommissioning. Counts of 1 minute in duration were made with the detector at various distances above the source.

The source-to-detector distance was evaluated using a Ludlum Model 43-68 gas proportional detector with a 0.8 mg/cm² window for beta emitters, including C-14, Ni-63, SrY-90, Tc-99 (two source geometries were used), and Tl-204, and for Pu-239 and Th-230 (two source geometries were used). Five 1-minute measurements were made at contact and at distances of 0.5 cm, 1 cm,

VARIABLES AFFECTING INSTRUMENT MDCs

and 2 cm. The distances were obtained by cutting out the specified thicknesses of plastic and using them to maintain the desired source-to-detector spacing. Tables 4.5 and 4.6 show the results of an increasing source-to-detector distance on instrument response. Specifically, the net count rate obtained at each distance was normalized to the net count rate obtained in contact with the source. These results demonstrate the significant reduction in instrument response that can occur when source-to-detector distance is increased by less than 1 cm.

As was expected, the greatest reduction in detector response per increased distance from the source was obtained for the alpha and low-energy beta emitters, i.e., Ni-63 and C-14. The modest reduction in instrument response for the alpha-emitting Pu-239 and Th-230 sources, from being in contact with the source to 1 cm, was somewhat unexpected. The C-14 and Ni-63 exhibited equal or greater reductions in instrument response over this range compared to the alpha emitters. Somewhat more anticipated was the dramatic reduction in instrument response from 1 to 2 cm for the Pu-239 and Th-230 sources. The instrument response to the Th-230 disc source at 2 cm was only 4% of the response obtained in contact with the source. This was contrasted to the Pu-239 disc source that exhibited 20% of the response at 2 cm relative to the contact measurement. The greater instrument response of Pu-239 at 2 cm relative to Th-230 at the same distance was likely due to the higher energy of the Pu-239 alpha emission (i.e., 5.1 MeV for Pu-239 versus 4.7 MeV for Th-230).

The data presented in Tables 4.5 and 4.6 were used to determine total efficiencies as a function of detector-to-source distance. It should be noted that although total efficiencies were determined and reported at each distance, the detector-to-source distance influences the instrument efficiency ϵ_i (as opposed to ϵ_s). These total efficiencies were used to calculate the MDCs presented in Tables 4.7 and 4.8. Figures 4.3 and 4.4 illustrate the effects of source-to-detector distance on the MDC for the beta emitters. These figures show that the source-to-detector distance effect on MDCs was relatively minor for the higher energy beta emitters (e.g., SrY-90 and Tl-204), but considerable for the low to mid-energy beta emitters. Figure 4.5 shows the effects of source-to-detector distance on the MDC for alpha emitters. For alpha emitters, the MDCs gradually increased as the detector-to-source spacing increased from contact to 1 cm. At 2-cm distance, consistent with the substantial reduction in total efficiency, the MDCs increased significantly. The MDC determined for Ni-63 at a detector-to-source distance of 2 cm was $52,000 \pm 56,000$ dpm/100 cm², with the relatively large uncertainty attributed to the error in the total efficiency determination. This magnitude of uncertainty in the MDC term suggests that the detection capability for the measurement process, i.e. detecting Ni-63 with a gas proportional detector 2 cm from the surface, is likely overestimated. This particular example illustrates the need for adjusting the MDC to account for uncertainties in the calibration factors (refer to Section 3.1 for discussion of MDC adjustment factor).

The practicality of these results may be realized by the deviation in instrument response that results when the source-to-detector distance during calibration is only slightly different (i.e., less than 1 cm for some radionuclides) from the detector-to-surface spacing maintained during field measurements of surface activity. That is, small changes in detector-to-surface distance produce significant changes in detector response, especially for alpha and low-energy beta radiation (1 to 2 cm spacing is not unusual for a roughly scabbled concrete surface). The effects on Tl-204 and SrY-90, although less than those on lower energy beta emitters, were still appreciable.

To minimize the effects of source-to-detector distance on MDCs, it is recommended that the detector be calibrated at a source-to-detector distance that is similar to the expected detector-to-surface spacing in the field.

4.3 Window Density Thickness

The detector-related factors that may change the instrument MDC are detector size (probe surface area), window density thickness, geotropism, instrument response time, and ambient conditions such as temperature, pressure, and humidity. In many instances, this information is already available. For example, the effects of ambient conditions and geotropism are usually tested by users concerned about the instrument or detector performance (Swinth & Kenoyer 1984; LA-10729).

One detector-related factor evaluated in this report was the effect of window density thickness on instrument response (using the Ludlum model 43-68) for C-14, Ni-63, Sr-90, Tc-99 (two source geometries were used for Tc-99), and Tl-204. Window density thickness for gas proportional detectors may be varied to provide a mechanism to control instrument response to various surface activity conditions. For example, in the assessment of low-energy beta emitters, a relatively thin window (e.g., 0.4 mg/cm²) provides greater sensitivity. Similarly, when beta radiation in the presence of alpha radiation must be assessed, it is possible to selectively discriminate out the alpha radiation using an alpha shield (i.e., using 3.8 mg/cm² window density thickness).

Measurements were performed for window density thicknesses of 0.3, 0.4, 0.8, and 3.8 mg/cm². In addition, MDC measurements at window density thicknesses of 1.3, 1.8, 2.3, 2.8, and 3.3 mg/cm² were performed for the two Tc-99 source geometries. Window density thicknesses were varied by adding sheets of 0.5-mg/cm² Mylar between the source and the detector. The results of these measurements are given in Table 4.9. Figures 4.6 and 4.7 illustrate the effects of window density thickness on the total efficiency. The total efficiency was reduced more significantly for the lower energy beta emitters as the window density thickness was increased.

The total efficiencies presented in Table 4.9 were used to determine MDCs as a function of window density thickness (Table 4.10). Figures 4.8 and 4.9 illustrate the effects of window density thickness on the MDC for the beta emitters. These figures show, as did the source-to-

VARIABLES AFFECTING INSTRUMENT MDCS

detector distance evaluation, that the window density thickness over the range of 0.3 to 3.8 mg/cm² has a trivial effect on MDCs for the higher energy beta emitters (e.g., SrY-90 and Tl-204), but was considerable for the low to mid-energy beta emitters. These figures illustrate how the detector MDC calibrated to lower energy beta emitters is significantly affected by the window density thickness. As with the effects of source-to-detector distance on MDCs, it is essential that the detector be calibrated with the same window density thickness that will be used for survey measurements in the field. This concern may arise if the window is replaced in the field with one of a different thickness and returned to service without recalibration.

4.4 Source Geometry Factors

The source geometry must be considered in determining the instrument MDC. The detector's response may be influenced, in part, by the contaminant's distribution on the surface being assessed. For example, if the contamination can be characterized by relatively large uniform areas of activity, then the detector should be calibrated to a distributed or extended source. Similarly, if the surface can be characterized by localized spots of surface contamination, that may be approximated by a point source, then the calibration source should be similar to a point source geometry.

The source geometry effect on detector response was evaluated by determining the instrument efficiencies (ϵ_i) for gas proportional, GM, and ZnS detectors placed in contact with both distributed and disc sources. The radionuclide sources used in this evaluation were Tc-99 and Th-230. The instrument efficiencies determined for each detector and geometry configuration are shown in Table 4.11. The instrument efficiencies determined with the disc sources were 6 to 42% greater than those obtained with the distributed sources. These results were expected because of the solid angle of the measurement geometry. That is, for the smaller disc source, a larger fraction of the radiation particles (α and β) emitted from the source intersect the detector probe area. Walker (1994) provides further information on the effects of source-to-detector geometry.

During the course of performing field survey measurements, it would be a time-consuming task to determine the contaminant geometry at each measurement location in an effort to select the most appropriate instrument efficiency. The benefits of a better defined contaminant geometry should be weighed against the increased labor expended in characterizing the contamination. It may be appropriate (conservative) to use the instrument efficiency obtained from a distributed source geometry for all surface activity measurement locations, except for those locations of elevated direct radiation. Only for locations of elevated direct radiation would effort be warranted to characterize the contaminant geometry in order to select the most appropriate instrument efficiency. Additionally, ISO-8769 recommends that the calibration source dimensions be sufficient to provide an area of 150 cm²—certainly a distributed source.

4.5 Ambient Background Count Rate

The effects of ambient background (in particular, relatively high ambient background) on the calculated MDC and measured activity concentration of a radioactive source using a GM detector were evaluated. The procedure included collecting five 1-minute measurements of the ambient background, followed by five 1-minute measurements of a NIST-traceable Tc-99 disc source (activity concentration was 1,500 dpm within a 5-cm² active area). A jig was used to ensure that a reproducible geometry was maintained for each measurement. The ambient background was increased by placing Cs-137 sources at various distances from the GM detector. The ambient background levels ranged from approximately 50 to 1,500 cpm. This procedure allowed a comparison of the *a priori* MDC and the measured activity concentration of the Tc-99 source. The measured activity concentration was calculated using a total efficiency of 0.17 count per disintegration (from Table 4.2); no probe area correction was made since it was known that the source activity was limited to a 5-cm² area. Results are tabulated in Table 4.12.

As expected from the MDC equation, the calculated detection sensitivity (or MDC) of the GM detector increased directly with the square root of the ambient background level (Figure 4.10). For ambient background levels ranging from 50 to 145 cpm (consistent with background levels typically encountered during final status surveys), the measured activity of the Tc-99 was very similar to the stated activity of the source. As the ambient background levels were increased to 1,000 cpm, the measured activity was, with one exception, consistently lower than the certified source activity. As the ambient background was further increased to 1,500 cpm, the measured activity was less than 60% of the certified source activity, with significant uncertainty at the 95% confidence level.

In general, as the ambient background increases, and the ratio of the calculated MDC to the actual activity concentration present approaches unity, the uncertainty in the measured activity increases. However, only when the calculated MDC was approximately 70% of the actual activity concentration (MDC equal to 1,070 dpm per 5 cm²), was there significant uncertainty and inaccuracy in the measured activity. For the case in which the MDC is a small fraction of the guideline value, significant uncertainty in the value is acceptable (e.g., $\pm 100\%$ uncertainty in a value that is 20% of the guideline gives adequate assurance that the compliance with the guideline has been achieved). If this is not the case, caution must be exercised when making measurements that are close to the MDC, because substantial uncertainties may be associated with the measurements.

VARIABLES AFFECTING INSTRUMENT MDCs

**Table 4.1 Characteristics of Radionuclide Sources
Used for Calibration and Static Measurements**

Radionuclide	Active Area (cm²)	Activity (Emission Rate) (cpm)	Source Backing Material^a	Surface Coating
C-14	13	12,860	S.S.	0.9 mg/cm ² aluminized Mylar
C-14	13	959,000	S.S.	0.9 mg/cm ² aluminized Mylar
Ni-63	15	16,600	Ni	NA
SrY-90	15	36,800	S.S./Kapton/Al	NA
SrY-90	13	8,080	Ni	NA
Tc-99	4.9	940	S.S.	NA
Tc-99	4.9	83,400	S.S.	NA
Tc-99	126	26,300	S.S./Al	NA
Tc-99	150	14,400	S.S.	NA
Tl-204	15	6,920	S.S.	NA
Th-230	150	25,100	S.S.	NA
Th-230	126	28,200	S.S./Al	NA
Th-230	5.1	52,700	Ni	NA
Pu-239	5.1	46,300	Ni	NA

^aS.S. is stainless steel.

Table 4.2 Average Total Efficiencies for Various Detectors and Radionuclides

Radionuclide (Average β Energy)	Total Efficiency (Counts per Disintegration) ^a				
	Gas Proportional			GM	ZnS
	α Only	β Only	$\alpha+\beta$		
Beta					
Ni-63 (17.1 keV)	--- ^b	---	0.08 ^c ,0.06 ^d	0.0025	---
C-14 49.4 (49.4 keV)	---	0.04 ^e	0.11 ^d	0.05	---
Tc-99 (84.6 keV)	---	0.16 ^e	0.22 ^d	0.17	---
Tl-204 (244 keV)	---	0.29 ^e	0.35 ^d	0.26	---
SrY-90 (563 keV)	---	0.36 ^e	0.42 ^d	0.32	---
Ru-106/Rh-106 (1410 keV)	---	0.55 ^e	0.57 ^c	0.56	---
Alpha					
Th-230	0.19 ^d	---	---	---	0.18
Pu-239	---	---	---	---	0.19

^aThe total efficiencies represent average values compiled from historical instrument calibration data. These values should be considered as the ideal efficiencies obtained under laboratory conditions. Note that calibration sources were typically on stainless steel or nickel backing material.

^bData not obtained.

^cFor window density thickness of 0.4 mg/cm².

^dFor window density thickness of 0.8 mg/cm².

^eFor window density thickness of 3.8 mg/cm².

VARIABLES AFFECTING INSTRUMENT MDCs

Table 4.3 Minimum Detectable Concentrations for Various Detectors and Radionuclides

Radionuclide (Endpoint β Energy)	Minimum Detectable Concentration (dpm/100 cm ²) ^a	
	Gas Proportional ($\alpha+\beta$)	GM
Ni-63 (66 keV)	1,160 ^b	70,000
C-14 (156 keV)	630	3,500
Tc-99 (294 keV)	320	1,000
Tl-204 (763 keV)	200	670
SrY-90 (1415 keV)	170	550

^aMDCs were calculated on the basis of the ambient background count rates presented in Table 5.1 for the gas proportional detector ($\alpha+\beta$ mode) and the GM detector, and the total efficiencies in Table 4.2. Probe area corrections of 126 and 20 cm², respectively, were made for the gas proportional and GM detectors. The following MDC equation was used for 1-minute counts:

$$MDC = \frac{3 + 4.65 \sqrt{C_B}}{KT}$$

^bMDC calculated using total efficiency for window density thickness of 0.8 mg/cm² (0.06 count per disintegration (c/dis)).

Table 4.4 Instrument Efficiencies

Radionuclide	Instrument Efficiency ^a					
	Active Area of Source (cm ²)	$\alpha + \beta$	β only	GM	α only	ZnS
C-14	13	0.254 ± 0.006	0.081 ± 0.002	0.099 ± 0.002	--- ^c	---
Tc-99	126	0.364 ± 0.029	0.191 ± 0.016	0.193 ± 0.021	---	---
Tl-204	15	0.450 ± 0.025	0.355 ± 0.021	0.278 ± 0.017	---	---
SrY-90	13	0.537 ± 0.027	0.465 ± 0.024	0.388 ± 0.020	---	---
Th-230	126	---	---	---	0.349 ± 0.015	0.259 ± 0.013

^aThe instrument efficiency was determined with the detector at contact with the source, separated by two sheets of Mylar (0.22 mg/cm² per sheet). The instrument efficiency was calculated by dividing the net count rate by the 2 π emission rate of the source.

^bUncertainties represent the 95% confidence interval, based on propagating the errors in the calibration source emission rate and in counting statistics.

^cMeasurement not performed.

VARIABLES AFFECTING INSTRUMENT MDCs

Table 4.5 Source-to-Detector Distance Effects for β Emitters

Distance From Source (cm)	Normalized Net Count Rate ^{a,b}					
	Ni-63 (Disc)	C-14 (Disc)	Tc-99 (Disc)	Tc-99 (Distributed)	Tl-204 (Disc)	SrY-90 (Disc)
Contact	1	1	1	1	1	1
0.5	0.381 ± 0.064 ^c	0.786 ± 0.047	0.864 ± 0.016	0.803 ± 0.015	0.910 ± 0.024	0.9189 ± 0.0065
1	0.196 ± 0.053	0.648 ± 0.048	0.7779 ± 0.0085	0.701 ± 0.023	0.836 ± 0.026	0.8534 ± 0.0088
2	0.038 ± 0.041	0.431 ± 0.034	0.5920 ± 0.0090	0.503 ± 0.014	0.645 ± 0.033	0.6995 ± 0.0063

^aNormalized net count rate determined by dividing the net count rate at each distance by the net count rate at contact with the source.

^bGas proportional detector operated in the $\alpha + \beta$ mode was used for all measurements.

^cUncertainties represent the 95% confidence interval, based on propagating the counting errors in each measurement.

Table 4.6 Source-to-Detector Distance Effects for α Emitters

Distance From Source (cm)	Normalized Net Count Rate ^{a,b}		
	Pu-239 (Disc)	Th-230 (Disc)	Th-230 (Distributed)
Contact	1	1	1
0.5	0.808 ± 0.013 ^c	0.812 ± 0.010	0.761 ± 0.026
1	0.656 ± 0.015	0.606 ± 0.012	0.579 ± 0.021
2	0.1974 ± 0.0046	0.0423 ± 0.0027	0.0990 ± 0.0093

^aNormalized net count rate determined by dividing the net count rate at each distance by the net count rate at contact with the source.

^bGas proportional detectors operated in the α mode were used for all measurements.

^cUncertainties represent the 95% confidence interval, based on propagating the counting errors in each measurement.

**Table 4.7 Minimum Detectable Concentrations
for Various Source-to-Detector Distances for β Emitters**

Distance from Source (cm)	Total Efficiency (c/dis) and Minimum Detectable Concentration (dpm/100 cm ²) ^{a,b}	
	Eff	MDC
Ni-63		
Contact	0.0360 ± 0.0041 ^c	2,000 ± 250
0.5	0.0137 ± 0.0019	5,250 ± 760
1	0.0071 ± 0.0018	10,200 ± 2,600
2	0.0014 ± 0.0015	52,000 ± 56,000
C-14		
Contact	0.1006 ± 0.0051	715 ± 51
0.5	0.0790 ± 0.0034	910 ± 61
1	0.0652 ± 0.0040	1,103 ± 88
2	0.0434 ± 0.0029	1,660 ± 140
Tc-99 (Disc)		
Contact	0.250 ± 0.010	287 ± 19
0.5	0.2164 ± 0.0090	332 ± 22
1	0.1947 ± 0.0076	369 ± 24
2	0.1482 ± 0.0060	485 ± 32
Tc-99 (Distributed)		
Contact	0.207 ± 0.016	347 ± 32
0.5	0.166 ± 0.013	433 ± 41
1	0.145 ± 0.012	496 ± 49
2	0.1042 ± 0.0086	690 ± 67
Tl-204		
Contact	0.338 ± 0.015	213 ± 14
0.5	0.308 ± 0.013	234 ± 16
1	0.282 ± 0.013	255 ± 18
2	0.218 ± 0.014	330 ± 27
SrY-90		
Contact	0.464 ± 0.016	154.9 ± 9.5
0.5	0.427 ± 0.014	169 ± 10
1	0.396 ± 0.014	181 ± 11
2	0.325 ± 0.011	221 ± 14

^aMeasurements performed with a gas proportional detector operated in the α + β mode with an 0.8-mg/cm² window density thickness.

^bThe instrument background was 355 counts and probe area corrections of 126 cm² were made for the gas proportional detectors. The following MDC equation was used for 1-minute counts:

$$MDC = \frac{3 + 4.65 \sqrt{C_B}}{KT}$$

^cUncertainties represent the 95% confidence interval, based on propagating the errors in the calibration source activity and in counting statistics.

Table 4.8 Minimum Detectable Concentrations for Various Source-to-Detector Distances for α Emitters

Distance From Source (cm)	Total Efficiency (c/dis) and Minimum Detectable Concentration (dpm/100 cm ²) ^{a,b}					
	Pu-239 (Disc)		Th-230 (Disc)		Th-230 (Distributed)	
	Eff	MDC	Eff	MDC	Eff	MDC
Contact	0.2549 ± 0.0053 ^c	24 ± 14	0.2495 ± 0.0044	24 ± 15	0.2002 ± 0.097	30 ± 18
0.5	0.2061 ± 0.0036	29 ± 18	0.1910 ± 0.0034	32 ± 19	0.1524 ± 0.0067	40 ± 24
1	0.1672 ± 0.0040	36 ± 22	0.1426 ± 0.0034	43 ± 26	0.1160 ± 0.0052	52 ± 32
2	0.0503 ± 0.0012	121 ± 73	0.00994 ± 0.00069	610 ± 370	0.0198 ± 0.0019	310 ± 190

^aMeasurements performed with a gas proportional detector operated in the α mode with a 0.8 mg/cm² window thickness.

^bThe instrument background was 1 count and probe area corrections of 126 cm² were made for the gas proportional detectors. The following MDC equation was used for 1-minute counts:

$$MDC = \frac{3 + 4.65 \sqrt{C_B}}{KT}$$

^cUncertainties represent the 95% confidence interval, based on propagating the errors in the calibration source activity and in counting statistics.

Table 4.9 Window Density Thickness Effects for β Emitters

Window Density Thickness (mg/cm ²)	Total Efficiency (c/dis) ^a					
	Ni-63 (Disc)	C-14 (Disc)	Tc-99 (Disc)	Tc-99 (Distributed)	Tl-204 (Disc)	SrY-90 (Disc)
0.3	0.0695 ± 0.0041 ^b	0.1273 ± 0.0032	0.288 ± 0.011	0.227 ± 0.018	0.354 ± 0.018	0.477 ± 0.017
0.4	0.0699 ± 0.0032	0.1302 ± 0.0039	0.291 ± 0.011	0.224 ± 0.018	0.359 ± 0.015	0.482 ± 0.019
0.8	0.0409 ± 0.0020	0.1096 ± 0.0032	0.266 ± 0.011	0.209 ± 0.017	0.342 ± 0.015	0.474 ± 0.017
1.3	--- ^c	---	0.247 ± 0.010	0.196 ± 0.016	---	---
1.8	---	---	0.2268 ± 0.0092	0.183 ± 0.015	---	---
2.3	---	---	0.2117 ± 0.0090	0.170 ± 0.013	---	---
2.8	---	---	0.1980 ± 0.0085	0.157 ± 0.012	---	---
3.3	---	---	0.1848 ± 0.0074	0.149 ± 0.012	---	---
3.8	0.0005 ± 0.0011	0.0383 ± 0.0018	0.1638 ± 0.0064	0.129 ± 0.010	0.275 ± 0.012	0.429 ± 0.015

^aGas proportional detectors operated in the $\alpha + \beta$ mode were used for all measurements.

^bUncertainties represent the 95% confidence interval, based on propagating the errors in the calibration source activity and in counting statistics.

^cMeasurement not performed.

Table 4.10 Minimum Detectable Concentrations for Various Window Density Thicknesses

Window Density Thickness (mg/cm ²)	Minimum Detectable Concentration (dpm/100 cm ²) ^{a,b}					
	Ni-63 (Disc)	C-14 (Disc)	Tc-99 (Disc)	Tc-99 (Distributed)	Tl-204 (Disc)	SrY-90 (Disc)
0.3	1,014 ± 80 ^c	554 ± 32	245 ± 16	311 ± 30	199 ± 14	147.9 ± 9.4
0.4	1,016 ± 71	546 ± 33	244 ± 16	317 ± 30	198 ± 13	147.3 ± 9.6
0.8	1,760 ± 120	656 ± 39	270 ± 18	344 ± 32	210 ± 14	151.8 ± 9.6
1.3	— ^d	—	291 ± 19	367 ± 34	—	—
1.8	—	—	317 ± 21	392 ± 38	—	—
2.3	—	—	340 ± 23	423 ± 40	—	—
2.8	—	—	363 ± 24	457 ± 43	—	—
3.3	—	—	389 ± 25	482 ± 46	—	—
3.8	130,000 ± 290,000	1,860 ± 130	435 ± 28	555 ± 52	259 ± 18	166 ± 10

^aGas proportional detectors operated in the $\alpha + \beta$ mode were used for all measurements.

^bBackground levels were determined for each window density thickness and efficiencies were used from Table 4.9. Probe area corrections of 126 cm² were made for the gas proportional detectors. The following MDC equation was used for 1-minute counts:

$$MDC = \frac{3 + 4.65 \sqrt{C_B}}{KT}$$

^cUncertainties represent the 95% confidence interval, based on propagating the errors in the calibration source activity and in counting statistics.

^dMeasurement not performed.

Table 4.11 Source Geometry Effects on Instrument Efficiency

Source Geometry	Instrument Efficiency ^a				
	Tc-99			Th-230	
	$\alpha + \beta$	β only	GM	α only	ZnS
Point (Disc) Source ^b	0.445 ± 0.017^c	0.253 ± 0.010	0.278 ± 0.012	0.4979 ± 0.0089	0.3304 ± 0.0068
Distributed Source ^d	0.382 ± 0.030	0.199 ± 0.016	0.195 ± 0.023	0.397 ± 0.020	0.313 ± 0.016
Ratio of Point-to-Distributed Source	1.16	1.27	1.42	1.25	1.06

^aThe instrument efficiency was determined by dividing the net count rate by the 2π emission rate of the source.

^bThe point (disc) source area for both Tc-99 and Th-230 was 5 cm².

^cUncertainties represent the 95% confidence interval, based on propagating the errors in the calibration source emission rate and in counting statistics.

^dThe distributed source area for both Tc-99 and Th-230 was 126 cm².

VARIABLES AFFECTING INSTRUMENT MDCs

Table 4.12 Ambient Background Effects

Background ^a (cpm)	Gross Counts (cpm)	Measured Activity ^b (dpm)	MDC ^c (dpm)
53.0 ± 9.2 ^d	295 ± 32	1,420 ± 190	220
117 ± 22	375 ± 26	1,520 ± 200	310
145 ± 20	413 ± 56	1,580 ± 350	350
192 ± 26	399 ± 38	1,220 ± 270	400
223 ± 26	458 ± 35	1,380 ± 280	430
291 ± 44	538 ± 54	1,450 ± 410	480
445 ± 46	725 ± 66	1,650 ± 480	590
594 ± 42	815 ± 38	1,300 ± 330	680
1,021 ± 38	1,223 ± 55	1,190 ± 390	890
1,490 ± 100	1,642 ± 91	880 ± 800	1,070

^aMeasurements performed with an Eberline HP-260 GM detector.

^bMeasured activity was calculated by subtracting the background from the gross counts and dividing by a total efficiency of 0.17 count per disintegration. Gross counts were determined by the average of five 1-minute measurements of a Tc-99 source.

^cThe following MDC equation was used for 1-minute counts and an assumed efficiency of 0.17 counts per disintegration:

$$MDC = \frac{3 + 4.65 \sqrt{C_B}}{KT}$$

^dUncertainties represent the 95% confidence interval, based on propagating the counting errors in each measurement.

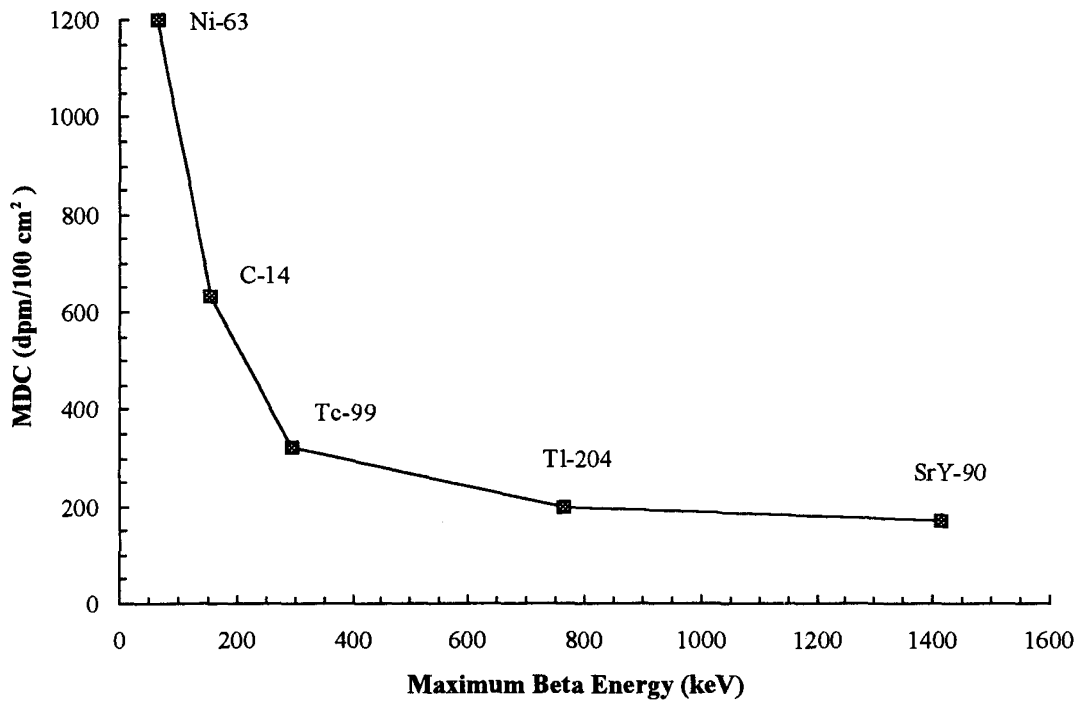


Figure 4.1: MDCs for Gas Proportional Detector ($\alpha+\beta$ Mode) for Various Radionuclides

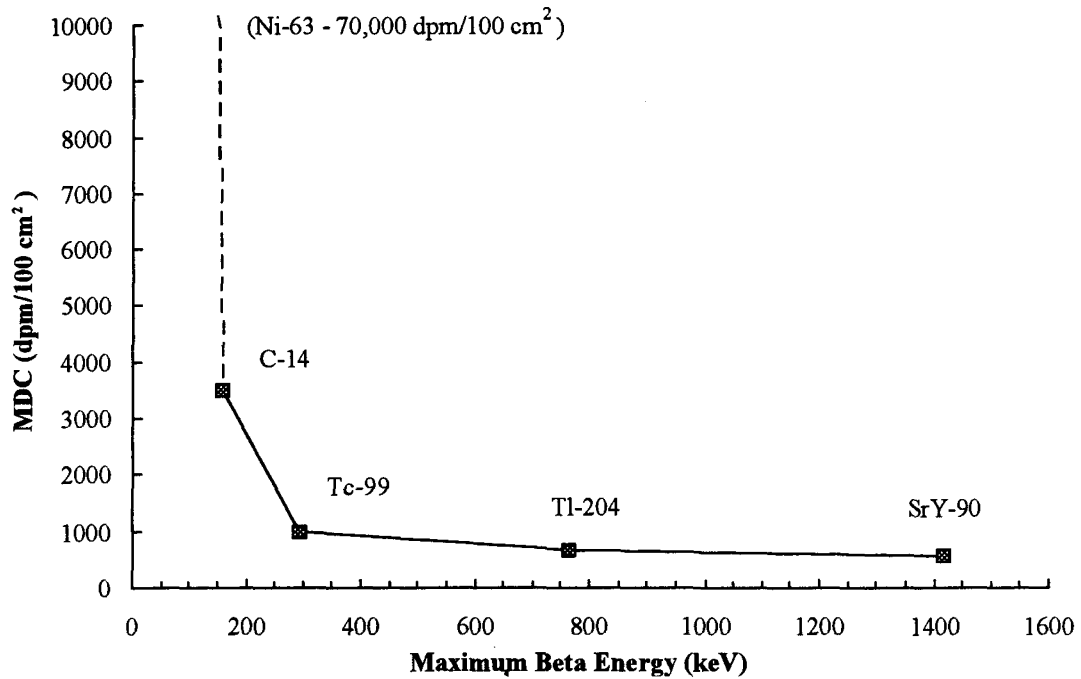


Figure 4.2: MDCs for GM Detector for Various Radionuclides

VARIABLES AFFECTING INSTRUMENT MDCs

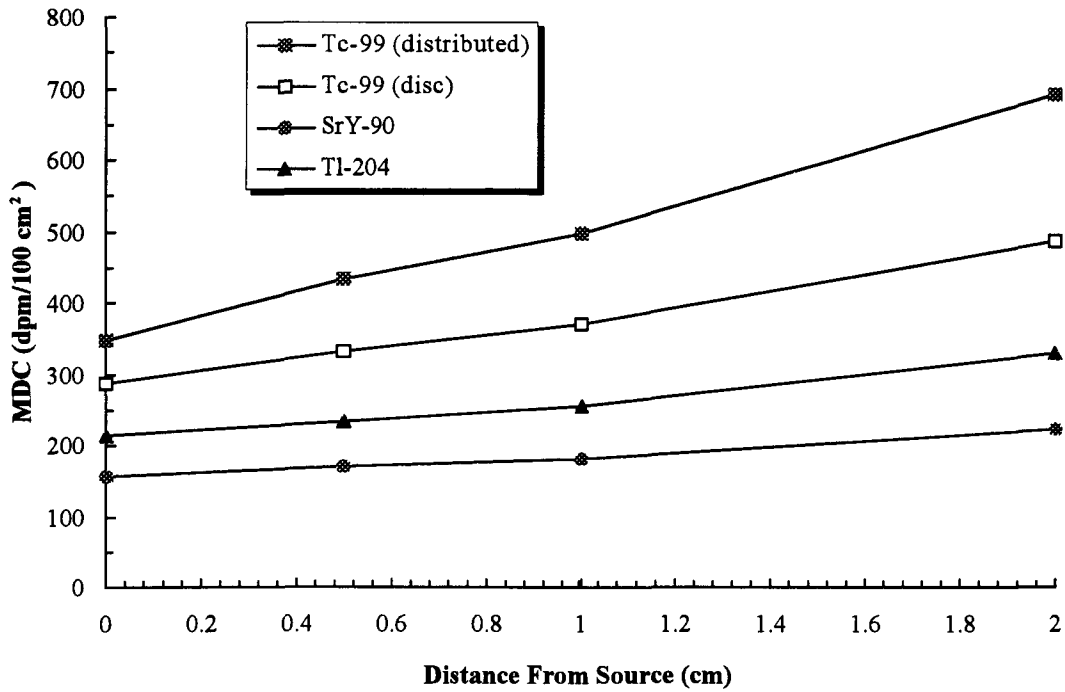


Figure 4.3: Source-to-Detector Distance Effects on MDC for Higher Energy β Emitters

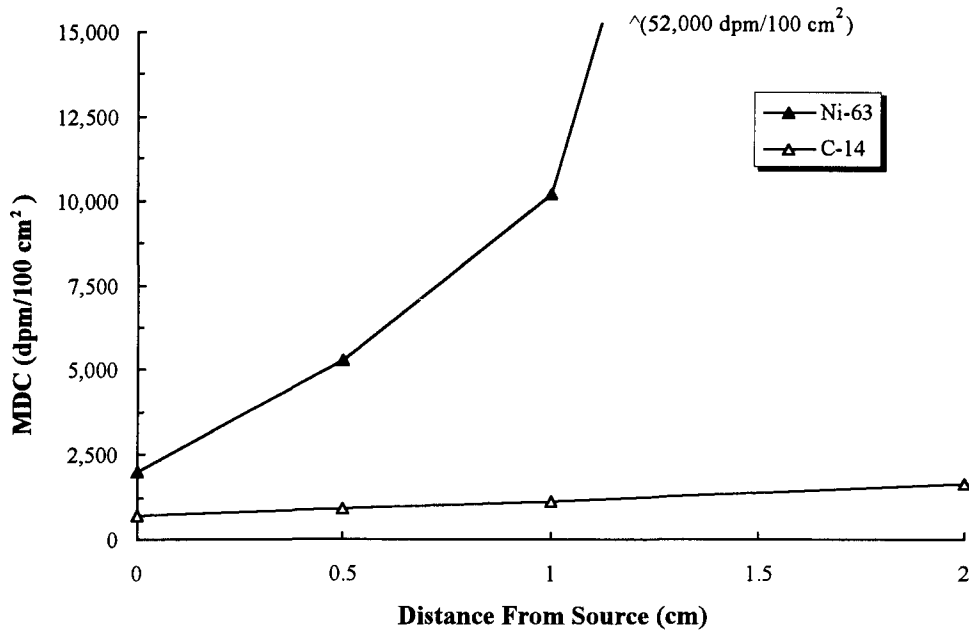


Figure 4.4: Source-to-Detector Distance Effects on MDC for Lower Energy β Emitters

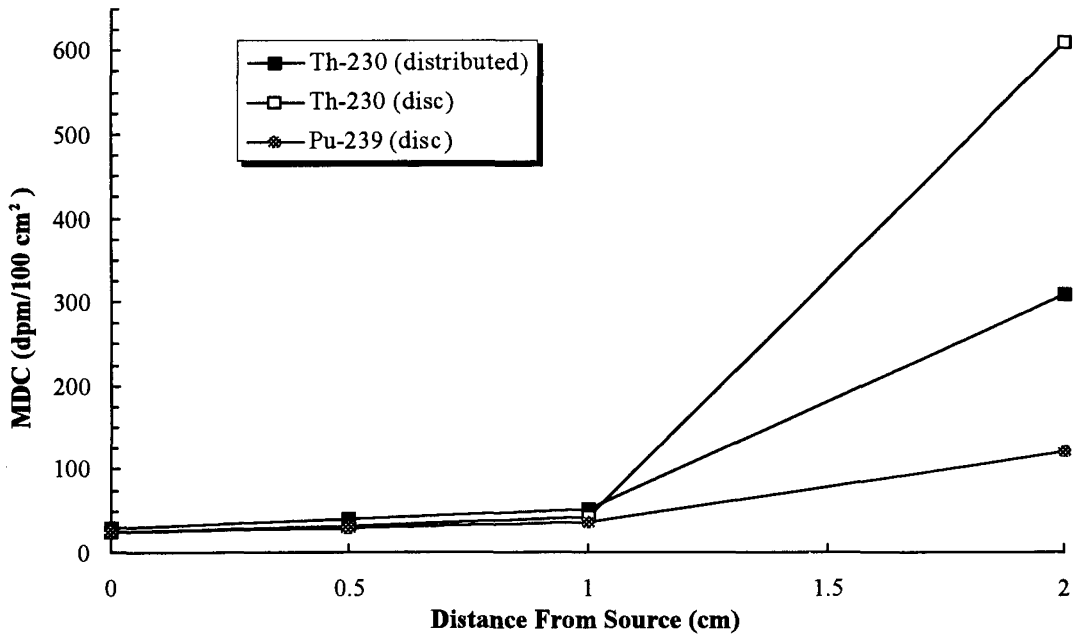


Figure 4.5: Source-to-Detector Effects on MDC for α Emitters

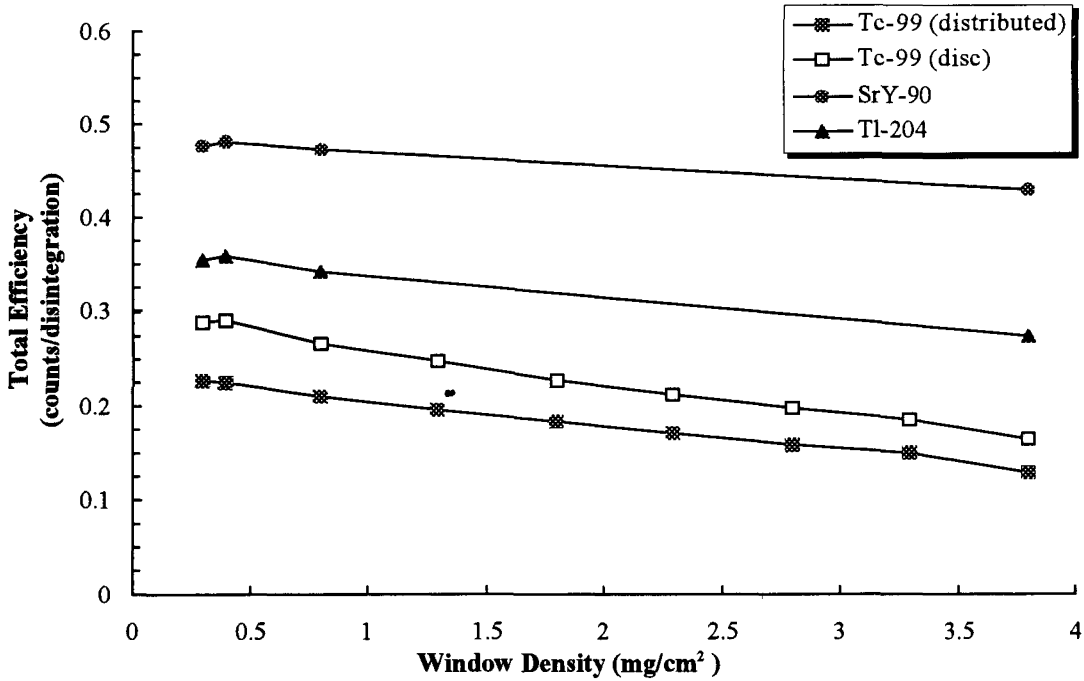


Figure 4.6: Effects of Window Density Thickness on Total Efficiency for Higher Energy β Emitters

VARIABLES AFFECTING INSTRUMENT MDCs

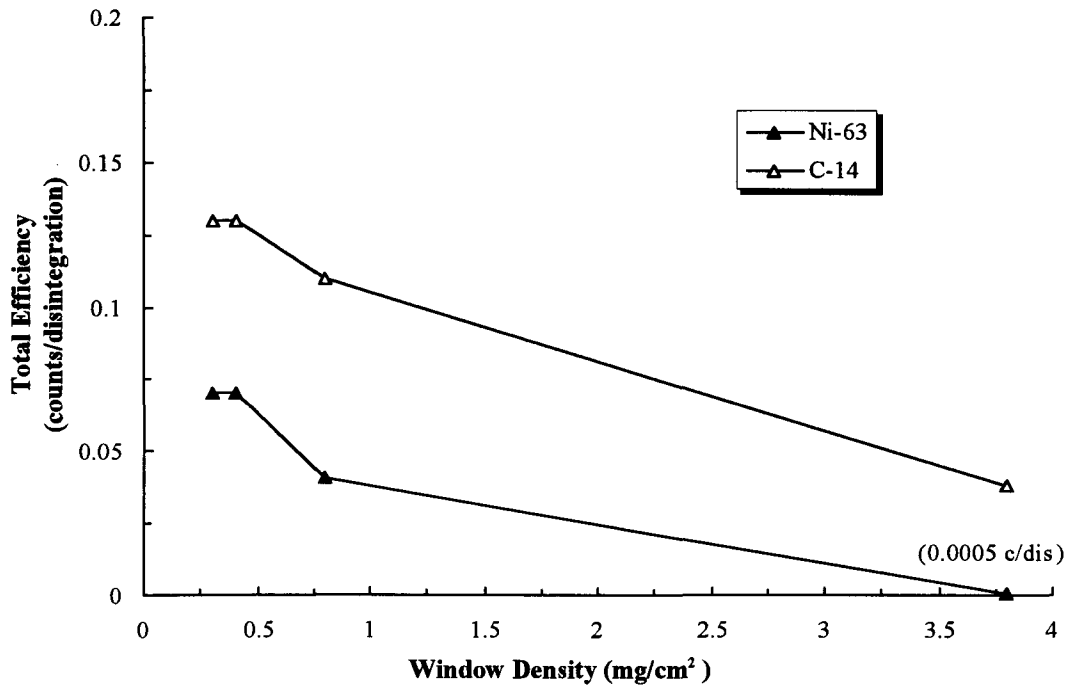


Figure 4.7: Effects of Window Density Thickness on Total Efficiency for Lower Energy β Emitters

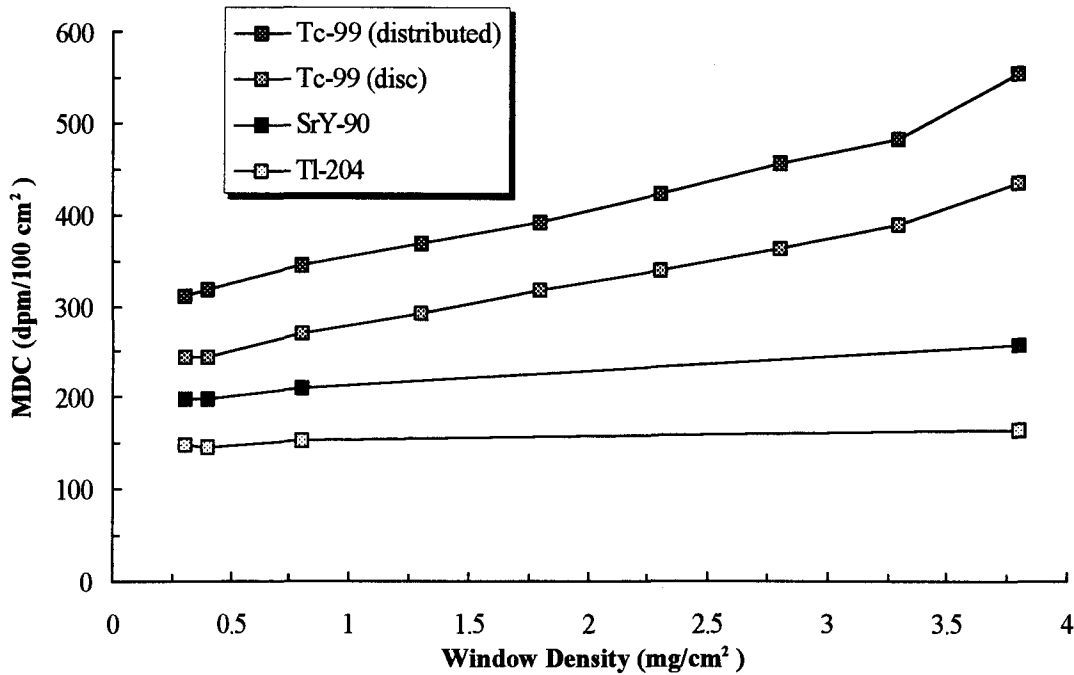


Figure 4.8: Effects of Window Density Thickness on MDC for Higher Energy β Emitters

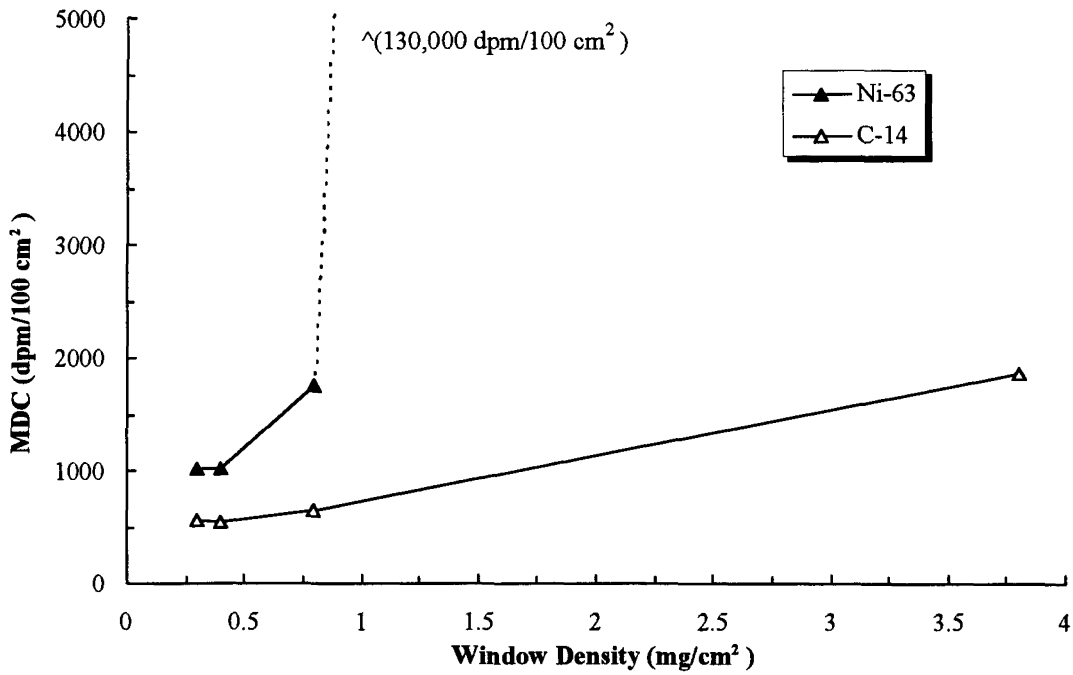


Figure 4.9: Effects of Window Density Thickness on MDC for Lower Energy β Emitters

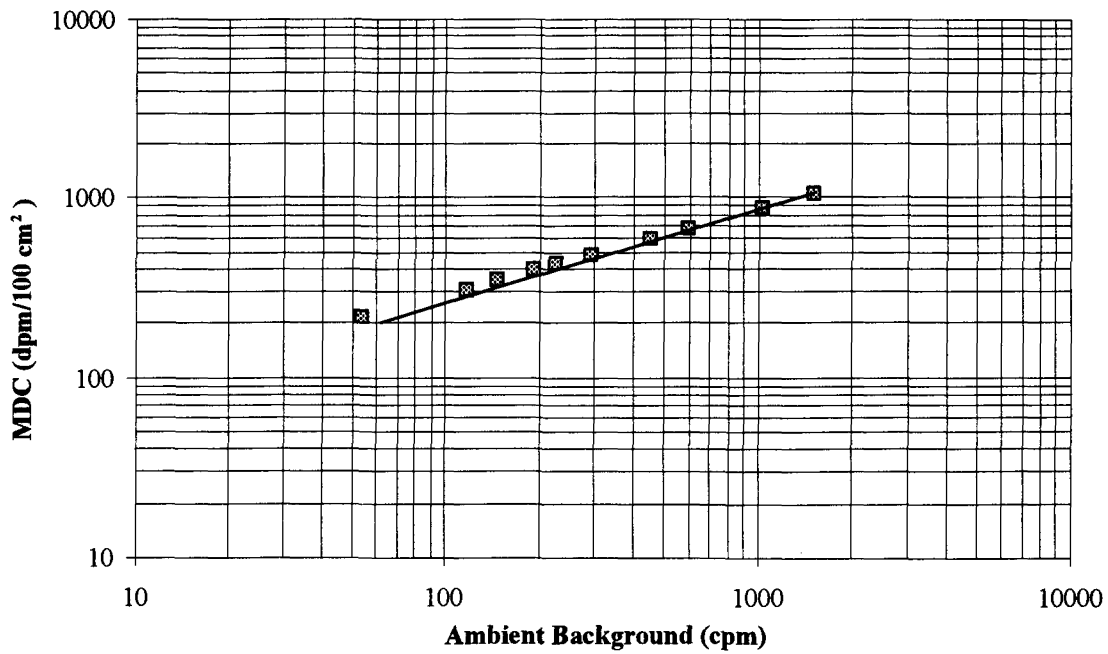


Figure 4.10: Effects of Ambient Background on MDC Calculation

5 VARIABLES AFFECTING MINIMUM DETECTABLE CONCENTRATIONS IN THE FIELD

Surface activity levels are assessed by converting detector response, through the use of a calibration factor, to radioactivity. Once the detector has been calibrated and an instrument efficiency (ϵ_i) established, several factors must still be carefully considered when using that instrument in the field. These factors involve the background count rate for the particular surface and the surface efficiency (ϵ_s), which addresses the physical composition of the surface and any surface coatings. Ideally, the surveyor should use experimentally determined surface efficiencies for the anticipated field conditions. The surveyor needs to know how and to what degree these different field conditions can affect the sensitivity of the instrument. A particular field condition may significantly affect the usefulness of a particular instrument (e.g., wet surfaces for alpha measurements or scabbled surfaces for low-energy beta measurements).

One of the more significant implicit assumptions commonly made during instrument calibration and subsequent use of the instrument in the field is that the composition and geometry of contamination in the field is the same as that of the calibration source. This may not be the case, considering that many calibration sources are fabricated from materials different from those that comprise the surfaces of interest in the field—e.g., activity plated on a metallic disc (Walker 1994). This difference usually manifests itself in the varying backscatter characteristics of the calibration and field surface materials.

Generally, it will not be necessary to recalculate the instrument MDC to adjust for the field conditions. For most of the items discussed below, the detection limit (in net counts or net count rate) remains the same, but the MDC may be different (due to the varying ϵ_s). In this study, the effects of typically encountered surface types and field conditions were evaluated quantitatively. These are discussed in the following sections.

5.1 Background Count Rates for Various Materials

Several different types of surface materials may be encountered in a facility undergoing decommissioning. Among the typical surface materials that were evaluated in this study were (a) brick, (b) ceramic block, (c) ceramic tile, (d) concrete block, (e) unpainted drywall, (f) vinyl floor tile, (g) linoleum, (h) steel, (i) wood pine treated with a commercially available water sealant product, and (j) untreated pine. The main difference considered was the background activity associated with each of these types of surface materials. In most cases, the background count rate for that type of surface needs to be determined and a new MDC established, provided that the specific surface type was not considered in the initial evaluation of the instrument's MDC.

Ambient background count rates were initially determined for gas proportional, ZnS scintillation, GM, and NaI scintillation detectors. Three variations were used for the gas proportional detectors: (a) detection of alpha radiation only (using a high voltage setting that discriminated all beta pulses), (b) detection of beta radiation only (using sufficient window density thickness to

VARIABLES AFFECTING MDCs IN THE FIELD

block alpha radiation), and (c) detection of alpha and beta radiation. Results of ambient background count rates are in Table 5.1. The ambient backgrounds were determined at the same location for all the tested surface materials and, as such, the ambient background was sometimes greater than a particular surface material background. This result was considered acceptable because a primary objective of this study was to evaluate detector responses in as close to field conditions as possible.

Background count rates were obtained for ten surface materials using the same instrument/detector combinations that were used to determine the ambient background. In general, background count rates were lowest for the linoleum, carbon steel, and wood, and highest for the brick and ceramic materials (Table 5.1). These background count rates will vary depending on the local area background radiation levels; however, the data provide information on the relative backgrounds in common construction materials.

MDCs for the gas proportional detectors operated in both the alpha-only and beta-only modes were calculated for each of the surface materials assuming a total efficiency (ϵ_{tot}) of 0.20 and 0.25 count per disintegration, for alpha and beta, respectively (Table 5.2). The MDCs were calculated from Equation 3-10, using the background count rates presented in Table 5.1. The MDCs in the alpha-only mode ranged from 28 to 83 dpm/100 cm², while the MDCs in the beta-only mode ranged from 268 to 425 dpm/100 cm². Since the detector MDC varies directly with the background count rate, the lowest MDCs were obtained for linoleum, carbon steel and wood, and concrete block and drywall, while the highest MDCs were for brick and ceramic materials. Figures 5.1 and 5.2 illustrate the effect of surface material background count rates on detector MDC for the gas proportional detectors operated in both the alpha-only and beta-only modes, respectively. These figures demonstrate the importance of carefully assessing the alpha background for various surface materials due to the wide range of MDC values. This is in contrast to the beta MDCs, which are fairly consistent for all materials examined, with the notable exception of brick and ceramics. In application, it is important that the surveyor establish specific material backgrounds that are representative of the surface types and field conditions.

The reader is referred to NUREG-1501, "Background as a Residual Radioactivity Criterion for Decommissioning," for additional information on background radionuclide concentrations.

5.2 Backscatter Effects

An experiment was performed to evaluate the backscatter characteristics of surfaces commonly encountered during the course of performing decommissioning surveys and to address their effect on surface activity assessments. A thin sheet of Mylar (0.22 mg/cm²) was stretched across a metal frame with an area of approximately 126 cm². Two milliliters of a liquid SrY-90 radionuclide standard was deposited on the Mylar and allowed to air dry—about 4,100 dpm was deposited on the Mylar sheet. Measurements were then performed on various surfaces with the same activity-spiked Mylar sheet positioned between the surface of interest and the gas flow

proportional detector. With this experimental setup, any differences in the detector response are solely attributable to the differences due to backscattered radiation. Gas flow proportional detectors were used to make surface activity measurements using both 0.4 and 3.8 mg/cm² window thicknesses. Table 5.3 depicts the different total efficiencies—determined by dividing the net count rate by deposited activity—obtained for the various surfaces used in this experiment. The efficiency data were normalized to the efficiency in air, which was assumed to produce negligible backscatter radiation. The backscatter factor, calculated by dividing the particular surface material efficiency by the efficiency in air, ranged from 1.20 to 1.43 for the detector with 0.4 mg/cm² window thickness, and ranged from 1.11 to 1.37 for the detector with 3.8 mg/cm² window thickness. Of particular interest is the backscatter factor for stainless steel—which is often the substrate material for calibration sources—as compared to the other surfaces. For the detector with 0.4 mg/cm² window thickness, the backscatter factor for stainless steel was 1.43, as compared to 1.20 for wood, 1.24 for drywall, 1.25 for a tile floor, and 1.30 for sealed concrete floor. Thus, efficiencies for surfaces other than stainless steel may be overestimated by 10 to 20% due to the backscatter effect alone (the efficiency overestimation for the 3.8 mg/cm² window thickness ranged from 11 to 24%). The relatively high efficiency obtained with stainless steel calibration sources may result in the surface activity for surfaces like wood, drywall and concrete being underestimated by 10 to 20%. Furthermore, the total efficiency for SrY-90 on stainless steel versus concrete surfaces exhibit similar differences (about 10%) when the SrY-90 source was deposited on each of these surfaces (discussed in Section 5.5 and shown in Table 5.29).

5.3 Effects of Surface Condition on Detection Sensitivity

The conversion of the surface emission rate to the activity of the contamination source is often a complicated task that may result in significant uncertainty if there are deviations from the assumed source geometry. For example, consider the measurement error associated with an alpha surface activity measurement on a rough surface, such as scabbled concrete, where substantial attenuation reduces the count rate as compared to the calibration performed on the smooth surface of a National Institute of Standards and Technology (NIST) traceable source.

The effects of surface condition on detection sensitivity were evaluated for surfaces commonly encountered during decommissioning surveys. The surfaces studied were abraded (scabbled) concrete, finished (sealed) concrete, carbon steel, stainless steel, and wood. The results of this study provide a quantitative range of how various surface conditions may affect the detectability of various contaminants.

5.3.1 Surface Preparation

For this study, known quantities of NIST traceable Tc-99 and Th-230 standard sources, in aqueous solutions, were dispensed on each of the surfaces. The preparation of the reference sources from the traceable solution involved measurement uncertainties (e.g., pipetting errors, volumetric determinations) that were propagated into the overall statement of uncertainty.

VARIABLES AFFECTING MDCS IN THE FIELD

Background count rates were obtained for instrument/surface combinations that were used to determine the surface activity measurements, so that the proper background could be subtracted from the gross counts. For the surface materials studied, the Tc-99 and Th-230 were dispensed to simulate both a point source and distributed source geometry (it should be noted that the Tc-99 and Th-230 were not mixed, but were dispensed on separate areas of each surface). The areal extent of the point source activity ranged from approximately 4 to 10 cm², while the distributed source geometry was fabricated by uniformly depositing droplets of the Tc-99 and Th-230 activity over a larger area (126 cm²). The total Tc-99 activity dispensed in the point source geometry was 2828 ± 91 dpm (5660 ± 110 dpm for the sealed concrete), while 4595 ± 79 dpm of Th-230 was dispensed in a point source geometry. The Tc-99 and Th-230 activity dispensed in the distributed source geometry was 2830 ± 100 dpm and 4600 ± 170 dpm, respectively. Once dispensed, the radioactive material was allowed to dry overnight in a ventilated hood.

Uniformity measurements with a GM detector for distributed sources were performed to evaluate how well the activity was spread over the surfaces (refer to Section 5.4.1 for a detailed description of uniformity measurements). It was important that the activity was precisely distributed the same for each of the materials. Because the instrument response is dependent on the source geometry (Section 4.4), the instrument efficiencies (ϵ_i) determined by placing the detectors in contact with the NIST-traceable plate sources were applicable to the measurements performed on the Oak Ridge Institute for Science and Education (ORISE) fabricated sources provided that the activity was uniformly deposited over the same active area (126 cm²) as the NIST-traceable source. It should be noted that the preparation of a scabbled surface source by deposition on a “pre-scabbled” surface may not be representative of the actual field surface condition. That is, on a real scabbled surface the activity will likely be concentrated in the “peaks” or undisturbed surface, and will be absent in the “valleys.”

5.3.2 Measurement Results for Various Surface Types

Beta measurements were performed with gas proportional and GM detectors. Two variations were used for the gas proportional detectors: detection of beta radiation only (using 3.8-mg/cm² window density thickness to block alpha radiation) and detection of alpha plus beta radiation. Five 1-minute measurements were made for each combination of material, geometry, and surface material. The results are presented in Table 5.4. Alpha measurements were performed with gas proportional (α -only mode) and ZnS detectors—results are presented in Table 5.5. Both alpha and beta measurements were taken at contact with the sources. The total efficiency for the point source geometry was determined by simply dividing the average net count rate by the total activity dispensed. No correction for the decay of Tc-99 or Th-230 was necessary because of their long half-lives. The total efficiency for the distributed source was determined by the following equation:

(5-1)

$$\text{Total Efficiency} = \frac{\text{Net Count Rate}}{\left(\frac{\text{Total Activity}}{126 \text{ cm}^2} \right) \text{ Probe Area}}$$

The total efficiencies determined for the distributed activity on surfaces should use the active or physical probe area, as opposed to the effective probe area, in converting instrument response to surface activity. During instrument calibration, the total efficiency is determined by placing the probe in contact with the calibration source and recording the net counts, and then dividing by the activity of the source. No correction is made for the fact that the probe has a protective screen; the total efficiency and instrument efficiency take into consideration the fact that part of the active area of the probe is covered and may be insensitive to incident radiation. Thus, surface activity measurements in the field should be corrected for the physical area of the probe, with no corrections made for the protective screen, to be consistent with the manner in which the instrument was calibrated. Refer to Section 2 for the comparison of the physical probe area and the effective probe area for each of the detectors studied.

The source efficiencies, ϵ_s , were calculated by dividing the total efficiency by the instrument efficiency. The instrument efficiencies were determined for each detector and geometry using appropriate NIST-traceable sources. As discussed in Section 4, following the ISO-7503-1 guidance for surface activity measurements requires knowledge of both the instrument and source efficiencies. The instrument efficiency, ϵ_i , is determined during calibration using the stated 2π emission rate of the source. Source efficiencies must be experimentally determined for a given surface type and coating. Tables 5.4 and 5.5 present experimental data on source efficiencies for several common surface types. The data indicate that the source efficiency varies widely depending on the amount of self-absorption and backscatter provided by the surface. The total efficiencies may be determined from Tables 5.4 and 5.5 by simply taking the product of ϵ_i and ϵ_s .

The total efficiencies for Tc-99 and Th-230 on various surfaces determined from this experiment may be compared to the average detector efficiencies (historical calibration data from the Environmental Survey and Site Assessment Program of ORISE) presented in Table 4.2. The average Tc-99 total efficiency for a gas proportional detector operated in an alpha plus beta mode was 0.22 c/dis (on a NIST-traceable source). This study indicates that this is an appropriate total efficiency to use for untreated wood in a point source geometry (for $\alpha + \beta$ on treated wood, ϵ_i multiplied by ϵ_s equals 0.23), but may be overly conservative for stainless steel surfaces and for sealed concrete. Similarly for the Th-230, the average total efficiencies during calibration were 0.18 and 0.19 c/dis, respectively, for the ZnS and gas proportional (alpha only mode). This study indicates that for a point source geometry on untreated wood, the total efficiency is less than 50% of the historical average alpha total efficiency (0.097 and 0.061, respectively, for α -only and ZnS detectors), and for scabbled concrete, the alpha total efficiency is approximately 50 to 75% of the total efficiency obtained from historic Environmental Survey and Site Assessment Program

VARIABLES AFFECTING MDCs IN THE FIELD

calibration data. The effect of reduced total efficiency in the field is an increase in the survey instrumentation MDCs. Table 5.6 gives information on the MDCs for these surface types.

The minimum detectable concentrations shown in Table 5.6 reflect the differences in the source efficiency for each surface. That is, the background, counting time, and instrument efficiency were constant for each given detector and geometry. The large variations in MDC for the surface types studied should be noted. For example, using an $\alpha + \beta$ gas proportional detector to measure Tc-99 distributed over a 126-cm² area has an MDC range of 260 to 950 dpm/100 cm², depending on the surface type. However, it is the lower bound value that is typically calculated and used as the MDC (because the calibration is performed on a clean, high-backscatter reference source, with no consideration given to the actual surface measured). Furthermore, if the uncertainty in the total efficiency is incorporated into the MDC equation (refer to Equation 3-12), the MDC for finished concrete is 2,300 dpm/100 cm² (compared to 950 dpm/100 cm²).

Instrument response can be affected by energy response to the source, backscatter from media, and self-absorption of radiation in the surface. It was possible that the relatively low efficiency obtained for some of the concrete surfaces was due to the penetration of the reference material into the surface and the resultant self-absorption. This porosity effect was also evident for the untreated wood

(Table 5.5). The high source efficiencies obtained on the stainless steel surface were due in part to the contribution from backscattered particles entering the detector. The backscatter contribution measured was approximately 50% for Tc-99 on stainless steel, somewhat higher than anticipated. The backscatter contribution from Tc-99 on a stainless steel surface has been estimated as 22% (NCRP 112).

The International Organization for Standardization recommends the use of factors to correct for alpha and beta self-absorption losses when determining the surface activity. Specifically, the recommendation is to use a source efficiency of 0.5 for maximum beta energies exceeding 0.4 MeV, and to use a source efficiency of 0.25 for maximum beta energies between 0.15 and 0.4 MeV and for alpha-emitters; these values "should be used in the absence of more precisely known values" (ISO 7503-1). Although this guidance provides a starting point for selecting source efficiencies, the data in Tables 5.4 and 5.5 illustrate the need for experimentally determined source efficiencies.

In summary, both backscatter and self-absorption effects may produce considerable error in the reported surface activity levels if the field surface is composed of material significantly different in atomic number from the calibration source. Therefore, it is important to consider the effects that result when the calibration source has backscatter and self-absorption characteristics different from the field surface to be measured. The following guidance should prove beneficial when making measurements on concrete surfaces and using the conventional total efficiency to convert count data to surface activity (i.e., source efficiencies are not considered separately): use a

calibration source that is mounted on an aluminum disc, since the backscatter characteristics for concrete and aluminum are similar (NCRP 112).

5.4 Attenuation Effects of Overlaying Material (Self-Absorption)

Calibration sources invariably consist of a clean, smooth surface and, as such, do not reproduce the self-absorption characteristics of surfaces in the field. Thus, the surface condition can affect the detection sensitivity of an instrument significantly, depending on the radionuclide of concern. For example, paint has a smaller impact on detection of Co-60 (beta radiation) than it does for Am-241 (alpha radiation). The effects that various surface conditions have on detection sensitivities were evaluated by depositing varying amounts of the material (i.e., water, dust, oil, paint) between the detector and the radioactive source.

5.4.1 Methodology

The effects of the following surface conditions were evaluated quantitatively: (a) dusty, (b) wet, (c) oily, and (d) painted surfaces. In order to allow intercomparison of the results from this study, it was necessary to simulate known thicknesses of materials such as dust, water, or paint on surfaces, reproducibly. Therefore, known quantities of soil (dust), water, oil, and paint were evenly spread over a surface with standard (known) dimensions to produce the desired thickness of material on the surface.

The material to be evaluated (e.g., water, dust, oil, paint) was uniformly deposited between two Mylar sheets, within the area of the Plexiglas jig. The net weight of the material was obtained and the density thickness of the material (in mg/cm²) was calculated by dividing the weight by the area over which the material was deposited (typically 126 cm²). It was necessary to ensure that the material was evenly spread over the active area of the Plexiglas. The following text describes how the surface coatings were prepared (oil is discussed in Section 5.4.2).

Paint

The Mylar was attached tightly to the Plexiglas jig and weighed for initial weight. A 126-cm² hole was cut in a piece of cardboard to match the exact active area of the 43-68 detector. The Mylar was placed beneath the cardboard jig. The paint was sprayed lightly over the surface of the Mylar at a distance that varied from 15 cm to as much as 30 cm. After the paint had dried, a new weight was obtained and subtracted from the initial weight. This yielded the test weight. After measurements were completed and the Mylar was checked for tears, the next quantity of paint was applied.

Water

A piece of Kimwipe was cut exactly to fit the active area of a 43-68 detector (126 cm²) and

VARIABLES AFFECTING MDCS IN THE FIELD

placed on a new piece of Mylar. In this case, the Mylar was not stretched or attached tightly across the Mylar jig. The initial weights for the Kimwipe and Mylar sheets were then determined. A known quantity of water was then pipetted onto the Kimwipe as evenly as possible. The water was uniformly absorbed over the Kimwipe. After measurements had been performed, the Kimwipe and Mylar were folded and reweighed to measure the amount of evaporation and to determine the next test weight. Evaporation was very rapid in most cases and weight determinations had to be made following each instrument measurement series.

Dust

Dust was obtained by grinding potting soil and sieving it through 250 mesh screen. An empty plastic dish was weighed and dust was added to the dish until the desired weight was obtained. Dust was then poured onto the Mylar that was tightly stretched across the Plexiglas jig. The dish was then reweighed to obtain the exact amount of dust applied to the Mylar. The dust was spread across the Mylar to 126 cm². This was done by using a small (1/4-inch-wide), very fine, bristle brush. The brush was first weighed. The dust was so fine that it could not be brushed or swept, instead it was blotted until it appeared evenly distributed and within the 126-cm² active area of the probe. Another sheet of Mylar was placed over the dust. After the dust was distributed, the brush was again weighed to determine if any dust remained in the brush and to obtain the final test weight. This process was repeated for each test weight.

Uniformity Measurements

The uniformity of the material deposition between the Mylar sheets was evaluated by measuring the attenuation produced by the two Mylar sheets and material at five locations within the active area of the Plexiglas. Specifically, at each location, the GM detector (20-cm² probe area) and radioactive disc source (a low-energy beta or alpha source was used to ensure that the source was being attenuated by the material) were placed on opposite sides of the Mylar sheets. Five 1-minute measurements were obtained at each location. The measurements were averaged and the standard error in the mean was calculated at each location. Uniformity of the material was assumed to be sufficient if the relative standard error in the mean of 25 measurements (5 measurements at each locations) was less than 15%. It was recognized that exact uniformity was not practical, or even desirable, since one objective of the study was to reproduce realistic field conditions.

If the uniformity test failed, efforts continued to evenly distribute the material until the material was distributed more uniformly. Once the desired level of uniformity had been achieved, measurements were performed using the necessary detectors and calibration sources. The instrument background was determined by a series of five 1-minute counts. For each data point (i.e., combination of material, thickness, detector, and source) evaluated, five 1-minute measurements were collected (in general, the radioactive sources used in this study possessed sufficient activity to ensure that the uncertainty due to counting statistics alone was less than 5%).

Each data point was statistically evaluated by calculating the mean of the gross counts and standard error in the mean of the gross counts. The background was subtracted from the mean of the gross counts, and the detector efficiency was calculated by dividing by the activity of the calibration source. The pressure and temperature in the measurement hood were recorded.

5.4.2 Measurement of Various Surface Coatings

Initially, this study was limited to performing MDC measurements with a gas proportional detector (Ludlum Model 43-68) with oil deposited between the Mylar sheets. The radioactive sources used in the pilot study were C-14, Tc-99, and SrY-90. The Tc-99 source used was a 100-cm² plate source; the C-14 and Sr-90 sources had 32-mm-diameter, disc-shaped geometries. The detector background for 1 minute was 326 counts. Table 5.7 presents the results of MDC measurements for each source under the following conditions: (a) detector face alone (0.4-mg/cm² window), (b) detector face and two sheets of Mylar (0.8-mg/cm², total density thickness), (c) plus 1.5 mg/cm² of 20W-50 motor oil (2.3-mg/cm², total density thickness), (d) plus 2.9 mg/cm² of 20W-50 motor oil (3.7-mg/cm², total density thickness), and (e) plus 4.5 mg/cm² of 20W-50 motor oil (5.3-mg/cm², total density thickness).

Figure 5.3 shows the effects of oil density thickness on the source efficiency. The first datum point for each source (at 0.4 mg/cm², not shown in figure) in Table 5.7 may be considered to yield the total efficiency under optimum laboratory conditions (smooth, clean surface). As various density thicknesses of oil were added, the source efficiency was decreased due to absorption losses. The source efficiency appeared to be reduced more significantly for the lower energy beta emitters as the density thickness of oil on the surface was increased. Figure 5.4 illustrates the effects of oil density thickness on the detector MDC (which is a function of source efficiency). The first data point for each source may be considered as the theoretical detector MDC under optimum laboratory conditions. This figure illustrates how the detector MDC, calibrated to lower energy beta emitters, was significantly affected by the oil density thickness on the surface.

This portion of the study continued with the evaluation of various thicknesses of paint, dust, and water deposited between the detector and the source. Measurements were performed with gas proportional, GM, and ZnS detectors. Three variations were used for the gas proportional detectors: (a) detection of alpha radiation only, (b) detection of beta radiation only (using 3.8-mg/cm² window density thickness to block alpha radiation), and (c) detection of alpha and beta radiation. The radioactive sources used in the pilot study were C-14, Tc-99, Tl-204, and SrY-90 for beta measurements, and Th-230 for alpha measurements. When measurements were performed over large area sources (i.e., 126 or 150 cm²), the source activity within the physical area of the detector was determined. This corrected activity was used to determine total efficiencies:

$$\text{Corrected Activity} = \frac{(\text{Source Activity}) (\text{Probe Area})}{(\text{Active Area of Source})} \quad (5-2)$$

VARIABLES AFFECTING MDCs IN THE FIELD

Tables 5.8 through 5.28 present the results of material density thicknesses for paint, dust, and water versus source efficiency for all of the detector types evaluated. These results are consistent with the results obtained with the oil deposition. As before, the source efficiency appeared to be reduced more significantly for the lower energy beta emitters as the density thickness of the material on the surface was increased. The instrument efficiency was determined with the Mylar in place above the source for the paint and dust studies, and with the Mylar and Kimwipe sheet for the water attenuation studies. The total efficiency may be calculated for any evaluated surface coating by multiplying the instrument efficiency by the source efficiency. Figures 5.5 through 5.19 illustrate the effects of material density thicknesses on source efficiency—each figure shows the measured data and the best-fit exponential curve. Figures 5.20 to 5.23 illustrate the effects of increasing dust density thickness on the MDC calculation.

The measured source efficiency versus density thickness was fit to an exponential curve. The results of this regression fit are provided in Tables 5.8 through 5.28. The data associated with the source efficiency and density thickness were examined for the best way to present the error associated with the given measurements. It was judged that regression techniques are the best approach to describe the data as well as providing the average source efficiency and 95% confidence interval at each density thickness. The density thickness was assumed to be known without error. This is undoubtedly incorrect but, it does not affect the results significantly because the error associated in the weight measurements is small compared with the error associated with the count measurements used to determine the source efficiency. This practice is common in most regression situations and is discussed in NUREG/CR-4604, "Statistical Methods for Nuclear Material Management". The regression was used to determine the intercept and slope of the line—transformed by taking the natural logarithm—using a least-squares fit. The regression also outputs the residual mean square which is an unbiased estimator of the variance associated with the source efficiency values. Using the slope and intercept, the predicted values associated with the density thickness measurements were determined. A confidence interval was also determined using (Myers 1994):

$$Y_o - t_{w/2} s \left((1/n) + [(x_o - \bar{x})^2 / S_x] \right)^{1/2} < Y < Y_o + t_{w/2} s \left((1/n) + [(x_o - \bar{x})^2 / S_x] \right)^{1/2} \quad (5-3)$$

where,

Y_o	= predicted source efficiency	x_o	= density thickness of interest
$t_{w/2}$	= test statistic for desired accuracy	\bar{x}	= average density thickness
s	= square root of residual mean square	S_x	= $\sum (x_i - \bar{x})^2$
n	= number of points in regression	Y	= measured source efficiency

One interesting finding was that the alpha and beta attenuation for a given radionuclide were similar, regardless of the specific material responsible for the attenuation. Figure 5.24 illustrates that the source efficiencies versus density thickness for SrY-90, Tl-204, Tc-99, and C-14 decrease fairly consistently for each of the materials tested, and may be considered independent of material

type (i.e., the source efficiency decreases with increasing density thickness in the same manner for water, dust, and paint).

The exponential term in each regression fit is a measure of the alpha or beta attenuation. That is, the exponential terms were consistent for each radionuclide—the terms ranged as follows: C-14, 0.211 to 0.291; Tc-99, 0.086 to 0.110; Tl-204, 0.031 to 0.046; SrY-90, 0.016 to 0.028; and Th-230, 0.331 to 0.906. The alpha radiation experienced the greatest variability in attenuation with different materials.

When using the fitted source efficiency data in Tables 5.8 to 5.28, it is important to note that the exponential reduction produced from a given density thickness is obtained from the exponential term alone. An example is provided to clarify the use of these data. Assume that a GM detector is calibrated to a Tc-99 point source, resulting in an ϵ_i equal to 0.278. It is determined that surface activity measurements will be performed on a concrete surface—refer to Table 5.4 to obtain ϵ_s equal to 0.630. Therefore, the total efficiency is calculated by multiplying ϵ_i by ϵ_s (equals 0.175). Now assume that there is a 2 mg/cm²-thick coating of dust on the concrete surface—therefore, the surface efficiency (ϵ_s) must be corrected for this dust layer. Table 5.16 provides the regression equation for Tc-99 with a GM detector: $\epsilon_s = 0.669 e^{-0.093 x}$

To correct the surface efficiency (0.630) for the dust layer, multiply ϵ_s by the exponential term, substituting the density thickness for x: ϵ_s (for 2 mg/cm² dust) = (0.630) * $e^{-0.093(2)} = 0.523$.

Now the total efficiency for this condition becomes $\epsilon_{tot} = \epsilon_i * \epsilon_s = (0.278) (0.523) = 0.146$, as compared to 0.175 without consideration of the dust layer.

5.5 Use of Alpha and/or Beta Measurements to Assess Surface Activity

The uranium and thorium decay series emit both alpha and beta radiation. A common practice has been to use beta measurements to demonstrate compliance with those surface activity guidelines expressed as alpha activity. In the case of uranium, the current surface activity guidelines are specified in alpha disintegrations per minute—e.g., 5,000 α dpm/100 cm². When applying beta measurements to assess compliance with uranium and thorium surface activity guidelines, consideration should be given to the radionuclide (specifically the energy of the radionuclide) used to calibrate the detector. For example, SrY-90, a high energy beta-emitter, is often used to calibrate a detector for surface activity measurements of uranium. That is, a SrY-90 calibration source is assumed to be sufficiently representative of the beta emissions from the uranium surface contamination and, therefore, it is assumed that the total efficiency using a SrY-90 source will provide an adequate representation of the uranium contamination. An experiment was designed to evaluate the agreement between total efficiencies obtained from a SrY-90 source and processed uranium contamination. Additionally, an experiment was performed with 3% enriched uranium (3% of U-235 by weight) to assess the applicability of calculating the total efficiency for uranium by considering the detector's response to each of the alpha and beta emissions in the decay series.

VARIABLES AFFECTING MDCs IN THE FIELD

For these experiments, known quantities of NIST-traceable SrY-90, Ru-106 (Rh-106), processed uranium, and 3% enriched uranium (in aqueous solutions), were dispensed on various surface materials (i.e., stainless steel, concrete, wood and drywall). Processed uranium includes U-238 that is in equilibrium with U-234, but with the remaining decay series radionuclides removed; and U-235 is present at the natural isotopic ratio (0.7% of U-235 by weight). The 3% enriched uranium exhibited a U-234-to-U-235 ratio of 24, and had the following alpha activity fractions: 0.167, U-238; 0.033, U-235; and 0.799, U-234. For each surface material, SrY-90, Ru-106 (Rh-106), and uranium were dispensed to simulate a small, disc-source geometry—the areal extent of the source activity was less than 20 cm². The total SrY-90 activity dispensed was 5,229 dpm and approximately 4,200 dpm for the Ru-106 (Rh-106). The total processed uranium activity was 7,840 alpha dpm—approximately comprised of 3,900 dpm U-238; 3,760 dpm U-234; and 180 dpm U-235. The amount of enriched uranium dispensed was 4,520 dpm; uranium isotopic fractions can be calculated using the alpha activity fractions provided above. Once dispensed, the radioactivity was allowed to dry overnight in a ventilated hood.

Background count rates were obtained for instrument/surface combinations that were used to make surface activity measurements of the deposited activity. Beta measurements were performed with gas proportional and GM detectors. As before, two variations were used for the gas proportional detectors, including detection of beta radiation only (using 3.8 mg/cm² window density thickness to absorb alpha radiation) and detection of alpha plus beta radiation. Alpha measurements were performed with gas proportional (alpha only mode) and ZnS detectors. Five, 1-minute measurements were performed for each source and surface material combination. Total efficiencies were calculated by dividing the net count rate by the activity dispensed on the particular surface. For uranium, the total alpha activity was used to determine the total efficiencies. Results are presented in Table 5.29.

The first observation that can be made is that the alpha efficiencies for the α -only gas proportional and ZnS detectors are low as compared to the historical efficiencies obtained from ESSAP electroplated calibration sources (refer to Table 4.2). One possible reason for this reduction in alpha efficiency is that the liquid sources were allowed to air dry—and as such, the resulting source deposition did not constitute a “weightless” source (i.e. source with virtually no self-absorption). That is, the uranium source deposition was probably responsible for measurable self-absorption of the alpha radiation. It should be noted that while experimental controls could have been exercised to make the uranium source deposition approximately “weightless,” the actual source deposition used is likely more realistic to the uranium contamination measured in the field.

The second observation made was that the SrY-90 source, deposited on stainless steel and concrete surfaces, exhibited total efficiencies for the alpha plus beta gas proportional and GM detectors very similar to those of processed uranium. The total efficiency for SrY-90 with the beta-only gas proportional detector was about 50% higher than the processed uranium total efficiency (i.e., 0.38 c/dis versus 0.24 c/dis on stainless steel). Therefore, the assessment of uranium contamination using a beta-only gas proportional detector calibrated to SrY-90 would result in an underestimate of the surface activity. An explanation for the difference is provided.

The alpha plus beta gas proportional and GM detector's response to processed uranium includes a measurable component due to the alpha radiation. Specifically, the detector is responding to a variety of radiations from the processed uranium—including alpha radiation from the three isotopes of uranium and beta radiations from the progeny of U-238 and U-235—and the total efficiency is only related to the total alpha activity of the uranium. Therefore, the total efficiency based on the alpha activity of processed uranium is similar to the efficiency of these detectors (alpha plus beta gas proportional and GM) calibrated to SrY-90. In the case of the beta-only gas proportional detector, the response to alpha radiation has been nearly eliminated through the use of the 3.8-mg/cm² window, and the resulting detector response to the beta component of processed uranium is much less than that of SrY-90 (a subsequent example will illustrate the components of the detector response to uranium). However, consistent with the scope of this document, the total efficiency for processed uranium should be considered under field conditions. That is, while there is agreement between the total efficiencies for SrY-90 and the processed uranium under ideal laboratory conditions, field conditions may affect the detector's response to these materials to varying degrees.

To evaluate the potential effect of overlaying material in the field, thin sheets of Mylar were placed over the processed uranium deposited on stainless steel. Five 1-minute measurements were performed for each Mylar thickness and detector combination. The total efficiencies were calculated by dividing the net count rate by the activity dispensed on the particular surface, and the results were normalized to the total efficiency obtained with no Mylar. Results are presented in Table 5.30. As expected, the total efficiency for the alpha detectors exhibited a significant reduction for the range of Mylar thicknesses evaluated (0.22 to 3.30 mg/cm²). Conversely, the detectors that respond primarily to beta radiation experienced only a modest reduction in total efficiency. Because a large fraction of the detector's response to processed uranium is due to the high-energy Pa-234m beta radiation, the addition of absorber sheets serves to primarily attenuate the lower energy beta radiation and alpha radiation associated with uranium. For comparison, the attenuation effects of overlaying material over this thickness range for SrY-90, discussed in Section 5.4 and illustrated in the corresponding tables, shows a normalized total efficiency of approximately 0.90 for 3.30 mg/cm² of Mylar (compared to 0.76 and 0.80 for the alpha plus beta and GM detectors, respectively, for processed uranium). Therefore, depending on the expected field conditions, the use of a SrY-90 calibration source for processed uranium may slightly underestimate the surface activity using alpha plus beta gas proportional and GM detectors. It is expected that only a minor correction (reduction in SrY-90 determined efficiency) would be necessary for field conditions because most of the response is from the high-energy beta.

As discussed previously, using the beta-only gas proportional detector calibrated to SrY-90 would result in an underestimate of the processed uranium surface activity, because of the comparison of total efficiencies (i.e., 0.38 c/dis for SrY-90 versus 0.24 c/dis for processed uranium). However, as Table 5.30 indicates, the total efficiency for the beta-only gas proportional detector is largely insensitive to the range of absorber thicknesses used to assess detector response under field conditions. Therefore, it may be desirable to use this detector for the assessment of processed uranium contamination using a detector calibrated to an appropriate beta energy (to yield about

VARIABLES AFFECTING MDCs IN THE FIELD

24% total efficiency). Table 4.2 indicates that an appropriate beta energy may be Tl-204, or a radionuclide with a slightly less average beta energy.

The total efficiencies for the 3% enriched uranium were less than those for processed uranium, because of the increased alpha activity fraction from U-234 (Table 5.29). The determination of an appropriate beta calibration energy is more difficult than for processed uranium because of the increase in alpha activity. The most representative calibration source would be one prepared from the radioactive material (e.g., uranium or thorium) that is being measured in the field. Because many detectors used for surface activity assessment can respond to alpha and beta radiations to varying degrees, using a single radionuclide (or even one in equilibrium with another radionuclide, SrY-90) for calibration may not be representative of the complex decay scheme of uranium and thorium decay series. In this situation, it may be more appropriate to determine the total efficiency by considering the detector's response to each of the alpha and beta emissions in the decay series. An example of this approach is discussed for 3% enriched uranium on stainless steel.

In order to evaluate the detector's response to each of the alpha and beta emissions in the decay of low enriched uranium, the decay scheme of the contamination must be completely understood in terms of radiation type, energy, and abundance. Table 5.31 illustrates the total efficiency calculation for 3% low enriched uranium, as measured by a 126-cm² alpha plus beta gas proportional detector. The alpha fractions of U-238, U-235 and U-234 were determined for 3% enriched uranium and the detector's total efficiency (4π) for each radiation emission was determined by experiment and/or empirical relationship. For example, the detector's response to the alpha emissions of U-238, U-235, and U-234 were assessed experimentally with Th-230 and Pu-239 calibration sources, the Th-231 beta energies from the U-235 series were determined using a Tc-99 calibration source. Beta energies that could not be determined via experiment due to the lack of an appropriate beta calibration standard, were calculated empirically. In this regard, the beta efficiency for Ru-106 (Rh-106) was determined to assist with the appropriate efficiency for the Pa-234m. As shown in Table 4.2, the total efficiency for SrY-90 (average beta energy of 563 keV) is about 0.42, while the total efficiency for Ru-106 (average beta from Rh-106 is 1410 keV) on stainless steel is 0.57; therefore, it was possible to determine the total efficiency for Pa-234m (819 keV average beta energy) using these data. The total weighted efficiency for 3% enriched uranium was 0.257—which compares favorably to the measured total efficiency of 0.23.

Using this approach, it is possible to assess the fractional detector response from each radionuclide in the decay series. In this example, about 33% of the gas proportional detector's response is due to the high energy beta of Pa-234m, while nearly 60% is from the alpha activity. Therefore, the 25.7% total efficiency calculated should be considered as the ideal laboratory efficiency, and should be corrected for expected field conditions. For example, each of the individual radionuclide total efficiencies could be corrected for field conditions using the exponential reduction discussed in Section 5.4.

VARIABLES AFFECTING MDCs IN THE FIELD

Alternatively, the same approach illustrated in Table 5.31 could be performed for the beta-only detector—which has the advantage of not being as sensitive to field conditions as are the detectors that respond to alpha radiation. This approach was performed and the resulting total efficiency was 0.096 (Table 5.32). The measured total efficiency (0.09) compared favorably. Most of the response (about 80%) is from the high energy beta of Pa-234m, which is not likely to be attenuated to a significant degree. It should be noted that this calculational technique is detector-dependent—i.e., the specific detector's response to various radiations must be carefully assessed.

Table 5.1 Background Count Rate for Various Materials

Surface Material	Background Count Rate (cpm) ^a					
	Gas Proportional			GM	ZnS	NaI
	α Only	β Only	$\alpha + \beta$			
Ambient ^b	1.00 ± 0.45 ^c	349 ± 12	331.6 ± 6.0	47.6 ± 2.6	1.00 ± 0.32	4702 ± 16
Brick	6.00 ± 0.84	567.2 ± 7.0	573.2 ± 6.4	81.8 ± 2.3	1.80 ± 0.73	5167 ± 23
Ceramic Block	15.0 ± 1.1	792 ± 11	770.2 ± 6.4	107.6 ± 3.8	8.0 ± 1.1	5657 ± 38
Ceramic Tile	12.6 ± 0.24	647 ± 14	648 ± 16	100.8 ± 2.7	7.20 ± 0.66	4649 ± 37
Concrete Block	2.60 ± 0.81	344.0 ± 6.2	325.0 ± 6.0	52.0 ± 2.5	1.80 ± 0.49	4733 ± 27
Drywall	2.60 ± 0.75	325.2 ± 8.0	301.8 ± 7.0	40.4 ± 3.0	2.40 ± 0.24	4436 ± 38
Floor Tile	4.00 ± 0.71	308.4 ± 6.2	296.6 ± 6.4	43.2 ± 3.6	2.20 ± 0.58	4710 ± 13
Linoleum	2.60 ± 0.98	346.0 ± 8.3	335.4 ± 7.5	51.2 ± 2.8	1.00 ± 0.45	4751 ± 27
Carbon Steel	2.40 ± 0.68	322.6 ± 8.7	303.4 ± 3.4	47.2 ± 3.3	1.00 ± 0.54	4248 ± 38
Treated Wood	0.80 ± 0.37	319.4 ± 8.7	295.2 ± 7.9	37.6 ± 1.7	1.20 ± 0.20	4714 ± 40
Untreated Wood	1.20 ± 0.37	338.6 ± 9.4	279.0 ± 5.7	44.6 ± 2.9	1.40 ± 0.51	4623 ± 34

^aBackground count rates determined from the mean of five 1-minute counts.

^bAmbient background determined at the same location as for all measurements, but without the surface material present.

^cUncertainties represent the standard error in the mean count rate, based only on counting statistics.

Table 5.2 Minimum Detectable Concentrations for Various Materials

Surface Material	Minimum Detectable Concentration (dpm/100 cpm ²) ^a	
	Gas Proportional	
	α Only	β Only
Ambient	30	285
Brick	57	361
Ceramic Block	83	425
Ceramic Tile	78	385
Concrete Block	41	283
Drywall	41	275
Floor Tile	49	268
Linoleum	41	284
Steel	40	275
Treated Wood	28	273
Untreated Wood	32	281

^aMDCs were calculated based on the background count rates presented in Table 5.1 for the gas proportional detector. The alpha only and beta only efficiencies were assumed to be 0.20 and 0.25 count per disintegration, respectively. Probe area corrections of 126 cm² were made for the gas proportional detectors. The following MDC equation was used for 1-minute counts:

$$MDC = \frac{3 + 4.65\sqrt{C_B}}{KT}$$

VARIABLES AFFECTING MDCs IN THE FIELD

Table 5.3 Efficiencies and Backscatter Factors for SrY-90

Surface Material	Gas Proportional Detector With 0.4-mg/cm ² Window		Gas Proportional Detector With 3.8-mg/cm Window	
	Total Efficiency ^a (c/dis)	Backscatter Factor ^b	Total Efficiency (c/dis)	Backscatter Factor
Air	0.28	1.00	0.25	1.00
Wood	0.34	1.20	0.29	1.14
Stainless Steel	0.40	1.43	0.35	1.37
Drywall	0.35	1.24	0.28	1.11
Carbon Steel	0.40	1.42	0.33	1.32
Floor Tile	0.35	1.25	0.31	1.23
Sealed Concrete	0.37	1.30	0.31	1.22
Concrete Block	0.35	1.25	0.31	1.22

^aTotal efficiency was determined by dividing the instrument net counts by the deposited SrY-90 activity.

^bThe backscatter factor was calculated by dividing the particular surface material efficiency by the efficiency in the air.

Table 5.4 Surface Material Effects on Source Efficiency for Tc-99 Distributed on Various Surfaces

Surface Material	Source Efficiency ^{a,b}		
	Gas Proportional		GM
	β Only	$\alpha + \beta$	
Point Source^c			
Sealed Concrete ^d	0.703 ± 0.079^e	0.694 ± 0.063	0.630 ± 0.076
Stainless Steel	0.755 ± 0.096	0.761 ± 0.076	0.773 ± 0.091
Untreated Wood	0.53 ± 0.11	0.504 ± 0.053	0.512 ± 0.061
Distributed Source^f			
Sealed Concrete	0.299 ± 0.096	0.20 ± 0.12	0.19 ± 0.18
Stainless Steel	0.81 ± 0.13	0.73 ± 0.11	--- ^g
Treated Wood	0.66 ± 0.11	0.551 ± 0.088	0.61 ± 0.52

^aSource efficiency determined by dividing the total efficiency by the instrument efficiency.

^bThe instrument efficiencies for the point source geometry were 0.25, 0.45, and 0.28, respectively, for the β only, $\alpha + \beta$, and GM detectors. Instrument efficiencies for the distributed source geometry were 0.20, 0.38, and 0.20, respectively, for the β only, $\alpha + \beta$, and GM detectors.

^cThe Tc-99 activity (2828 ± 91 dpm) was dispensed over an area less than 5 cm^2 .

^dFor sealed concrete, the Tc-99 activity ($5,660 \pm 110$ dpm) was dispensed over an area of approximately 4 cm^2 .

^eUncertainties represent the 95% confidence interval, based on propagating the errors in pipetting, volumetric measurements, calibration source activity, and in counting statistics.

^fThe Tc-99 activity (2830 ± 100 dpm) was evenly distributed over an area of 126 cm^2 .

^gMeasurement not performed.

VARIABLES AFFECTING MDCs IN THE FIELD

Table 5.5 Surface Material Effects on Source Efficiency for Th-230 Distributed on various Surfaces

Surface Material	Source Efficiency ^{a,b}	
	Gas Proportional (α only)	ZnS
Point Source^c		
Scabbled Concrete	0.276 ± 0.013^d	0.288 ± 0.026
Stainless Steel	0.499 ± 0.028	0.555 ± 0.043
Untreated Wood	0.194 ± 0.023	0.185 ± 0.025
Distributed Source^e		
Sealed Concrete	0.473 ± 0.053	0.428 ± 0.054
Carbon Steel	0.250 ± 0.042	0.216 ± 0.031
Treated Wood	0.527 ± 0.057	0.539 ± 0.065

^aSource efficiency determined by dividing the total efficiency by the instrument efficiency.

^bThe instrument efficiencies for the point source geometry were 0.50 and 0.33, respectively, for the α -only and ZnS detectors. Instrument efficiencies for the distributed source geometry were 0.40 and 0.31, respectively, for the α -only and ZnS detectors.

^cThe Th-230 activity ($4,595 \pm 79$ dpm) was dispensed over an area less than 10 cm^2 .

^dUncertainties represent the 95% confidence interval, based on propagating the errors in pipetting, volumetric measurements, calibration source activity, and in counting statistics.

^eThe Th-230 activity ($4,600 \pm 170$ dpm) was evenly distributed over an area of 126 cm^2 .

Table 5.6 Surface Material Effects on MDC for Tc-99 and Th-230 Distributed on Various Surfaces

Surface Material	Minimum Detectable Concentration ^a (dpm/100 cm ²)				
	Tc-99			Th-230	
	$\alpha + \beta$	β only	GM	α only	ZnS
Point Source^b					
Sealed Concrete	242 ± 13 ^c	396 ± 46	1,090 ± 180	---	---
Scabbled Concrete	---	---	---	88 ± 16	131 ± 89
Stainless Steel	192 ± 19	359 ± 47	850 ± 130	32 ± 13	68 ± 28
Untreated Wood	285 ± 31	520 ± 110	1,200 ± 150	67 ± 30	190 ± 100
Distributed Source^d					
Sealed Concrete	950 ± 560	1,220 ± 380	5,100 ± 4,800	37 ± 23	84 ± 40
Stainless Steel	260 ± 34	446 ± 64	---	---	---
Treated Wood	312 ± 44	523 ± 79	1,500 ± 1300	27.1 ± 7.7	64.8 ± 9.8
Carbon Steel	---	---	---	81 ± 21	153 ± 54

^aThe minimum detectable concentration was calculated using 1-minute counts and total efficiencies determined on the basis of the known amount of activity deposited.

^bThe point (disc) source area for Tc-99 and Th-230 were approximately 5 and 10 cm², respectively.

^cUncertainties represent the 95% confidence interval, based on propagating the errors in pipetting, volumetric measurements, calibration source activity, and in counting statistics.

^dThe distributed source area for both Tc-99 and Th-230 was 126 cm².

**Table 5.7 Effects of Oil Density Thickness on Source Efficiency and MDC
(Gas Proportional— $\alpha + \beta$)**

Surface Material	Density Thickness (mg/cm ²)	C-14 (0.254) ^a		Tc-99 (0.364)		SrY-90 (0.536)	
		Source Efficiency ^b	MDC ^c (dpm/100 cm ²)	Source Efficiency	MDC (dpm/100 cm ²)	Source Efficiency	MDC (dpm/100 cm ²)
Detector Face ^d	0.4	NA	605	NA	304	NA	164
Detector Face ^e Plus 2 Sheets Mylar	0.8	0.386	703	0.596	317	0.772	167
Plus 1.5 mg/cm ² Oil ^f	2.3	0.236	1,148	0.467	406	0.744	173
Plus 2.9 mg/cm ² Oil	3.7	0.193	1,406	0.401	472	0.700	184
Plus 4.5 mg/cm ² Oil	5.3	0.102	2,651	0.349	543	0.677	190

^aInstrument efficiency provided in parentheses.

^bSource efficiency was determined by dividing the total efficiency by the instrument efficiency.

^cProbe area corrections of 126 cm² were made for the gas proportional detectors. The following MDC equation was used for 1-minute counts and a background of 326 cpm:

$$MDC = \frac{3 + 4.65 \sqrt{C_B}}{KT}$$

^dMeasurements performed with a Ludlum 43-68 gas proportional detector with a standard 0.4 mg/cm² window.

^eEach sheet of Mylar has a density thickness of 0.22 mg/cm².

^f20W-50 motor oil used for study.

**Table 5.8 Effects of Paint Density Thickness on Source Efficiency and MDC
(Gas Proportional— $\alpha + \beta$)**

Surface Material	Density Thickness (mg/cm ²)	C-14 (0.254 ± 0.006) ^a			Tc-99 (0.364 ± 0.029)			Tl-204 (0.450 ± 0.025)			SrY-90 (0.537 ± 0.027)		
		Source Efficiency		MDC ^d (dpm/100 cm ²)	Source Efficiency		MDC (dpm/100 cm ²)	Source Efficiency		MDC (dpm/100 cm ²)	Source Efficiency		MDC (dpm/100 cm ²)
		Meas. ^b	Fit ^c		Meas.	Fit		Meas.	Fit		Meas.	Fit	
Detector Face ^c	0.4	NA	NA	510	NA	NA	278	NA	NA	202	NA	NA	177
Detector Face ^f Plus 2 Sheets Mylar	0.84	0.437	0.426 ± 0.065	600	0.626	0.572 ± 0.100	291	0.716	0.675 ± 0.079	206	0.697	0.643 ± 0.103	178
Plus 1.93 mg/cm ² Paint ^g	2.77	0.252	0.243 ± 0.030	1,037	0.427	0.463 ± 0.066	427	0.596	0.622 ± 0.060	247	0.584	0.615 ± 0.080	212
Plus 2.48 mg/cm ² Paint	3.32	0.215	0.207 ± 0.024	1,215	---	---	---	---	---	---	---	---	---
Plus 5.54 mg/cm ² Paint	6.38	0.074	0.085 ± 0.008	3,542	0.300	0.311 ± 0.034	608	0.515	0.535 ± 0.039	286	0.530	0.565 ± 0.056	233
Plus 9.48 mg/cm ² Paint	10.32	0.026	0.027 ± 0.004	9,955	0.201	0.202 ± 0.027	907	0.449	0.454 ± 0.042	329	0.513	0.515 ± 0.064	241
Plus 12.63 mg/cm ² Paint	13.47	0.012	0.011 ± 0.002	22,593	0.147	0.143 ± 0.027	1,238	0.410	0.398 ± 0.051	360	0.498	0.479 ± 0.083	249
Regression Equation		$\epsilon_s = 0.544 e^{-0.291 x}$			$\epsilon_s = 0.628 e^{-0.110 x}$			$\epsilon_s = 0.699 e^{-0.042 x}$			$\epsilon_s = 0.656 e^{-0.023 x}$		

^aInstrument efficiency provided in parentheses; uncertainties represent the 95% confidence interval.

^bSource efficiency was determined by dividing the total efficiency by the instrument efficiency.

^cThe measured source efficiency versus density thickness was fit to an exponential curve; uncertainties represent the 95% confidence interval.

^dProbe area corrections of 126 cm² were made for the gas proportional detectors. The following MDC equation was used for 1-minute counts and a background of 301 cpm:

$$MDC = \frac{3 + 4.65\sqrt{C_B}}{KT}$$

^eMeasurements performed with a Ludlum 43-68 gas proportional detector with a standard 0.4 mg/cm² window.

^fEach sheet of Mylar has a density thickness of 0.22 mg/cm².

^gOrange fluorescent water base paint.

^hMeasurement not performed.

VARIABLES AFFECTING MDCs IN THE FIELD

**Table 5.9 Effects of Paint Density Thickness on Source Efficiency and MDC
(Gas Proportional— α -Only)**

Surface Material	Density Thickness (mg/cm ²)	Th-230 (0.349 ± 0.015) ^a		
		Source Efficiency		MDC ^d (dpm/100 cm ²)
		Meas. ^b	Fit ^c	
Detector Face ^e	0.4	NA	NA	30
Detector Face ^f plus 2 Sheets of Mylar	0.84	0.509	0.513 ± 0.085	34
Plus 1.93 mg/cm ² Paint ^g	2.77	0.129	0.123 ± 0.013	135
Plus 2.48 mg/cm ² Paint	3.32	0.078	0.082 ± 0.009	223
Plus 5.54 mg/cm ² Paint	6.38	0.008	0.008 ± 0.002	2,060
Plus 9.48 mg/cm ² Paint	10.32 ^h	0.001	NA	17,369
Regression Equation		$\epsilon_s = 0.956 e^{-0.741 x}$		

^aInstrument efficiency provided in parentheses; uncertainties represent the 95% confidence interval.

^bSource efficiency was determined by dividing the total efficiency by the instrument efficiency.

^cThe measured source efficiency versus density thickness was fit to an exponential curve; uncertainties represent the 95% confidence interval.

^dProbe area corrections of 126 cm² were made for the gas proportional detectors. The following MDC equation was used for 1-minute counts and a background of 1 cpm:

$$MDC = \frac{3 + 4.65\sqrt{C_B}}{KT}$$

^eMeasurements performed with a Ludlum 43-68 gas proportional detector with a standard 0.4-mg/cm² window.

^fEach sheet of Mylar has a density thickness of 0.22 mg/cm².

^gOrange fluorescent water base paint.

^hData point not used in regression fit due to limited alpha range.

**Table 5.10 Effects of Paint Density Thickness on Source Efficiency and MDC
(Gas Proportional—β-Only)**

VARIABLES AFFECTING MDCs IN THE FIELD

Surface Material	Density Thickness (mg/cm ²)	C-14 (0.081 ± 0.002) ^a			Tc-99 (0.191 ± 0.016)			Tl-204 (0.355 ± 0.021)			SrY-90 (0.465 ± 0.024)		
		Source Efficiency		MDC ^d (dpm/100 cm ²)	Source Efficiency		MDC (dpm/100 cm ²)	Source Efficiency		MDC (dpm/100 cm ²)	Source Efficiency		MDC (dpm/100 cm ²)
		Meas. ^b	Fit ^c		Meas.	Fit		Meas.	Fit		Meas.	Fit	
Detector Face ^e	3.8	NA	NA	1,823	NA	NA	577	N/A	NA	280	NA	NA	222
Detector Face ^f Plus 2 Sheets Mylar	4.24	0.435	0.445 ± 0.055	2,039	0.628	0.625 ± 0.008	599	0.715	0.707 ± 0.040	283	0.696	0.691 ± 0.021	222
Plus 1.93 mg/cm ² Paint ^g	6.17	0.269	0.255 ± 0.026	3,296	0.521	0.522 ± 0.005	722	0.657	0.663 ± 0.030	308	0.669	0.669 ± 0.017	231
Plus 2.48 mg/cm ² Paint	6.72	0.228	0.217 ± 0.021	3,882	---	---	---	---	---	---	---	---	---
Plus 5.54 mg/cm ² Paint	9.78	0.081	0.090 ± 0.007	10,893	0.370	0.373 ± 0.003	1,105	0.592	0.588 ± 0.021	342	0.627	0.631 ± 0.012	246
Plus 9.48 mg/cm ² Paint	13.72	0.028	0.029 ± 0.003	31,920	0.259	0.258 ± 0.002	1,450	0.499	0.516 ± 0.023	405	0.583	0.592 ± 0.014	265
Plus 12.63 mg/cm ² Paint	16.87	0.012	0.012 ± 0.002	72,542	0.192	0.192 ± 0.003	1,958	0.475	0.465 ± 0.028	426	0.570	0.562 ± 0.019	271
Regression Equation		$\epsilon_s = 1.51 e^{-0.289 x}$			$\epsilon_s = 0.929 e^{-0.093 x}$			$\epsilon_s = 0.813 e^{-0.033 x}$			$\epsilon_s = 0.740 e^{-0.016 x}$		

^aInstrument efficiency provided in parentheses; uncertainties represent the 95% confidence interval.

^bSource efficiency was determined by dividing the total efficiency by the instrument efficiency.

^cThe measured source efficiency versus density thickness was fit to an exponential curve; uncertainties represent the 95% confidence interval.

^dProbe area corrections of 126 cm² were made for the gas proportional detectors. The following MDC equation was used for 1-minute counts and a background of 354 cpm:

$$MDC = \frac{3 + 4.65\sqrt{C_B}}{KT}$$

^eMeasurements performed with a Ludlum 43-68 gas proportional detector with a standard alpha-blocking 3.8-mg/cm² window.

^fEach sheet of Mylar has a density thickness of 0.22 mg/cm².

^gOrange fluorescent water base paint.

^hMeasurement not performed.

Table 5.11 Effects of Paint Density Thickness on Source Efficiency and MDC (GM Detector)

Surface Material	Density Thickness (mg/cm ²)	C-14 (0.099 ± 0.002) ^a			Tc-99 (0.193 ± 0.021)			Tl-204 (0.278 ± 0.017)			SrY-90 (0.388 ± 0.020)		
		Source Efficiency		MDC ^d (dpm/100 cm ²)	Source Efficiency		MDC (dpm/100 cm ²)	Source Efficiency		MDC (dpm/100 cm ²)	Source Efficiency		MDC (dpm/100 cm ²)
		Meas. ^b	Fit ^c		Meas.	Fit		Meas.	Fit		Meas.	Fit	
Detector Face ^o	— ^f	NA	NA	3,757	NA	NA	1,454	NA	NA	888	NA	NA	648
Detector Face ^e Plus 2 Sheets of Mylar	0.44	0.436	0.465 ± 0.050	4,098	0.627	0.646 ± 0.061	1,468	0.716	0.712 ± 0.028	894	0.697	0.681 ± 0.056	657
Plus 1.93 mg/cm ² Paint ^h	2.37	0.284	0.266 ± 0.023	6,294	0.527	0.530 ± 0.041	1,748	0.671	0.670 ± 0.021	952	0.666	0.660 ± 0.044	688
Plus 2.48 mg/cm ² Paint	2.92	0.239	0.227 ± 0.019	7,485	— ⁱ	—	—	—	—	—	—	—	—
Plus 5.54 mg/cm ² Paint	5.98	0.089	0.094 ± 0.007	20,012	0.388	0.366 ± 0.022	2,373	0.599	0.599 ± 0.015	1,068	0.594	0.622 ± 0.032	771
Plus 9.48 mg/cm ² Paint	9.92	0.029	0.030 ± 0.003	61,664	0.245	0.244 ± 0.018	3,767	0.517	0.529 ± 0.016	1,238	0.575	0.584 ± 0.038	797
Plus 12.63 mg/cm ² Paint	13.07	0.012	0.012 ± 0.002	145,037	0.172	0.177 ± 0.018	5,362	0.487	0.479 ± 0.020	1,312	0.571	0.554 ± 0.050	802
Regression Equation		$\epsilon_s = 0.528 e^{-0.289 x}$			$\epsilon_s = 0.676 e^{-0.103 x}$			$\epsilon_s = 0.722 e^{-0.031 x}$			$\epsilon_s = 0.686 e^{-0.016 x}$		

^aInstrument efficiency provided in parentheses; uncertainties represent the 95% confidence interval.

^bSource efficiency was determined by dividing the total efficiency by the instrument efficiency.

^cThe measured source efficiency versus density thickness was fit to an exponential curve; uncertainties represent the 95% confidence interval.

^dThe following MDC equation was used for 1-minute counts, with a background of 49 cpm and a probe area of 20 cm²:

$$MDC = \frac{3 + 4.65\sqrt{C_B}}{KT}$$

^eMeasurements performed with an Eberline HP-260 GM detector with a standard mica window, typical thickness 1.4 to 2.0 mg/cm².

^fDetector face is fixed part of detector and is not removable.

^gEach sheet of Mylar has a density thickness of 0.22 mg/cm².

^hOrange fluorescent water base paint.

ⁱMeasurement not performed.

Table 5.12 Effects of Paint Density Thickness on Source Efficiency and MDC (ZnS Scintillation Detector)

Surface Material	Density Thickness (mg/cm ²)	Th-230 (0.259 ± 0.013) ^a		
		Source Efficiency		MDC ^d (dpm/100 cm ²)
		Meas. ^b	Fit ^c	
Detector Face ^e	--- ^f	NA	NA	65
Detector Face ^g Plus 2 Sheets of Mylar	0.44	0.509	0.523 ± 0.125	294
Plus 1.93 mg/cm ² Paint ^h	2.37	0.099	0.091 ± 0.014	404
Plus 2.48 mg/cm ² Paint	2.92	0.053	0.055 ± 0.008	756
Plus 5.54 mg/cm ² Paint	5.98	0.003	0.004 ± 0.001	11,619
Plus 9.48 mg/cm ² Paint	9.92 ⁱ	0.001	NA	67,400
Regression Equation		$\epsilon_s = 0.779 e^{-0.906 x}$		

^aInstrument efficiency provided in parentheses; uncertainties represent the 95% confidence interval.

^bSource efficiency was determined by dividing the total efficiency by the instrument efficiency.

^cThe measured source efficiency versus density thickness was fit to an exponential curve; uncertainties represent the 95% confidence interval.

^dThe following MDC equation was used for 1-minute counts, with a background of 1 cpm and a probe area of 74 cm²:

$$MDC = \frac{3 + 4.65\sqrt{C_B}}{KT}$$

^eMeasurements performed with an Eberline AC3-7 ZnS scintillation detector with a standard 1.5-mg/cm² window.

^fDetector face is fixed part of detector and is not removable.

^gEach sheet of Mylar has a density thickness of 0.22 mg/cm².

^hOrange fluorescent water base paint.

ⁱData point not used in regression fit due to limited alpha range.

**Table 5.13 Effects of Dust Density Thickness on Source Efficiency and MDC
(Gas Proportional— $\alpha + \beta$)**

Surface Material	Density Thickness (mg/cm ²)	C-14 (0.254 ± 0.006) ^a			Tc-99 (0.364 ± 0.029)			Tl-204 (0.450 ± 0.025)			SrY-90 (0.537 ± 0.027)		
		Source Efficiency		MDC ^d (dpm/100 cm ²)	Source Efficiency		MDC (dpm/100 cm ²)	Source Efficiency		MDC (dpm/100 cm ²)	Source Efficiency		MDC (dpm/100 cm ²)
		Meas. ^b	Fit ^c		Meas.	Fit		Meas.	Fit		Meas.	Fit	
		Meas. ^b	Fit ^c	MDC ^d (dpm/100 cm ²)	Meas.	Fit	MDC (dpm/100 cm ²)	Meas.	Fit	MDC (dpm/100 cm ²)	Meas.	Fit	MDC (dpm/100 cm ²)
Detector Face ^c	0.4	NA	NA	510	NA	NA	278	NA	NA	202	NA	NA	177
Detector Face ^f plus 2 Sheets of Mylar	0.84	0.437	0.432 ± 0.148	599	0.626	0.592 ± 0.086	292	0.716	0.706 ± 0.037	206	0.697	0.691 ± 0.031	178
Plus 2.28 mg/cm ² Dust ^g	3.12	0.218	0.265 ± 0.064	1,201	0.425	0.465 ± 0.045	430	0.620	0.636 ± 0.024	238	0.642	0.649 ± 0.021	193
Plus 4.11 mg/cm ² Dust	4.95	0.205	0.179 ± 0.035	1,276	0.407	0.383 ± 0.032	449	0.595	0.585 ± 0.018	248	0.616	0.617 ± 0.016	201
Plus 6.10 mg/cm ² Dust	6.94	0.142	0.116 ± 0.023	1,847	0.297	0.310 ± 0.026	614	0.536	0.534 ± 0.016	275	0.594	0.583 ± 0.015	208
Plus 7.99 mg/cm ² Dust	8.83	0.071	0.078 ± 0.019	3,675	0.245	0.253 ± 0.027	745	0.474	0.490 ± 0.019	311	0.536	0.553 ± 0.018	231
Plus 9.99 mg/cm ² Dust	10.83	0.047	0.050 ± 0.017	5,534	0.215	0.205 ± 0.029	848	0.456	0.447 ± 0.023	323	0.532	0.523 ± 0.023	233
Regression Equation	$\epsilon_s = 0.518 e^{-0.215 x}$			$\epsilon_s = 0.647 e^{-0.106 x}$			$\epsilon_s = 0.733 e^{-0.046 x}$			$\epsilon_s = 0.708 e^{-0.028 x}$			

^aInstrument efficiency provided in parentheses; uncertainties represent the 95% confidence interval.

^bSource efficiency was determined by dividing the total efficiency by the instrument efficiency.

^cThe measured source efficiency versus density thickness was fit to an exponential curve; uncertainties represent the 95% confidence interval.

^dProbe area corrections of 126 cm² were made for the gas proportional detectors. The following MDC equation was used for 1-minute counts and a background of 301 cpm:

$$MDC = \frac{3 + 4.65\sqrt{C_B}}{KT}$$

^eMeasurements performed with a Ludlum 43-68 gas proportional detector with a standard 0.4-mg/cm² window.

^fEach sheet of Mylar has a density thickness of 0.22 mg/cm².

^gDust obtained by grinding potting soil and sieving through 250 mesh screen.

**Table 5.14 Effects of Dust Density Thickness on Source Efficiency and MDC
(Gas Proportional— α Only)**

Surface Material	Density Thickness (mg/cm ²)	Th-230 (0.349 ± 0.015) ^a		
		Source Efficiency		MDC ^d (dpm/100 cm ²)
		Meas. ^b	Fit ^c	
Detector Face ^e	0.4	NA	NA	30
Detector Face ^f Plus 2 Sheets of Mylar	0.84	0.509	0.428 ± 0.215	34
Plus 2.28 mg/cm ² Dust ^g	3.12	0.145	0.201 ± 0.071	120
Plus 4.11 mg/cm ² Dust	4.95	0.134	0.110 ± 0.031	130
Plus 6.10 mg/cm ² Dust	6.94	0.056	0.057 ± 0.016	310
Plus 7.99 mg/cm ² Dust	8.83	0.026	0.030 ± 0.011	674
Plus 9.99 mg/cm ² Dust	10.83	0.018	0.016 ± 0.008	974
Regression Equation		$\epsilon_s = 0.565 e^{-0.331 x}$		

^aInstrument efficiency provided in parentheses; uncertainties represent the 95% confidence interval.

^bSource efficiency was determined by dividing the total efficiency by the instrument efficiency.

^cThe measured source efficiency versus density thickness was fit to an exponential curve; uncertainties represent the 95% confidence interval.

^dProbe area corrections of 126 cm² were made for the gas proportional detectors. The following MDC equation was used for 1-minute counts and a background of 1 cpm:

$$MDC = \frac{3 + 4.65\sqrt{C_B}}{KT}$$

^eMeasurements performed with a Ludlum 43-68 gas proportional detector with a standard 0.4-mg/cm² window.

^fEach sheet of Mylar has a density thickness of 0.22 mg/cm².

^gDust obtained by grinding potting soil and sieving through 250 mesh screen.

**Table 5.15 Effects of Dust Density Thickness on Source Efficiency and MDC
(Gas Proportional—β Only)**

Surface Material	Density Thickness (mg/cm ²)	C-14 (0.081 ± 0.002) ^a			Tc-99 (0.191 ± 0.016)			Tl-204 (0.355 ± 0.021)			SrY-90 (0.465 ± 0.024)		
		Source Efficiency		MDC ^d (dpm/100 cm ²)	Source Efficiency		MDC (dpm/100 cm ²)	Source Efficiency		MDC (dpm/100 cm ²)	Source Efficiency		MDC (dpm/100 cm ²)
		Meas ^b	Fit ^c		Meas.	Fit		Meas.	Fit		Meas.	Fit	
Detector Face ^e	3.8	NA	NA	1,823	NA	NA	577	NA	NA	280	NA	NA	222
Detector Face ^f Plus 2 Sheets of Mylar	4.24	0.435	0.448 ± 0.136	2,039	0.628	0.632 ± 0.061	599	0.715	0.715 ± 0.031	283	0.696	0.696 ± 0.028	222
Plus 2.28 mg/cm ² Dust ^g	6.52	0.242	0.278 ± 0.060	3,659	0.501	0.519 ± 0.036	751	0.648	0.660 ± 0.020	312	0.649	0.665 ± 0.019	238
Plus 4.11 mg/cm ² Dust	8.35	0.218	0.189 ± 0.033	4,074	0.479	0.443 ± 0.025	785	0.626	0.619 ± 0.015	323	0.655	0.641 ± 0.015	236
Plus 6.10 mg/cm ² Dust	10.34	0.149	0.124 ± 0.022	5,957	0.371	0.373 ± 0.021	1,013	0.594	0.577 ± 0.014	340	0.627	0.617 ± 0.014	246
Plus 7.99 mg/cm ² Dust	12.23	0.076	0.083 ± 0.018	11,680	0.305	0.317 ± 0.022	1,233	0.529	0.540 ± 0.017	382	0.593	0.594 ± 0.017	260
Plus 9.99 mg/cm ² Dust	14.23	0.051	0.055 ± 0.016	17,243	0.270	0.267 ± 0.025	1,395	0.502	0.504 ± 0.021	403	0.564	0.571 ± 0.022	274
Regression Equation		$\epsilon_s = 1.10 e^{-0.211 x}$			$\epsilon_s = 0.912 e^{-0.086 x}$			$\epsilon_s = 0.830 e^{-0.035 x}$			$\epsilon_s = 0.757 e^{-0.020 x}$		

^aInstrument efficiency provided in parentheses; uncertainties represent the 95% confidence interval.

^bSource efficiency was determined by dividing the total efficiency by the instrument efficiency.

^cThe measured source efficiency versus density thickness was fit to an exponential curve; uncertainties represent the 95% confidence interval.

^dProbe area corrections of 126 cm² were made for the gas proportional detectors. The following MDC equation was used for 1-minute counts and a background of 354 cpm:

$$MDC = \frac{3 + 4.65\sqrt{C_B}}{KT}$$

^eMeasurements performed with a Ludlum 43-68 gas proportional with a standard alpha-blocking 3.8-mg/cm² window.

^fEach sheet of Mylar has a density thickness of 0.22 mg/cm².

^gDust obtained by grinding potting soil and sieving through 250 mesh screen.

Table 5.16 Effects of Dust Density Thickness on Source Efficiency and MDC (GM Detector)

Surface Material	Density Thickness (mg/cm ²)	C-14 (0.099 ± 0.002) ^a			Tc-99 (0.193 ± 0.021)			Tl-204 (0.278 ± 0.017)			SrY-90 (0.388 ± 0.020)		
		Measured Source Efficiency		MDC ^d (dpm/100 cm ²)	Source Efficiency		MDC (dpm/100 cm ²)	Source Efficiency		MDC (dpm/100 cm ²)	Source Efficiency		MDC (dpm/100 cm ²)
		Meas. ^b	Fit ^c		Meas.	Fit		Meas.	Fit		Meas.	Fit	
Detector Face ^e	... ^h	NA	NA	3,758	NA	NA	1,454	NA	NA	888	NA	NA	648
Detector Face ^f Plus 2 Sheets of Mylar	0.44	0.436	0.474 ± 0.176	4,098	0.627	0.642 ± 0.087	1,469	0.716	0.715 ± 0.015	894	0.697	0.706 ± 0.031	657
Plus 2.28 mg/cm ² Dust ^h	2.72	0.257	0.291 ± 0.077	6,941	0.490	0.520 ± 0.050	1,877	0.658	0.661 ± 0.010	973	0.668	0.670 ± 0.021	686
Plus 4.11 mg/cm ² Dust	4.55	0.234	0.196 ± 0.041	7,644	0.473	0.439 ± 0.034	1,949	0.617	0.621 ± 0.007	1,036	0.645	0.642 ± 0.016	710
Plus 6.10 mg/cm ² Dust	6.54	0.160	0.128 ± 0.027	11,133	0.392	0.365 ± 0.028	2,345	0.590	0.580 ± 0.007	1,084	0.632	0.613 ± 0.015	725
Plus 7.99 mg/cm ² Dust	8.43	0.080	0.085 ± 0.023	22,344	0.300	0.306 ± 0.030	3,067	0.543	0.543 ± 0.008	1,178	0.591	0.587 ± 0.019	776
Plus 9.99 mg/cm ² Dust	10.43	0.049	0.056 ± 0.020	36,720	0.243	0.255 ± 0.034	3,789	0.504	0.507 ± 0.010	1,270	0.547	0.560 ± 0.024	838
Regression Equation		$\epsilon_s = 0.521 e^{-0.215 x}$			$\epsilon_s = 0.669 e^{-0.093 x}$			$\epsilon_s = 0.726 e^{-0.034 x}$			$\epsilon_s = 0.713 e^{-0.023 x}$		

^aInstrument efficiency provided in parentheses; uncertainties represent the 95% confidence interval.

^bSource efficiency was determined by dividing the total efficiency by the instrument efficiency.

^cThe measured source efficiency versus density thickness was fit to an exponential curve; uncertainties represent the 95% confidence interval.

^dThe following equation was used for 1 minute counts, with a background of 49 cpm and a probe area of 20 cm²:

$$MDC = \frac{3 + 4.65\sqrt{C_B}}{KT}$$

^eMeasurements performed with an Eberline HP-260 GM detector with a standard mica window with typical thickness 1.4 to 2.0 mg/cm².

^fDetector face is fixed part of detector and is not removable.

^gEach sheet of Mylar has a density thickness of 0.22 mg/cm².

^hDust obtained by grinding potting soil and sieving through 250 mesh screen.

VARIABLES AFFECTING MDCs IN THE FIELD

Table 5.17 Effects of Dust Density Thickness on Source Efficiency and MDC (ZnS Scintillation Detector)

Surface Material	Density Thickness (mg/cm ²)	Th-230 (0.259 ± 0.013) ^a		
		Source Efficiency		MDC ^d (dpm/100 cm ²)
		Meas. ^b	Fit ^c	
Detector Face ^e	--- ^f	NA	NA	65
Detector Face ^g Plus 2 Sheets of Mylar	0.44	0.509	0.410 ± 0.327	78
Plus 2.28 mg/cm ² Dust ^h	2.72	0.118	0.179 ± 0.092	340
Plus 4.11 mg/cm ² Dust	4.55	0.109	0.092 ± 0.039	367
Plus 6.10 mg/cm ² Dust	6.54	0.045	0.045 ± 0.024	885
Plus 7.99 mg/cm ² Dust	8.43	0.023	0.022 ± 0.017	1,735
Plus 9.99 mg/cm ² Dust	10.43	0.017 ⁱ	NA	2,390
Regression Equation		$\epsilon_s = 0.481 e^{-0.364 x}$		

^aInstrument efficiency provided in parentheses; uncertainties represent the 95% confidence interval.

^bSource efficiency was determined by dividing the total efficiency by the instrument efficiency.

^cThe measured source efficiency versus density thickness was fit to an exponential curve; uncertainties represent the 95% confidence interval.

^dThe following MDC equation was used for 1-minute counts, with a background of 1 cpm and a probe area of 74 cm²:

$$MDC = \frac{3 + 4.65\sqrt{C_B}}{KT}$$

^eMeasurements performed with an Eberline AC3-7 ZnS scintillation detector with a standard 1.5-mg/cm² window.

^fDetector face is fixed part of detector and is not removable.

^gEach sheet of Mylar has a density thickness of 0.22 mg/cm².

^hDust obtained by grinding potting soil and sieving through 250 mesh screen.

ⁱData point not used in regression fit due to limited alpha range.

**Table 5.18 Effects of Water Density Thickness on Source Efficiency and MDC
(Gas Proportional— $\alpha+\beta/C-14$)**

Surface Material	Density Thickness (mg/cm ²)	C-14 (0.139 ± 0.003) ^a		
		Source Efficiency		MDC ^d (dpm/100 cm ²)
		Meas. ^b	Fit ^c	
Detector Face ^e	0.4	NA	NA	629
Detector Face Plus 2 Mylar Sheets With 1 Kimwipe ^f	2.70	0.436	0.442 ± 0.042	1,249
Plus 0.44 mg/cm ² Water ^g	3.14	0.362	0.397 ± 0.035	1,502
Plus 0.62 mg/cm ² Water	3.32	0.360	0.380 ± 0.032	1,513
Plus 0.78 mg/cm ² Water	3.48	0.349	0.365 ± 0.030	1,558
Plus 1.23 mg/cm ² Water	3.93	0.333	0.327 ± 0.025	1,637
Plus 2.29 mg/cm ² Water	4.99	0.284	0.252 ± 0.017	1,920
Plus 3.04 mg/cm ² Water	5.74	0.237	0.210 ± 0.014	2,297
Plus 5.14 mg/cm ² Water	7.84	0.138	0.125 ± 0.011	3,940
Plus 6.49 mg/cm ² Water	9.19	0.083	0.090 ± 0.010	6,533
Plus 7.62 mg/cm ² Water	10.32	0.063	0.068 ± 0.009	8,599
Regression Equation	$\epsilon_s = 0.858 e^{-0.245 x}$			

^aInstrument efficiency provided in parentheses; uncertainties represent the 95% confidence interval.

^bSource efficiency was determined by dividing the total efficiency by the instrument efficiency.

^cThe measured source efficiency versus density thickness was fit to an exponential curve; uncertainties represent the 95% confidence interval.

^dProbe area corrections of 126 cm² were made for the gas proportional detectors. The following MDC equation was used for 1-minute counts and a background of 396 cpm:

$$MDC = \frac{3 + 4.65\sqrt{C_B}}{KT}$$

^eMeasurements performed with a Ludlum 43-68 gas proportional detector with a standard 0.4 mg/cm² window.

^fEach sheet of Mylar has a density thickness of 0.22 mg/cm² and one Kimwipe has a density thickness of 1.86 mg/cm².

^gReagent water used in analytical procedures from radiochemistry laboratory.

VARIABLES AFFECTING MDCs IN THE FIELD

**Table 5.19 Effects of Water Density Thickness on Source Efficiency and MDC
(Gas Proportional— $\alpha+\beta/\text{Tc-99}$)**

Surface Material	Density Thickness (mg/cm ²)	Tc-99 (0.239 ± 0.020) ^a		
		Source Efficiency		MDC ^d (dpm/100 cm ²)
		Meas. ^b	Fit ^c	
Detector Face ^e	0.4	NA	NA	368
Detector Face Plus 2 Mylar Sheets With 1 Kimwipe ^f	2.70	0.626	0.642 ± 0.020	506
Plus 0.19 mg/cm ² Water ^g	2.89	0.628	0.630 ± 0.019	505
Plus 0.76 mg/cm ² Water	3.46	0.595	0.596 ± 0.016	533
Plus 2.85 mg/cm ² Water	5.55	0.501	0.487 ± 0.010	633
Plus 3.97 mg/cm ² Water	6.67	0.443	0.436 ± 0.009	716
Plus 5.49 mg/cm ² Water	8.19	0.386	0.377 ± 0.009	822
Plus 6.67 mg/cm ² Water	9.37	0.327	0.336 ± 0.010	969
Plus 8.17 mg/cm ² Water	10.87	0.287	0.290 ± 0.011	1,104
Regression Equation		$\epsilon_s = 0.834 e^{-0.097 x}$		

^aInstrument efficiency provided in parentheses; uncertainties represent the 95% confidence interval.

^bSource efficiency was determined by dividing the total efficiency by the instrument efficiency.

^cThe measured source efficiency versus density thickness was fit to an exponential curve; uncertainties represent the 95% confidence interval.

^dProbe area corrections of 126 cm² were made for the gas proportional detectors. The following MDC equation was used for 1-minute counts and a background of 396 cpm:

$$MDC = \frac{3 + 4.65\sqrt{C_B}}{KT}$$

^eMeasurements performed with a Ludlum 43-68 gas proportional detector with a standard 0.4-mg/cm² window.

^fEach sheet of Mylar has a density thickness of 0.22 mg/cm² and one Kimwipe has a density thickness of 1.86 mg/cm².

^gReagent water used in analytical procedures from radiochemistry laboratory.

**Table 5.20 Effects of Water Density Thickness on Source Efficiency and MDC
(Gas Proportional— $\alpha+\beta$ /SrY-90)**

Surface Material	Density Thickness (mg/cm ²)	SrY-90 (0.484 ± 0.025) ^a		
		Source Efficiency		MDC ^d (dpm/100 cm ²)
		Meas. ^b	Fit ^c	
Detector Face ^e	0.4	NA	NA	207
Detector Face Plus 2 Mylar Sheets With 1 Kimwipe ^f	2.70	0.697	0.705 ± 0.018	225
Plus 2.56 mg/cm ² Water ^g	5.26	0.666	0.664 ± 0.010	235
Plus 3.25 mg/cm ² Water	5.95	0.666	0.653 ± 0.009	235
Plus 4.81 mg/cm ² Water	7.51	0.627	0.630 ± 0.009	250
Plus 6.28 mg/cm ² Water	8.98	0.608	0.608 ± 0.011	258
Plus 7.88 mg/cm ² Water	10.58	0.582	0.586 ± 0.014	269
Regression Equation		$\epsilon_s = 0.751 e^{-0.023 x}$		

^aInstrument efficiency provided in parentheses; uncertainties represent the 95% confidence interval.

^bSource efficiency was determined by dividing the total efficiency by the instrument efficiency.

^cThe measured source efficiency versus density thickness was fit to an exponential curve; uncertainties represent the 95% confidence interval.

^dProbe area corrections of 126 cm² were made for the gas proportional detectors. The following MDC equation was used for 1-minute counts and a background of 396 cpm:

$$MDC = \frac{3 + 4.65\sqrt{C_B}}{KT}$$

^eMeasurements performed with a Ludlum 43-68 gas proportional detector with a standard 0.4-mg/cm² window.

^fEach sheet of Mylar has a density thickness of 0.22 mg/cm² and one Kimwipe has a density thickness of 1.86 mg/cm².

^gReagent water used in analytical procedures from radiochemistry laboratory.

VARIABLES AFFECTING MDCs IN THE FIELD

Table 5.21 Effects of Water Density Thickness on Source Efficiency and MDC (Gas Proportional— α -Only)

Surface Material	Density Thickness (mg/cm ²)	Th-230 (0.085 ± 0.005) ^a		
		Source Efficiency		MDC ^d (dpm/100 cm ²)
		Meas. ^b	Fit ^c	
Detector Face ^e	0.4	NA	NA	30
Detector Face Plus 2 Mylar Sheets With 1 Kimwipe ^f	2.70	0.508	0.516 ± 0.071	140
Plus 0.11 mg/cm ² Water ^g	2.81	0.469	0.485 ± 0.065	151
Plus 0.25 mg/cm ² Water	2.95	0.441	0.448 ± 0.058	161
Plus 0.48 mg/cm ² Water	3.18	0.372	0.393 ± 0.048	191
Plus 1.23 mg/cm ² Water	3.93	0.274	0.257 ± 0.027	259
Plus 2.03 mg/cm ² Water	4.73	0.168	0.163 ± 0.016	423
Plus 3.51 mg/cm ² Water	6.21	0.090	0.071 ± 0.009	787
Plus 4.23 mg/cm ² Water	6.93	0.039	0.047 ± 0.007	1,827
Plus 5.88 mg/cm ² Water	8.58	0.018	0.018 ± 0.004	3,983
Regression Equation		$\epsilon_s = 2.39 e^{-0.567 x}$		

^aInstrument efficiency provided in parentheses; uncertainties represent the 95% confidence interval.

^bSource efficiency was determined by dividing the total efficiency by the instrument efficiency.

^cThe measured source efficiency versus density thickness was fit to an exponential curve; uncertainties represent the 95% confidence interval.

^dProbe area corrections of 126 cm² were made for the gas proportional detectors. The following MDC equation was used for 1-minute counts and a background of 1 cpm:

$$MDC = \frac{3 + 4.65\sqrt{C_B}}{KT}$$

^eMeasurements performed with a Ludlum 43-68 gas proportional detector with a standard 0.4-mg/cm² window.

^fEach sheet of Mylar has a density thickness of 0.22 mg/cm² and one Kimwipe has a density thickness of 1.86 mg/cm².

^gReagent water used in analytical procedures from radiochemistry laboratory.

**Table 5.22 Effects of Water Density Thickness on Source Efficiency and MDC
(Gas Proportional—β-Only/C-14)**

Surface Material	Density Thickness (mg/cm ²)	C-14 (0.046 ± 0.001) ^a		
		Source Efficiency		MDC ^d (dpm/100 cm ²)
		Meas. ^b	Fit ^c	
Detector Face ^e	3.8	NA	NA	1,869
Detector Face Plus 2 Mylar Sheets With 1 Kimwipe ^f	6.10	0.436	0.445 ± 0.041	3,544
Plus 0.44 mg/cm ² Water ^g	6.54	0.367	0.399 ± 0.034	4,209
Plus 0.62 mg/cm ² Water	6.72	0.358	0.382 ± 0.031	4,317
Plus 0.78 mg/cm ² Water	6.88	0.354	0.367 ± 0.029	4,363
Plus 1.23 mg/cm ² Water	7.33	0.338	0.329 ± 0.024	4,576
Plus 2.29 mg/cm ² Water	8.39	0.282	0.253 ± 0.016	5,480
Plus 3.04 mg/cm ² Water	9.14	0.239	0.210 ± 0.013	6,457
Plus 5.14 mg/cm ² Water	11.24	0.136	0.125 ± 0.011	11,359
Plus 6.49 mg/cm ² Water	12.59	0.084	0.090 ± 0.010	18,320
Plus 7.62 mg/cm ² Water	13.72	0.063	0.068 ± 0.009	24,606
Regression Equation		$\epsilon_s = 2.01 e^{-0.247 x}$		

^aInstrument efficiency provided in parentheses; uncertainties represent the 95% confidence interval.

^bSource efficiency was determined by dividing the total efficiency by the instrument efficiency.

^cThe measured source efficiency versus density thickness was fit to an exponential curve; uncertainties represent the 95% confidence interval.

^dProbe area corrections of 126 cm² were made for the gas proportional detectors. The following MDC equation was used for 1-minute counts and a background of 354 cpm:

$$MDC = \frac{3 + 4.65\sqrt{C_B}}{KT}$$

^eMeasurements performed with a Ludlum 43-68 gas proportional detector with a standard alpha-blocking 3.8-mg/cm² window.

^fEach sheet of Mylar has a density thickness of 0.22 mg/cm² and one Kimwipe has a density thickness of 1.86 mg/cm².

^gReagent water used in analytical procedures from radiochemistry laboratory.

VARIABLES AFFECTING MDCs IN THE FIELD

**Table 5.23 Effects of Water Density Thickness on Source Efficiency and MDC
(Gas Proportional—β-Only/Tc-99)**

Surface Material	Density Thickness (mg/cm ²)	Tc-99 (0.148 ± 0.013) ^a		
		Source Efficiency		MDC ^d (dpm/100 cm ²)
		Meas. ^b	Fit ^c	
Detector Face ^e	3.8	NA	NA	620
Detector Face Plus 2 Mylar Sheets With 1 Kimwipe ^f	6.10	0.626	0.643 ± 0.026	773
Plus 0.19 mg/cm ² Water ^g	6.29	0.630	0.632 ± 0.025	769
Plus 0.74 mg/cm ² Water	6.84	0.590	0.602 ± 0.022	821
Plus 2.85 mg/cm ² Water	8.95	0.518	0.500 ± 0.013	934
Plus 3.97 mg/cm ² Water	10.07	0.469	0.452 ± 0.012	1,033
Plus 5.49 mg/cm ² Water	11.59	0.402	0.396 ± 0.012	1,206
Plus 6.67 mg/cm ² Water	12.77	0.357	0.356 ± 0.014	1,356
Plus 8.17 mg/cm ² Water	14.27	0.300	0.312 ± 0.015	1,614
Regression Equation		$\epsilon_s = 1.10 e^{-0.088 x}$		

^aInstrument efficiency provided in parentheses; uncertainties represent the 95% confidence interval.

^bSource efficiency was determined by dividing the total efficiency by the instrument efficiency.

^cThe measured source efficiency versus density thickness was fit to an exponential curve; uncertainties represent the 95% confidence interval.

^dProbe area corrections of 126 cm² were made for the gas proportional detectors. The following MDC equation was used for 1-minute counts and a background of 354 cpm:

$$MDC = \frac{3 + 4.65\sqrt{C_B}}{KT}$$

^eMeasurements performed with a Ludlum 43-68 gas proportional detector with a standard alpha-blocking 3.8-mg/cm² window.

^fEach sheet of Mylar has a density thickness of 0.22 mg/cm² and one Kimwipe has a density thickness of 1.86 mg/cm².

^gReagent water used in analytical procedures from radiochemistry laboratory.

**Table 5.24 Effects of Water Density Thickness on Source Efficiency and MDC
(Gas Proportional—β-Only/SrY-90)**

Surface Material	Density Thickness (mg/cm ²)	SrY-90 (0.429 ± 0.023) ^a		
		Source Efficiency		MDC ^d (dpm/100 cm ²)
		Meas. ^b	Fit ^c	
Detector Face ^e	3.8	NA	NA	222
Detector Face Plus 2 Mylar Sheets With 1 Kimwipe ^f	6.10	0.697	0.700 ± 0.021	241
Plus 2.56 mg/cm ² Water ^g	8.66	0.665	0.666 ± 0.013	252
Plus 3.25 mg/cm ² Water	9.35	0.661	0.657 ± 0.011	253
Plus 4.81 mg/cm ² Water	10.91	0.635	0.637 ± 0.011	264
Plus 6.28 mg/cm ² Water	12.38	0.632	0.619 ± 0.013	265
Plus 7.88 mg/cm ² Water	13.98	0.590	0.600 ± 0.017	284
Regression Equation		$\epsilon_s = 0.790 e^{-0.020 x}$		

^aInstrument efficiency provided in parentheses; uncertainties represent the 95% confidence interval.

^bSource efficiency was determined by dividing the total efficiency by the instrument efficiency.

^cThe measured source efficiency versus density thickness was fit to an exponential curve; uncertainties represent the 95% confidence interval.

^dProbe area corrections of 126 cm² were made for the gas proportional detectors. The following MDC equation was used for 1-minute counts and a background of 354 cpm:

$$MDC = \frac{3 + 4.65\sqrt{C_B}}{KT}$$

^eMeasurements performed with a Ludlum 43-68 gas proportional detector with a standard alpha-blocking 3.8-mg/cm² window.

^fEach sheet of Mylar has a density thickness of 0.22 mg/cm² and one Kimwipe has a density thickness of 1.86 mg/cm².

^gReagent water used in analytical procedures from radiochemistry laboratory.

VARIABLES AFFECTING MDCs IN THE FIELD

Table 5.25 Effects of Water Density Thickness on Source Efficiency and MDC (GM Detector/C-14)

Surface Material	Density Thickness (mg/cm ²)	C-14 (0.056 ± 0.001) ^a		
		Source Efficiency		MDC ^d (dpm/100 cm ²)
		Meas. ^b	Fit ^c	
Detector Face ^e	--- ^f	NA	NA	3,758
Detector Face Plus 2 Mylar Sheets With 1 Kimwipe ^g	2.30	0.436	0.494 ± 0.053	7,294
Plus 0.44 mg/cm ² Water ^h	2.74	0.422	0.445 ± 0.044	7,526
Plus 0.62 mg/cm ² Water	2.92	0.412	0.427 ± 0.041	7,716
Plus 0.78 mg/cm ² Water	3.08	0.405	0.411 ± 0.038	7,847
Plus 1.23 mg/cm ² Water	3.53	0.382	0.369 ± 0.032	8,320
Plus 2.29 mg/cm ² Water	4.59	0.320	0.287 ± 0.021	9,925
Plus 3.04 mg/cm ² Water	5.34	0.277	0.241 ± 0.018	11,481
Plus 5.14 mg/cm ² Water	7.44	0.162	0.146 ± 0.015	19,622
Plus 6.49 mg/cm ² Water	8.79	0.104	0.106 ± 0.014	30,496
Plus 7.62 mg/cm ² Water	9.92	0.071	0.082 ± 0.013	44,680
Regression Equation		$\epsilon_s = 0.851 e^{-0.236 x}$		

^aInstrument efficiency provided in parentheses; uncertainties represent the 95% confidence interval.

^bSource efficiency was determined by dividing the total efficiency by the instrument efficiency.

^cThe measured source efficiency versus density thickness was fit to an exponential curve; uncertainties represent the 95% confidence interval.

^dThe following MDC equation was used for 1-minute counts, with a background of 49 cpm and probe area of 20 cm²:

$$MDC = \frac{3 + 4.65\sqrt{C_B}}{KT}$$

^eMeasurements performed with an Eberline HP-260 GM detector with a standard mica window, typical thickness 1.4 to 2.0 mg/cm².

^fDetector face is fixed part of detector and is not removable.

^gEach sheet of Mylar has a density thickness of 0.22 mg/cm² and one Kimwipe has a density thickness of 1.86 mg/cm².

^hReagent water used in analytical procedures from radiochemistry laboratory.

Table 5.26 Effects of Water Density Thickness on Source Efficiency and MDC (GM Detector/Tc-99)

Surface Material	Density Thickness (mg/cm ²)	Tc-99 (0.161 ± 0.018) ^a		
		Source Efficiency		MDC ^d (dpm/100 cm ²)
		Meas. ^b	Fit ^c	
Detector Face ^e	--- ^f	NA	NA	1,454
Detector Face Plus 2 Mylar Sheets With 1 Kimwipe ^g	2.30	0.627	0.631 ± 0.022	1,762
Plus 0.19 mg/cm ² Water ^h	2.49	0.611	0.621 ± 0.021	1,805
Plus 0.76 mg/cm ² Water	3.06	0.580	0.590 ± 0.018	1,902
Plus 2.85 mg/cm ² Water	5.15	0.501	0.490 ± 0.011	2,204
Plus 3.97 mg/cm ² Water	6.27	0.463	0.444 ± 0.010	2,383
Plus 5.49 mg/cm ² Water	7.79	0.392	0.387 ± 0.010	2,814
Plus 6.67 mg/cm ² Water	8.97	0.347	0.349 ± 0.012	3,179
Plus 8.17 mg/cm ² Water	10.47	0.296	0.305 ± 0.013	3,731
Regression Equation		$\epsilon_s = 0.775 e^{-0.089 x}$		

^aInstrument efficiency provided in parentheses; uncertainties represent the 95% confidence interval.

^bSource efficiency was determined by dividing the total efficiency by the instrument efficiency.

^cThe measured source efficiency versus density thickness was fit to an exponential curve; uncertainties represent the 95% confidence interval.

^dThe following MDC equation was used for 1-minute counts, with a background of 49 cpm and probe area of 20 cm²:

$$MDC = \frac{3 + 4.65\sqrt{C_B}}{KT}$$

^eMeasurements performed with an Eberline HP-260 GM detector with a standard mica window, typical thickness 1.4 to 2.0 mg/cm².

^fDetector face is fixed part of detector and is not removable.

^gEach sheet of Mylar has a density thickness of 0.22 mg/cm² and one Kimwipe has a density thickness of 1.86 mg/cm².

^hReagent water used in analytical procedures from radiochemistry laboratory.

VARIABLES AFFECTING MDCs IN THE FIELD

Table 5.27 Effects of Water Density Thickness on Source Efficiency and MDC (GM Detector/SrY-90)

Surface Material	Density Thickness (mg/cm ²)	SrY-90 (0.373 ± 0.020) ^a		
		Source Efficiency		MDC ^d (dpm/100 cm ²)
		Meas. ^b	Fit ^c	
Detector Face ^e	--- ^f	NA	NA	648
Detector Face Plus 2 Mylar Sheets With 1 Kimwipe ^g	2.30	0.697	0.708 ± 0.029	684
Plus 2.56 mg/cm ² Water ^h	4.86	0.678	0.676 ± 0.017	703
Plus 3.25 mg/cm ² Water	5.55	0.678	0.668 ± 0.015	703
Plus 4.81 mg/cm ² Water	7.11	0.665	0.649 ± 0.015	717
Plus 6.28 mg/cm ² Water	8.58	0.620	0.632 ± 0.018	768
Plus 7.88 mg/cm ² Water	10.18	0.608	0.613 ± 0.024	783
Regression Equation		$\epsilon_s = 0.739 e^{-0.018 x}$		

^aInstrument efficiency provided in parentheses; uncertainties represent the 95% confidence interval.

^bSource efficiency was determined by dividing the total efficiency by the instrument efficiency.

^cThe measured source efficiency versus density thickness was fit to an exponential curve; uncertainties represent the 95% confidence interval.

^dThe following MDC equation was used for 1-minute counts, with a background of 49 cpm and probe area of 20 cm²:

$$MDC = \frac{3 + 4.65\sqrt{C_B}}{KT}$$

^eMeasurements performed with an Eberline HP-260 GM detector with a standard mica window, typical thickness 1.4 to 2.0 mg/cm².

^fDetector face is fixed part of detector and is not removable.

^gEach sheet of Mylar has a density thickness of 0.22 mg/cm² and one Kimwipe has a density thickness of 1.86 mg/cm².

^hReagent water used in analytical procedures from radiochemistry laboratory.

Table 5.28 Effects of Water Density Thickness on Source Efficiency and MDC (ZnS Scintillation Detector)

Surface Material	Density Thickness (mg/cm ²)	Th-230 (0.069 ± 0.005) ^a		
		Source Efficiency		MDC ^d (dpm/100 cm ²)
		Meas. ^b	Fit ^c	
Detector Face ^e	--- ^f	NA	NA	65
Detector Face Plus 2 Mylar Sheets With 1 Kimwipe ^g	2.30	0.508	0.453 ± 0.060	294
Plus 0.11 mg/cm ² Water ^h	2.41	0.433	0.423 ± 0.054	345
Plus 0.25 mg/cm ² Water	2.55	0.366	0.389 ± 0.048	407
Plus 0.48 mg/cm ² Water	2.78	0.296	0.338 ± 0.040	504
Plus 1.23 mg/cm ² Water	3.53	0.232	0.214 ± 0.021	645
Plus 2.03 mg/cm ² Water	4.33	0.145	0.131 ± 0.012	1,030
Plus 3.51 mg/cm ² Water	5.81	0.046	0.053 ± 0.006	3,265
Plus 4.23 mg/cm ² Water	6.53	0.031	0.034 ± 0.005	4,814
Plus 5.88 mg/cm ² Water	8.18	0.014	0.012 ± 0.003	10,465
Regression Equation		$\epsilon_s = 1.84 e^{-0.610 x}$		

^aInstrument efficiency provided in parentheses; uncertainties represent the 95% confidence interval.

^bSource efficiency was determined by dividing the total efficiency by the instrument efficiency.

^cThe measured source efficiency versus density thickness was fit to an exponential curve; uncertainties represent the 95% confidence interval.

^dThe following MDC equation was used for 1-minute counts, with a background of 1 cpm and probe area of 74 cm²:

$$MDC = \frac{3 + 4.65\sqrt{C_B}}{KT}$$

^eMeasurements performed with an Eberline AC3-7 ZnS scintillation detector with a standard 1.5-mg/cm² window.

^fDetector face is fixed part of detector and is not removable.

^gEach sheet of Mylar has a density thickness of 0.22 mg/cm² and one Kimwipe has a density thickness of 1.86 mg/cm².

^hReagent water used in analytical procedures from radiochemistry laboratory.

VARIABLES AFFECTING MDCS IN THE FIELD

Table 5.29 Total Efficiencies for Detectors Used To Assess Uranium Surface Activity

Radioactive Material (Surface Type)	Total Efficiency (counts per disintegration) ^a				
	Gas Proportional			GM	ZnS
	α Only ^b	β Only ^c	$\alpha + \beta$ ^b		
Processed Uranium^d					
Stainless Steel	0.13	0.24	0.45	0.28	0.08
Concrete	0.10	0.22	0.44	0.19	0.06
Wood	0.04	0.21	0.32	0.22	0.02
Drywall	0.10	0.23	0.43	0.27	0.06
Enriched Uranium (3%)					
Stainless Steel	0.10	0.09	0.23	0.12	0.06
Concrete	0.07	0.07	0.18	0.10	0.05
Wood	0.06	0.08	0.17	0.10	0.03
Drywall	0.07	0.07	0.18	0.10	0.04
Ru-106 (Rh-106)					
Stainless Steel	--- ^e	0.55	0.57	0.56	---
Concrete	---	0.50	0.51	0.47	---
Wood	---	0.46	0.46	0.45	---
Drywall	---	0.35	0.34	0.30	---
SrY-90					
Stainless Steel	---	0.38	0.43	0.27	---
Concrete	---	0.34	0.38	0.23	---

^aThe total efficiencies were calculated by dividing net detector counts by radioactivity dispensed on the particular surface. All measurements were at contact with surface. For uranium, the alpha radioactivity (U-238, U-235, and U-234) was used. Activity was distributed over a 20 cm² area.

^bUsing window density thickness of 0.4 mg/cm².

^cUsing window density thickness of 3.8 mg/cm².

^dProcessed uranium includes U-238 in equilibrium with U-234, and U-235 present at natural isotopic ratios; the only other radionuclides present include the immediate progeny of U-238 and U-235.

^eData not obtained.

Table 5.30 Normalized Total Efficiencies for Processed Uranium With Various Absorber Thicknesses

Processed Uranium ^a on Stainless Steel With Mylar Absorber Thicknesses	Normalized Total Efficiency ^b				
	Gas Proportional			GM	ZnS
	α Only ^c	β Only ^d	$\alpha + \beta$ ^c		
No Mylar (at contact)	1.0	1.0	1.0	1.0	1.0
0.22 mg/cm ² Mylar	0.85	1.0	0.96	1.0	0.69
0.44 mg/cm ² Mylar	0.72	1.0	0.93	0.99	0.58
0.88 mg/cm ² Mylar	0.53	1.0	0.90	0.97	0.33
1.32 mg/cm ² Mylar	0.32	1.0	0.84	0.94	0.17
2.20 mg/cm ² Mylar	0.05	0.98	0.77	0.90	0.03
3.30 mg/cm ² Mylar	0.02	0.97	0.76	0.80	0.01

^aProcessed uranium includes U-238 in equilibrium with U-234, and U-235 present at natural isotopic ratios; the only other radionuclides present include the immediate progeny of U-238 and U-235.

^bThe total efficiencies were calculated by dividing net detector counts by radioactivity dispensed on the particular surface. Total efficiencies were then normalized to the total efficiency obtained with no Mylar. The alpha radioactivity (U-238, U-235, and U-234) was distributed over a 20-cm² area.

^cUsing window density thickness of 0.4 mg/cm².

^dUsing window density thickness of 3.8 mg/cm².

Table 5.31 Detector Efficiency for Low Enriched Uranium (3%) Using a 126-cm² Proportional Detector With a 0.4 mg cm⁻² Window (Gas Proportional— $\alpha + \beta$)

Radionuclide	Radiation/Average Energy (MeV)	Alpha Fraction	Radiation Yield	Detection Efficiency	Weighted Efficiency
²³⁸ U	Alpha/4.2	0.167	100%	0.15	2.51×10 ⁻²
²³⁴ Th	Beta/0.0435	0.167	100%	0.11	1.84×10 ⁻²
^{234m} Pa	Beta/0.819	0.167	100%	0.49	8.17×10 ⁻²
²³⁴ U	Alpha/4.7	0.799	100%	0.15	1.20×10 ⁻¹
²³⁵ U	Alpha/4.4	0.033	100%	0.15	5.00×10 ⁻³
²³¹ Th	Beta/0.0764	0.033	100%	0.22	7.27×10 ⁻³
Total Weighted Efficiency					0.257

VARIABLES AFFECTING MDCs IN THE FIELD

**Table 5.32 Detector Efficiency for Low Enriched Uranium (3%)
Using a 126-cm² Proportional Detector with a 3.8 mg cm⁻² Window
(Gas Proportional—β only)**

Radionuclide	Radiation/Average Energy (MeV)	Alpha Fraction	Radiation Yield	Detection Efficiency	Weighted Efficiency
²³⁸ U	Alpha/4.2	0.167	100%	0.01	1.67×10 ⁻³
²³⁴ Th	Beta/0.0435	0.167	100%	0.038	6.36×10 ⁻³
^{234m} Pa	Beta/0.819	0.167	100%	0.453	7.58×10 ⁻²
²³⁴ U	Alpha/4.7	0.799	100%	0.01	7.99×10 ⁻³
²³⁵ U	Alpha/4.4	0.033	100%	0.01	3.33×10 ⁻⁴
²³¹ Th	Beta/0.0764	0.033	100%	0.118	3.93×10 ⁻³
Total Weighted Efficiency					0.096

VARIABLES AFFECTING MDCs IN THE FIELD

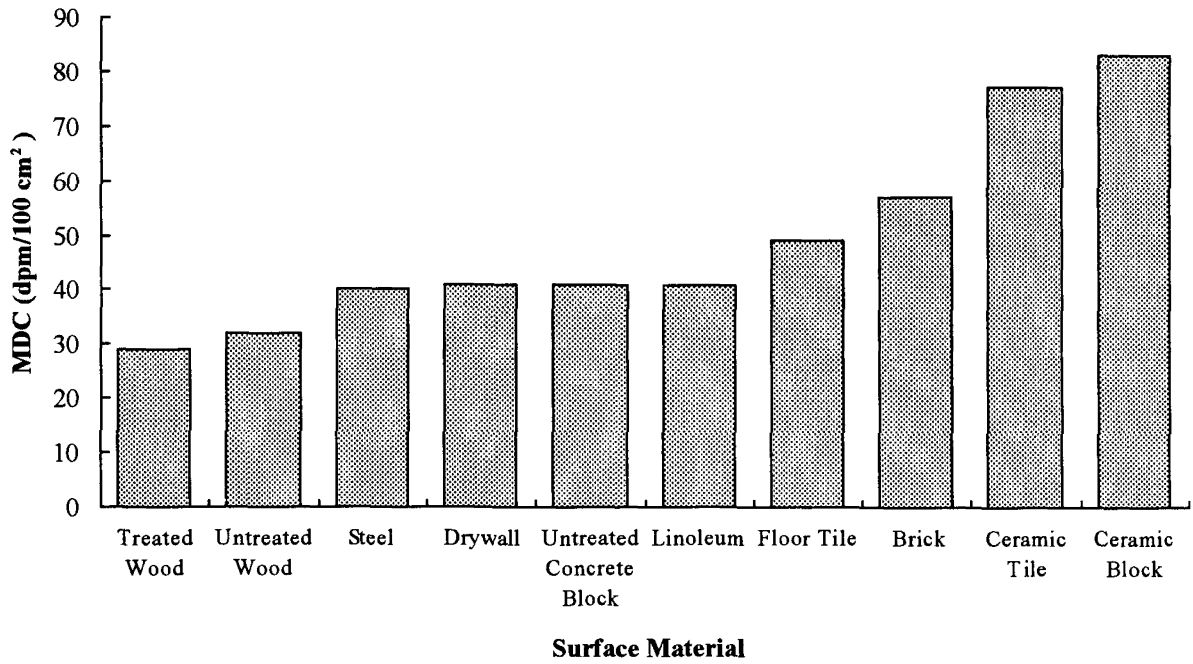


Figure 5.1: Effect of Surface Material on Gas Proportional Detector (α only) MDC

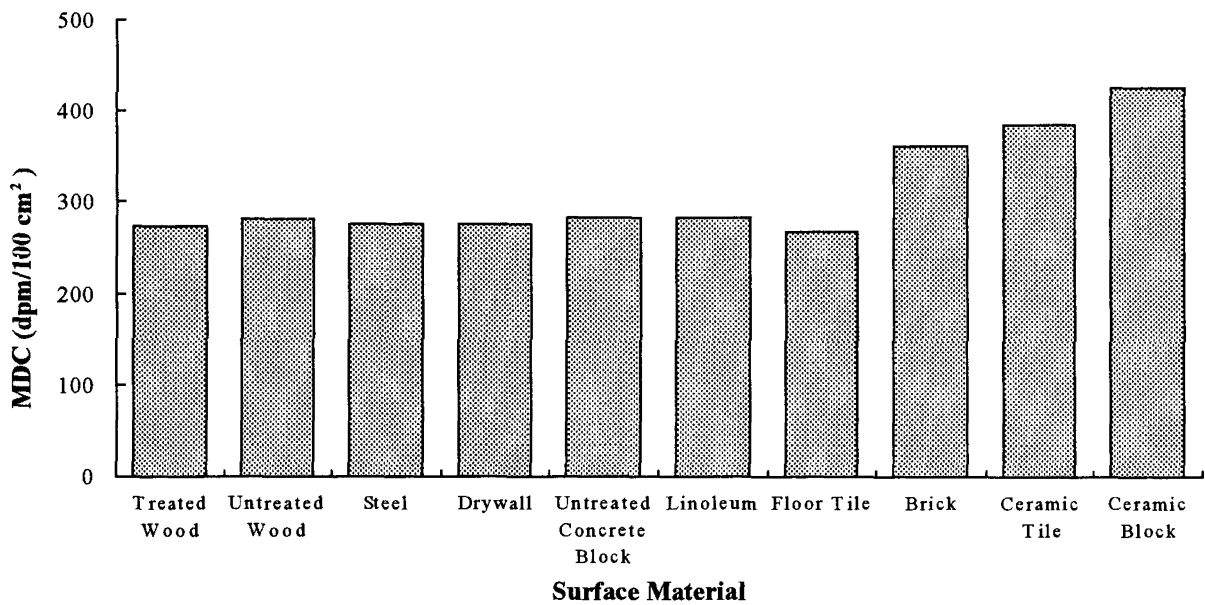


Figure 5.2: Effect of Surface Material on Gas Proportional Detector (β only) MDC

VARIABLES AFFECTING MDCs IN THE FIELD

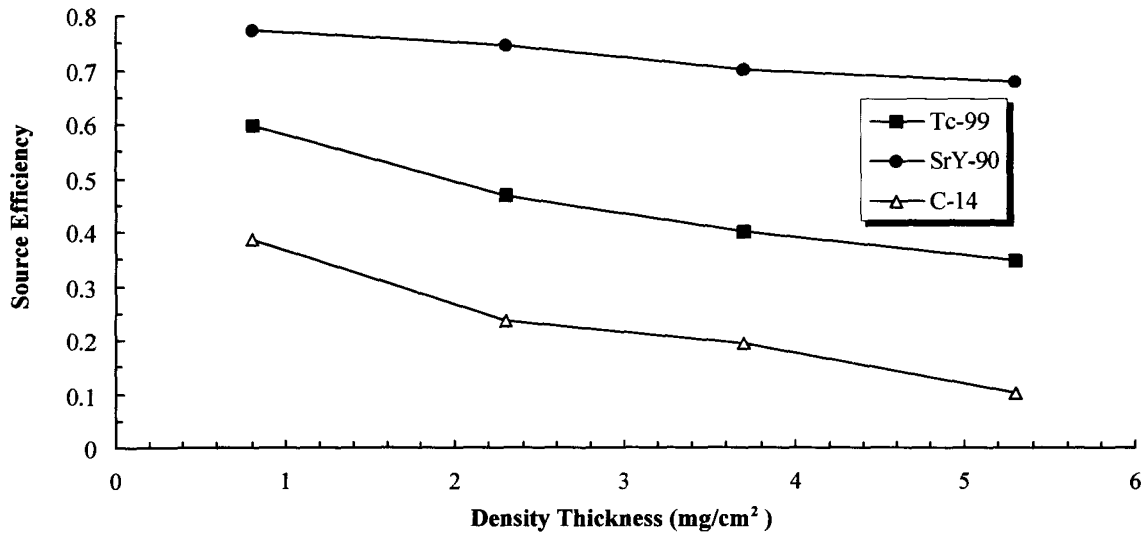


Figure 5.3: Effects of Oil Density Thickness on Source Efficiency for Various Sources

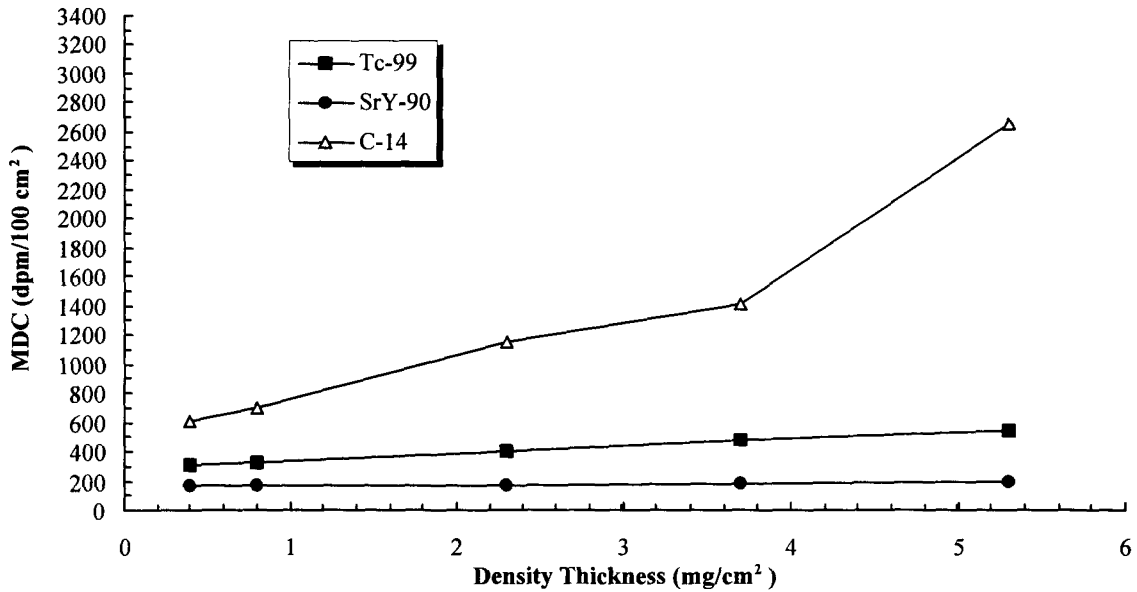


Figure 5.4: Effects of Oil Density Thickness on MDC

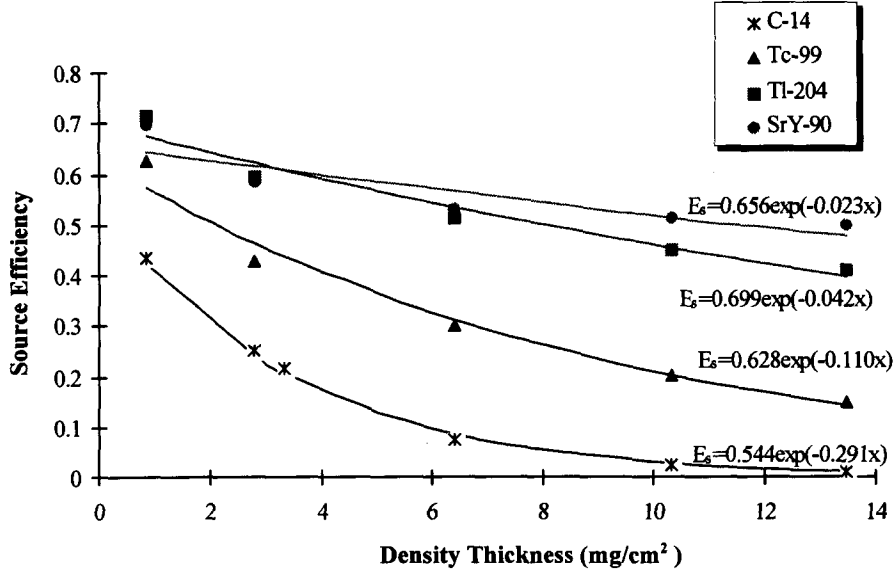


Figure 5.5: Effects of Paint Density Thickness on Source Efficiency (Gas Proportional— $\alpha+\beta$)

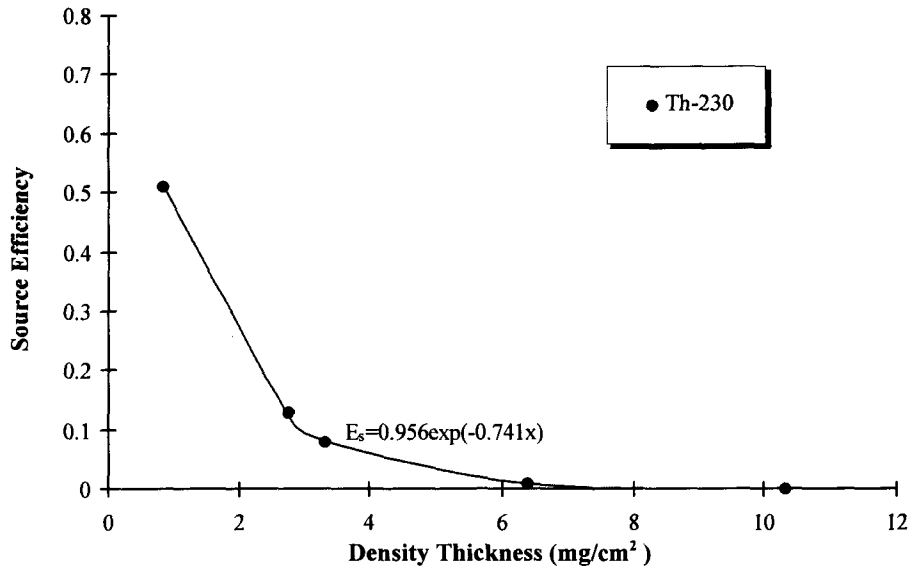


Figure 5.6: Effects of Paint Density Thickness on Source Efficiency (Gas Proportional— α -Only)

VARIABLES AFFECTING MDCs IN THE FIELD

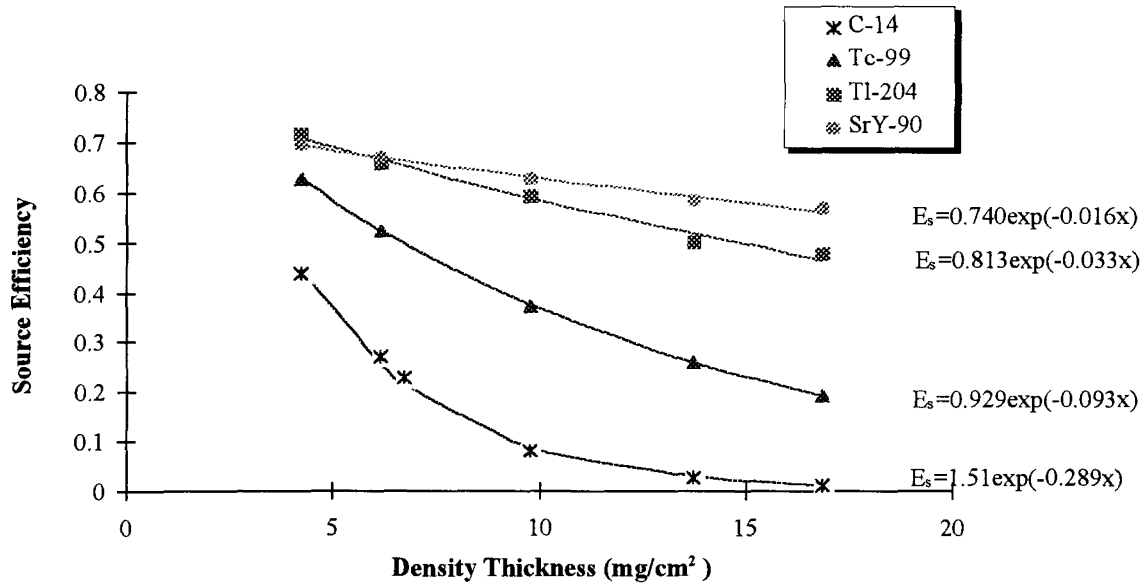


Figure 5.7: Effects of Paint Density Thickness on Source Efficiency (Gas Proportional—β only)

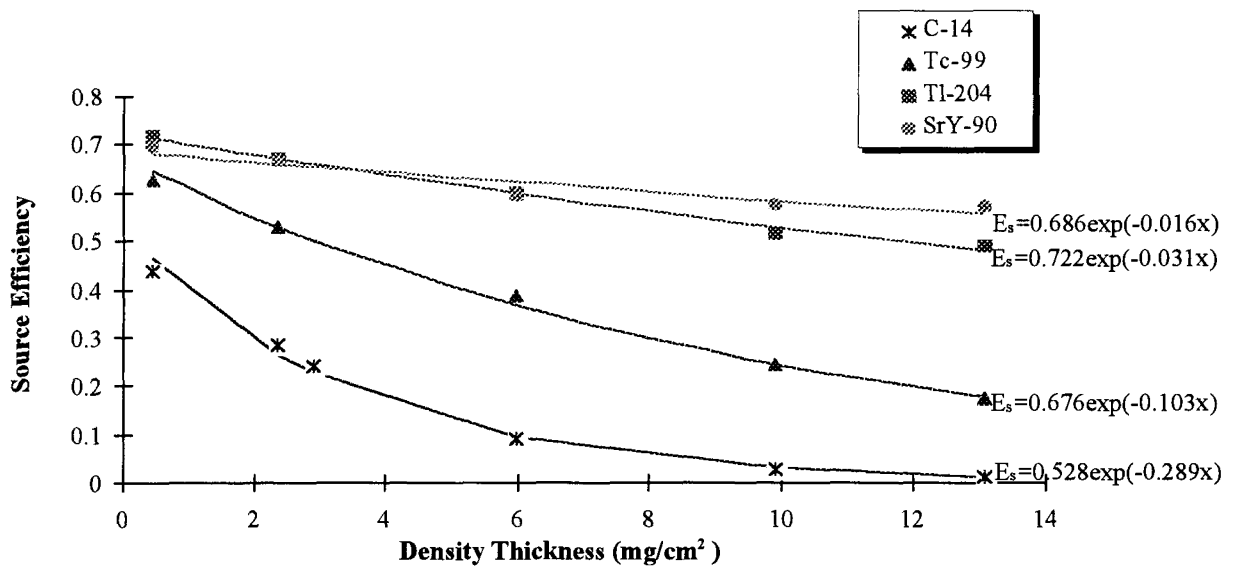


Figure 5.8: Effects of Paint Density Thickness on Source Efficiency (GM Detector)

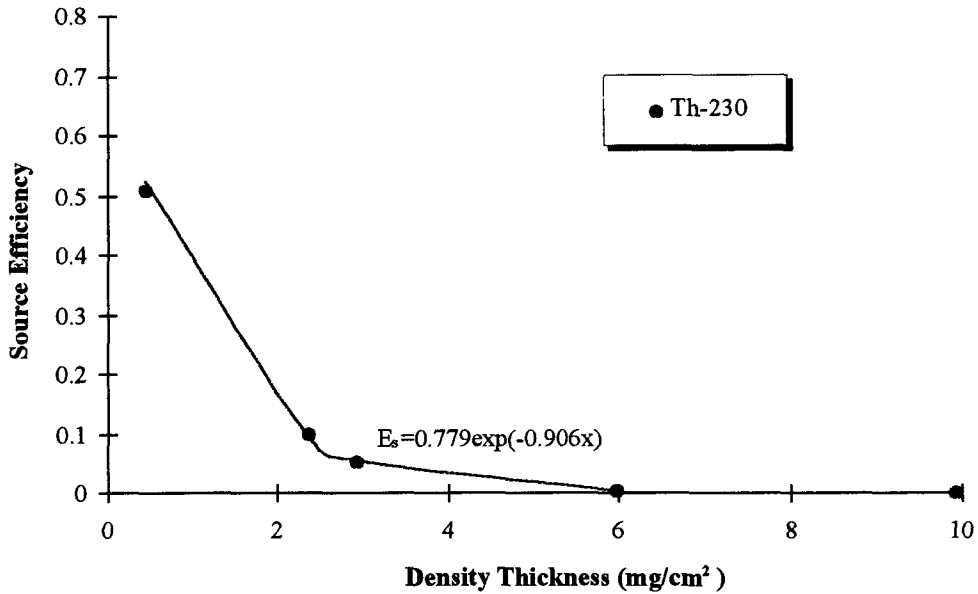


Figure 5.9: Effects of Paint Density Thickness on Source Efficiency (ZnS Scintillation Detector)

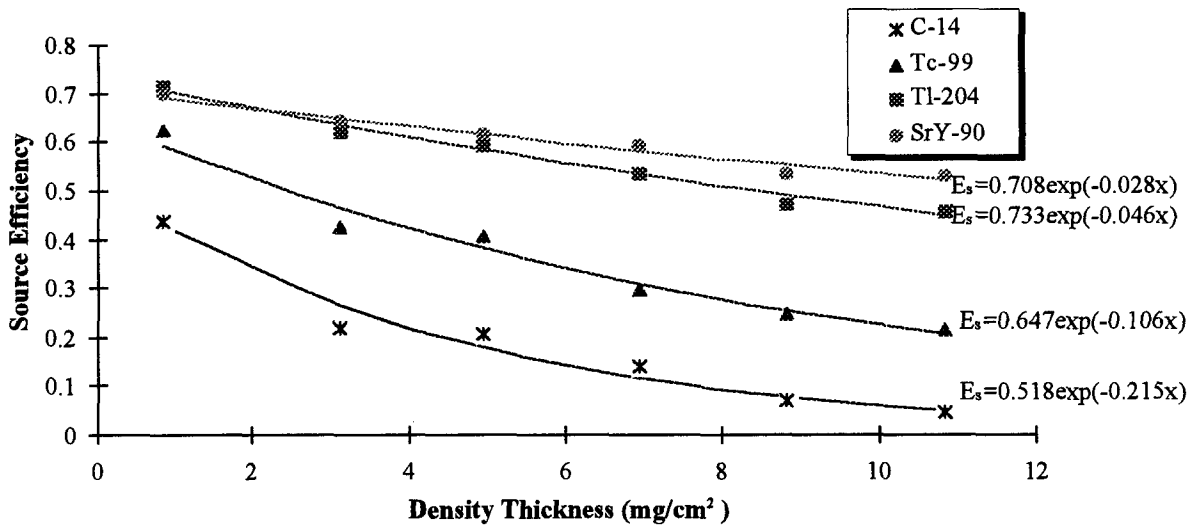


Figure 5.10: Effects of Dust Density Thickness on Source Efficiency (Gas Proportional— $\alpha+\beta$)

VARIABLES AFFECTING MDCs IN THE FIELD

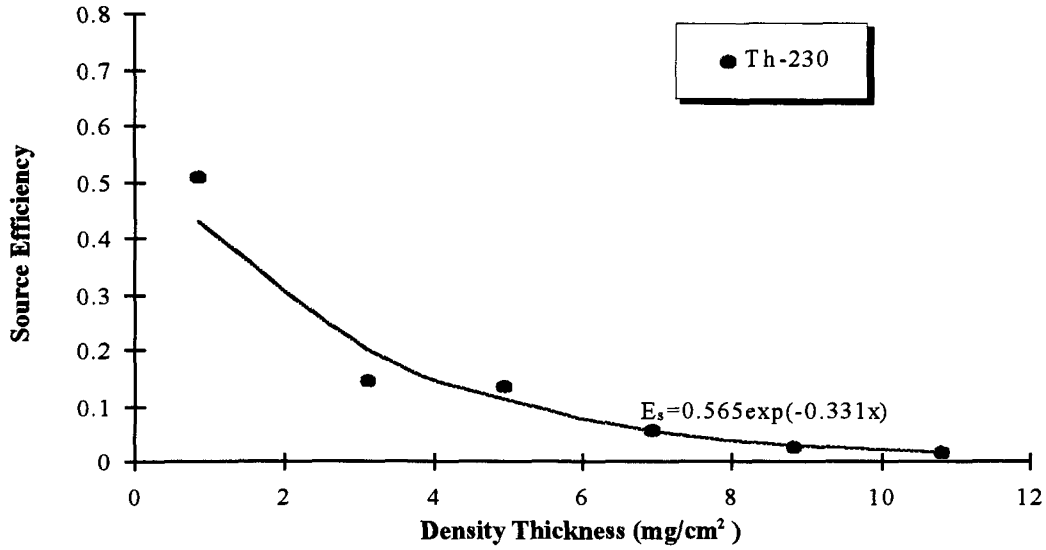


Figure 5.11: Effects of Dust Density Thickness on Source Efficiency (Gas Proportional— α only)

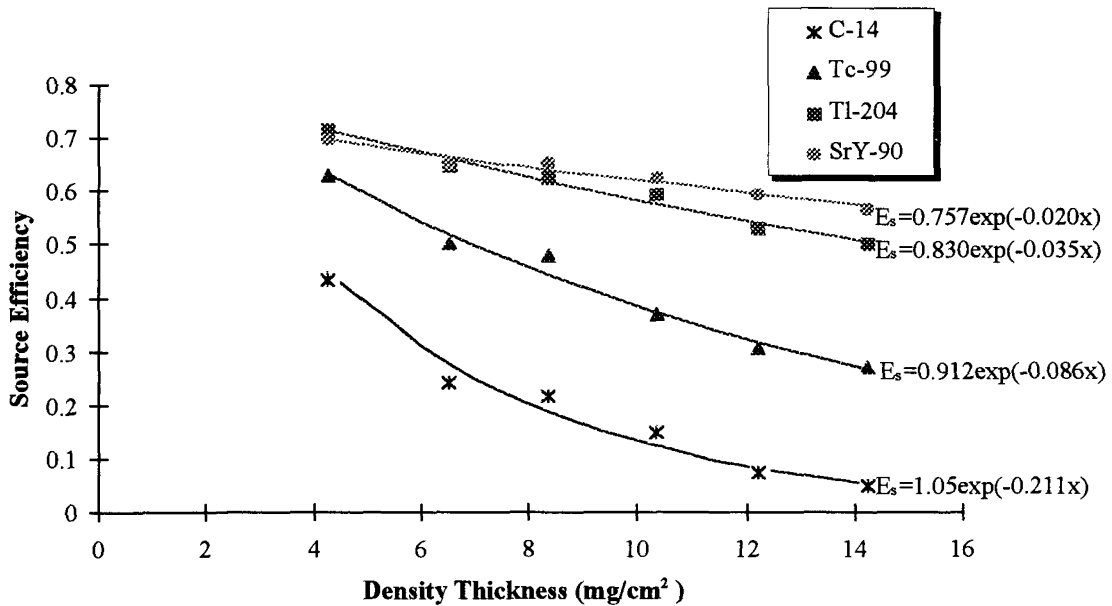


Figure 5.12: Effects of Dust Density Thickness on Source Efficiency (Gas Proportional— β only)

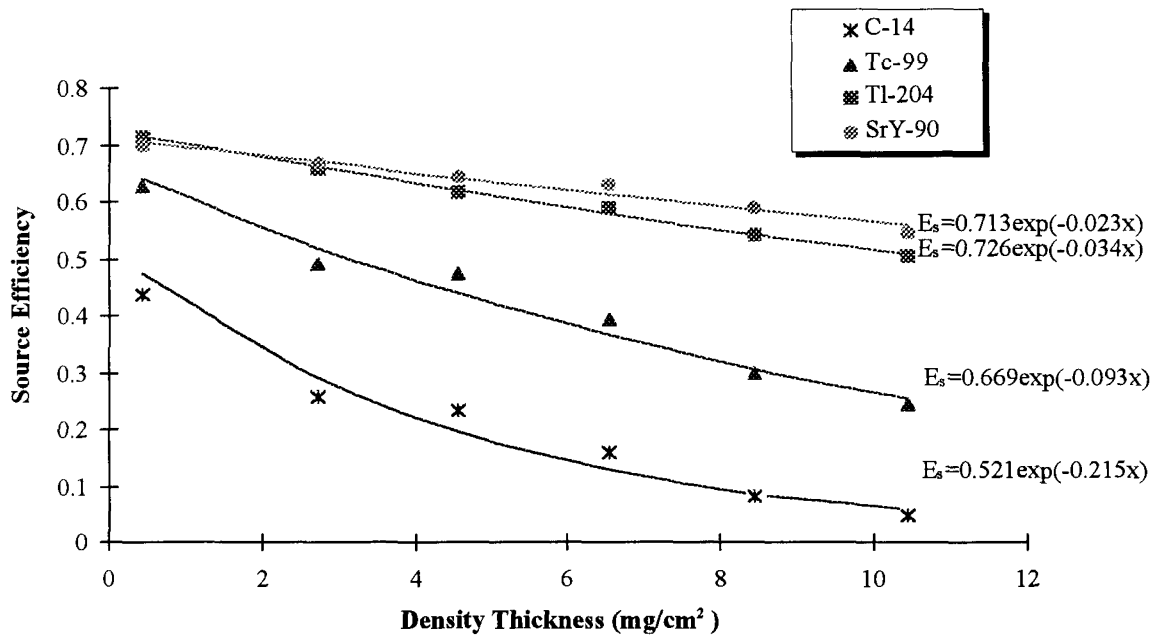


Figure 5.13: Effects of Dust Density Thickness on Source Efficiency (GM Detector)

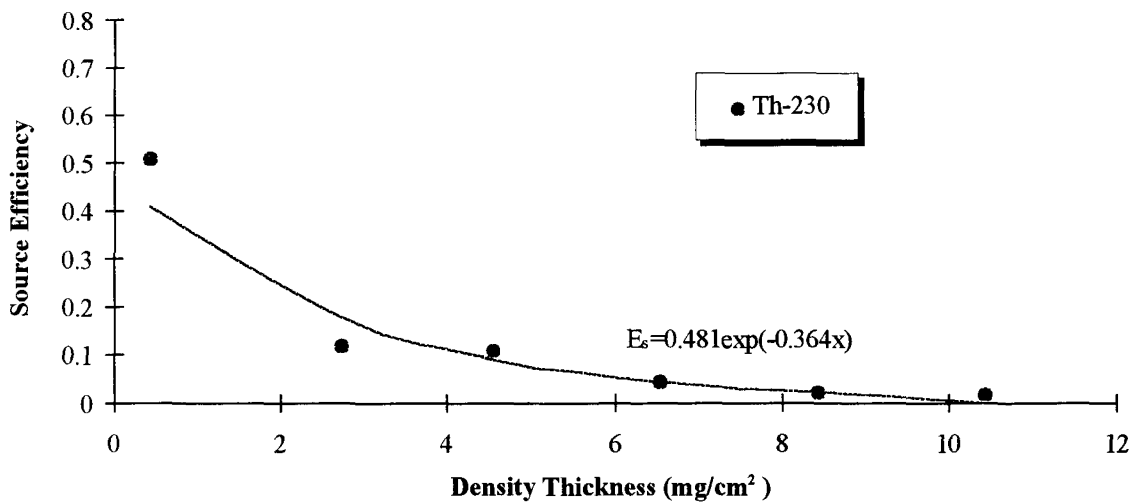


Figure 5.14: Effects of Dust Density Thickness on Source Efficiency (ZnS Scintillation Detector)

VARIABLES AFFECTING MDCs IN THE FIELD

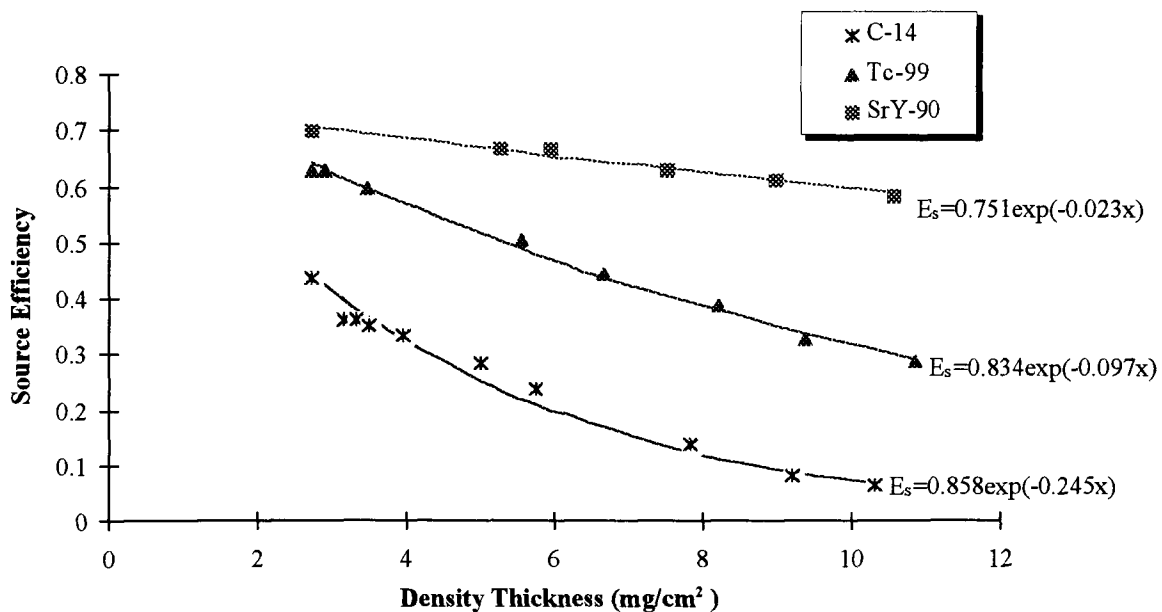


Figure 5.15: Effects of Water Density Thickness on Source Efficiency (Gas Proportional— $\alpha+\beta$)

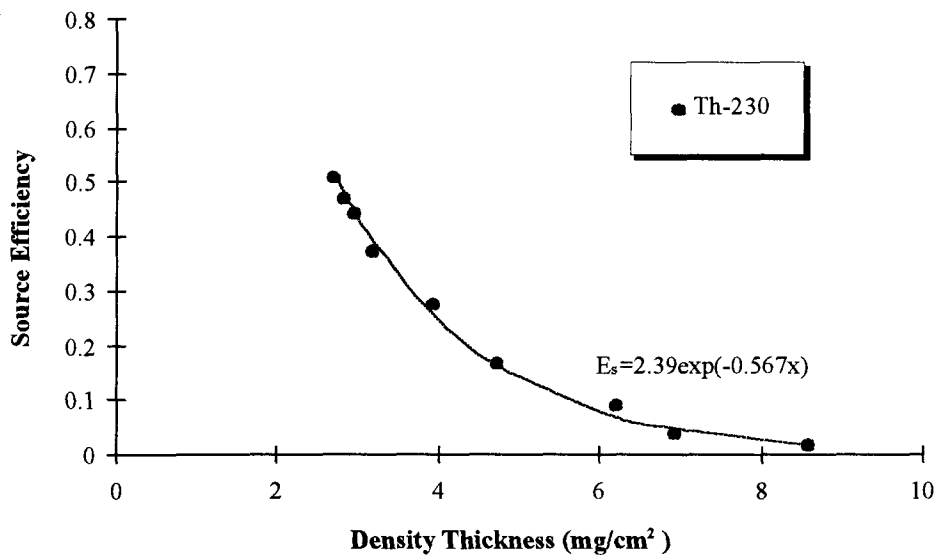


Figure 5.16: Effects of Water Density Thickness on Source Efficiency (Gas Proportional— α only)

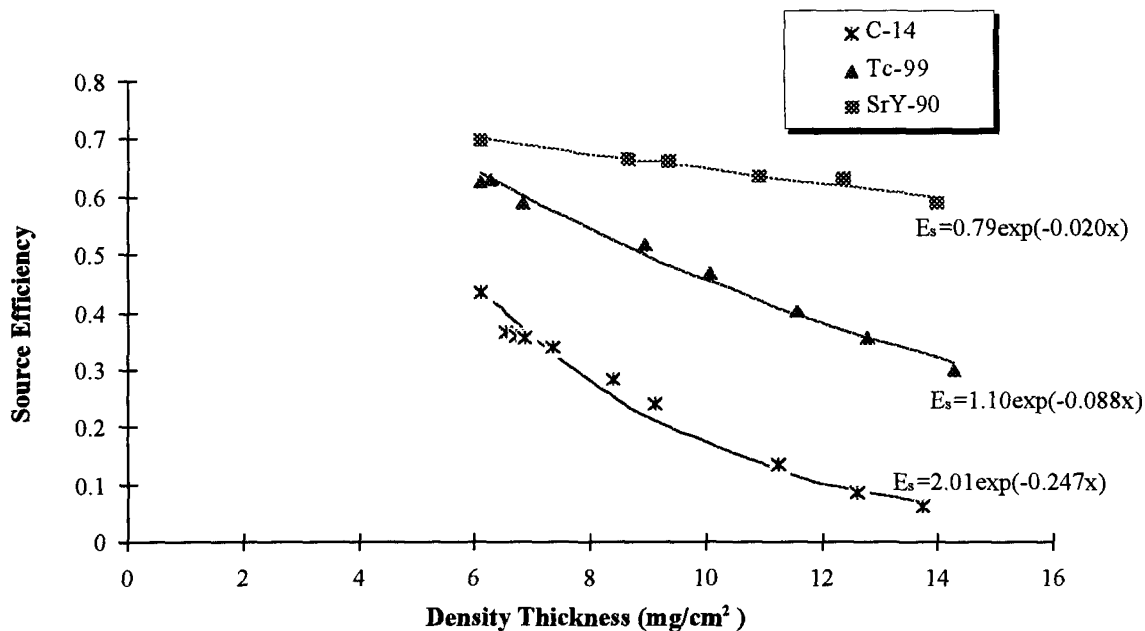


Figure 5.17: Effects of Water Density Thickness on Source Efficiency (Gas Proportional— β only)

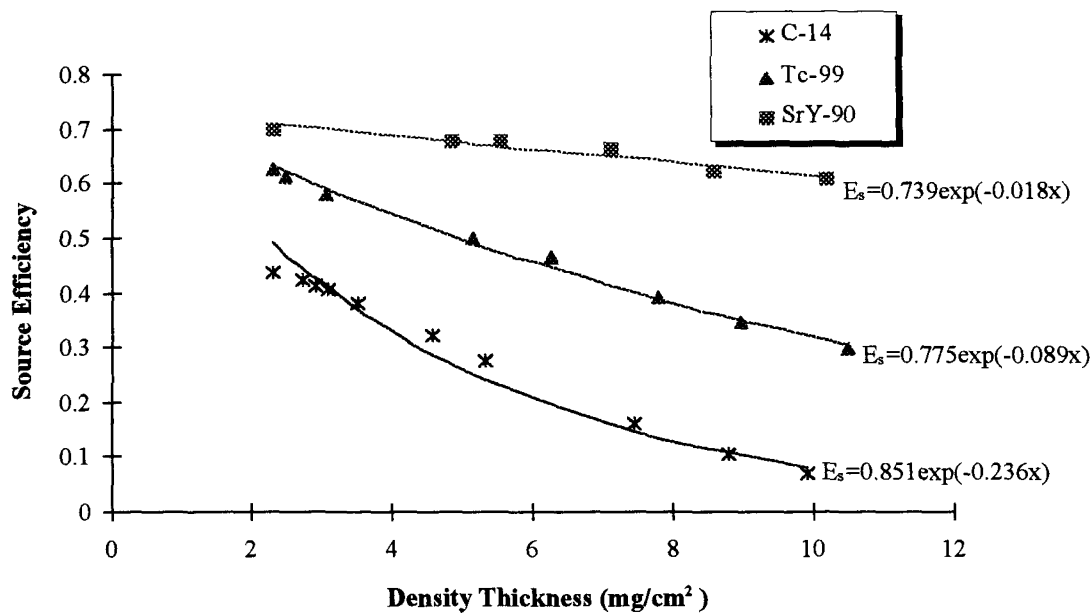


Figure 5.18: Effects of Water Density Thickness on Source Efficiency (GM Detector)

VARIABLES AFFECTING MDCs IN THE FIELD

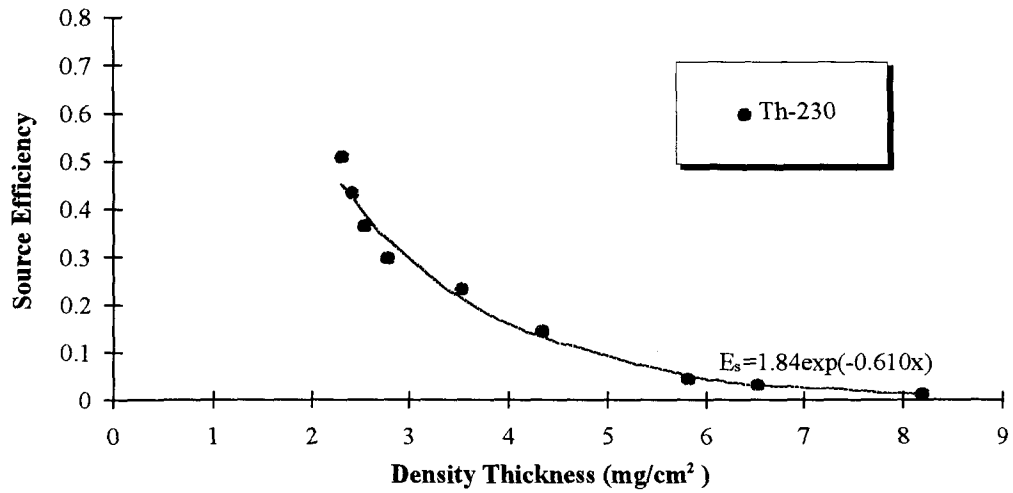


Figure 5.19: Effects of Water Density Thickness on Source Efficiency (ZnS Scintillation Detector)

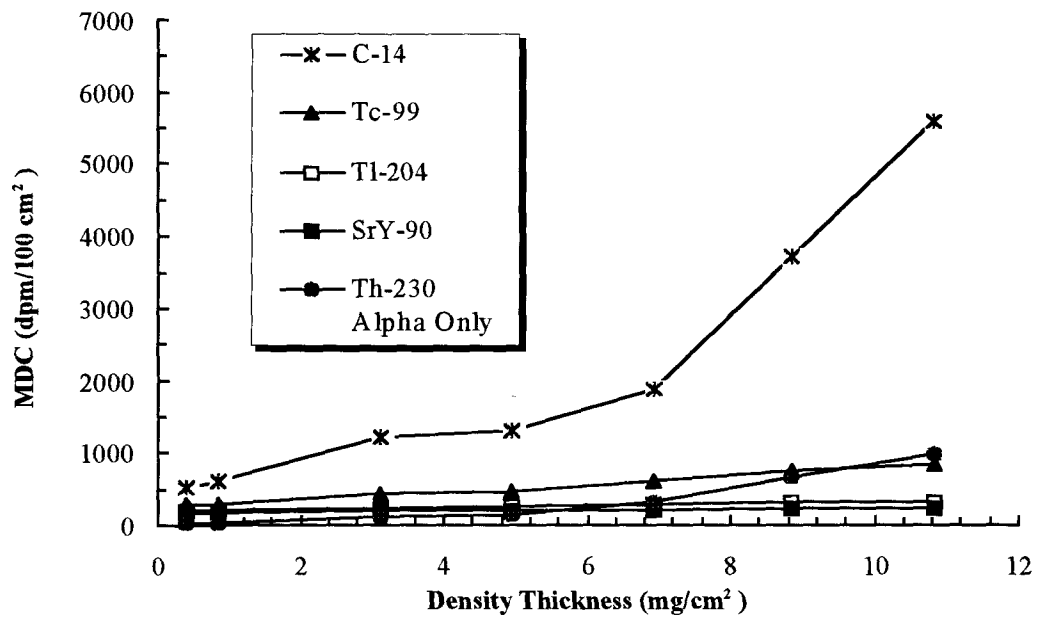


Figure 5.20: Effects of Dust Density Thickness on MDC for Various Sources Using the Gas Proportional Detector in $\alpha+\beta$ and α -Only Modes

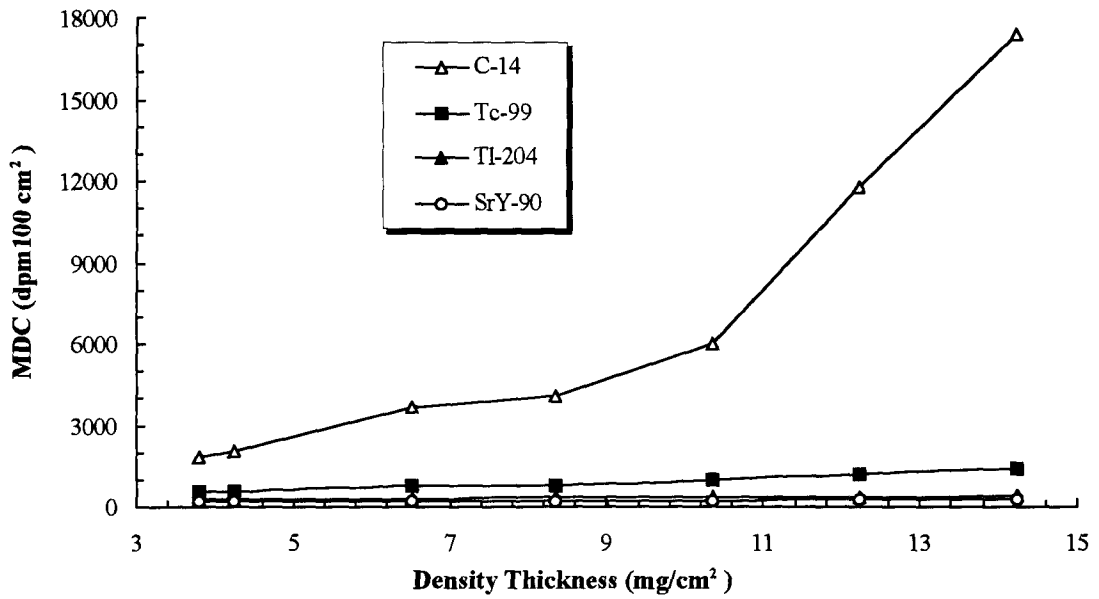


Figure 5.21: Effects of Dust Density Thickness on MDC for Various Sources Using the Gas Proportional in β -Only Mode

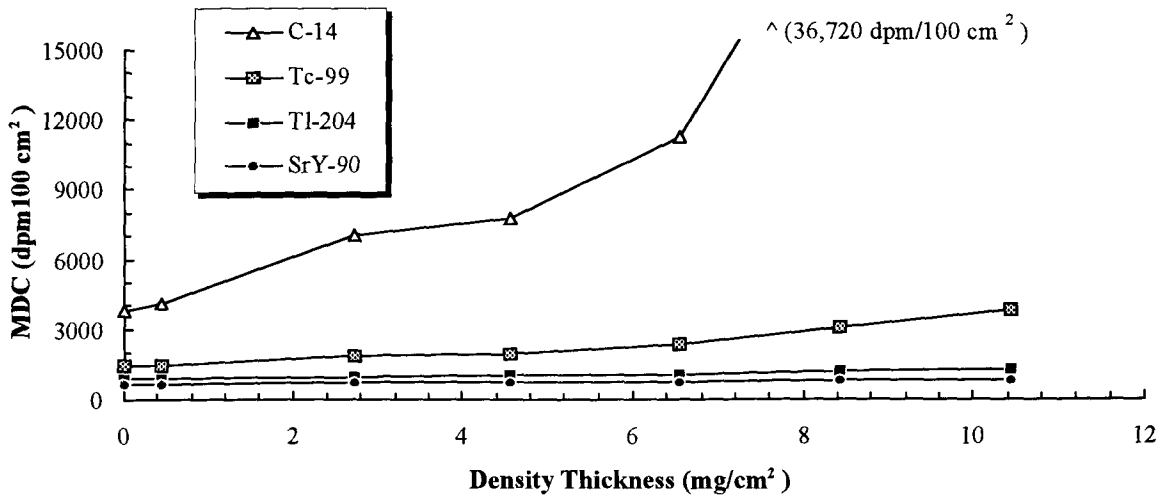


Figure 5.22: Effects of Dust Density Thickness on MDC for Various Sources Using the GM Detector

VARIABLES AFFECTING MDCs IN THE FIELD

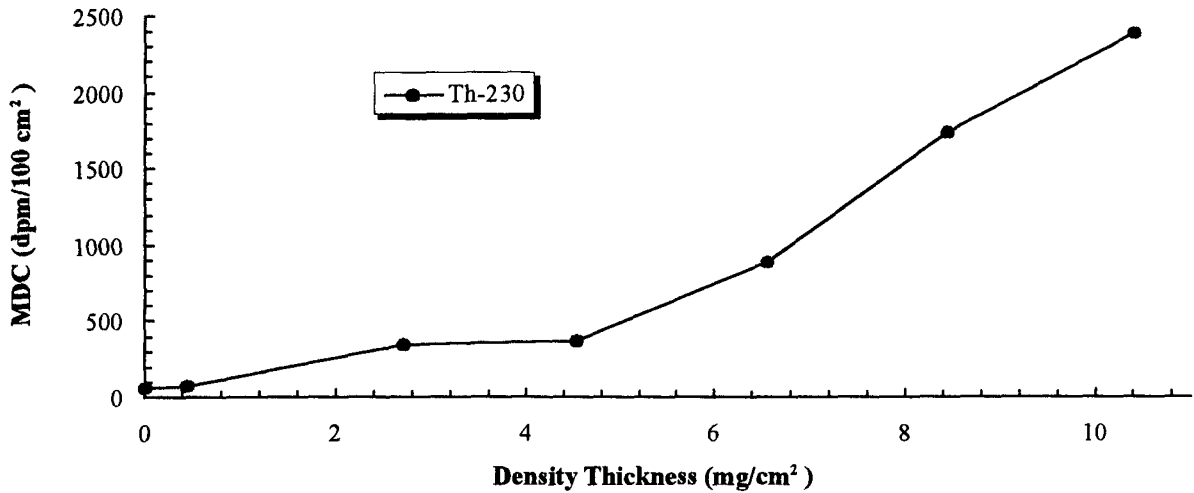


Figure 5.23: Effects of Dust Density Thickness on MDC for an Alpha Source Using the ZnS Scintillation Detector

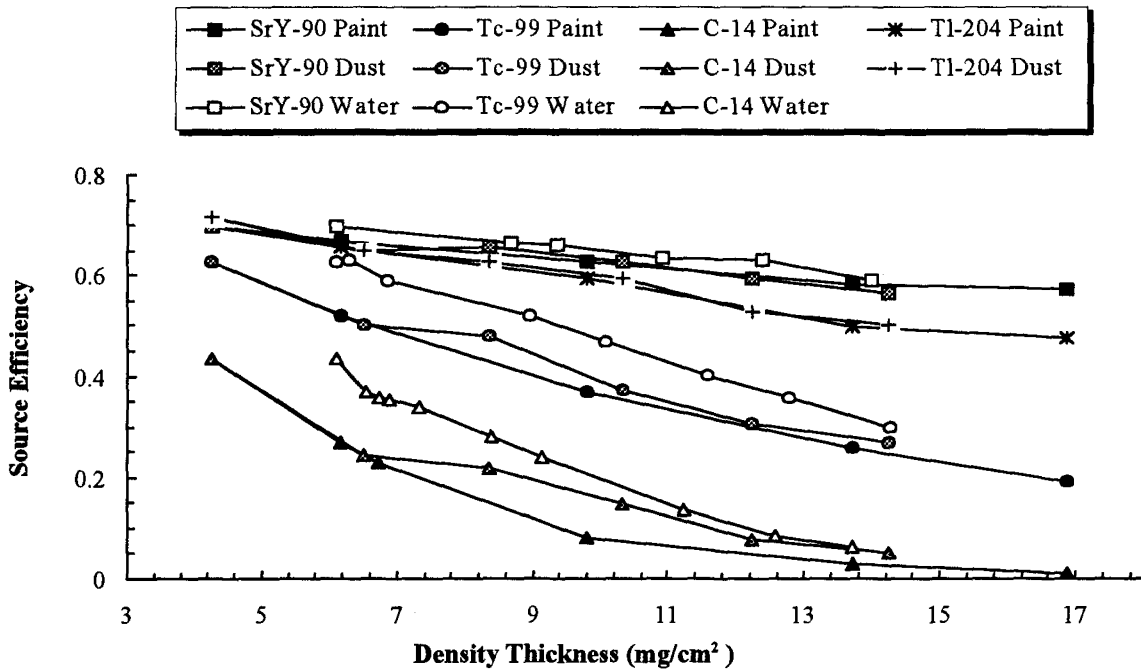


Figure 5.24: Overall Effects of Paint, Dust, and Water Density Thickness on Source Efficiency for Various Sources Using the Gas Proportional Detector in β -Only Mode

6 HUMAN PERFORMANCE AND SCANNING SENSITIVITY

6.1 Introduction

Scanning is performed during radiological surveys in support of decommissioning to identify the presence of any locations of elevated direct radiation. The probability of detecting residual contamination in the field is affected not only by the sensitivity of the survey instrumentation when used in the scanning mode of operation, but also by the surveyor's ability. The surveyor must decide whether the signals represent only the background activity, or whether they represent residual contamination in excess of background.

The minimum detectable concentration of a scan survey (scan MDC) depends on the intrinsic characteristics of the detector (efficiency, window area, etc.), the nature (type and energy of emissions) and relative distribution of the potential contamination (point versus distributed source and depth of contamination), scan rate and other characteristics of the surveyor. Some factors that may affect the surveyor's performance include the costs associated with various outcomes—e.g., cost of missed contamination versus cost of incorrectly identifying areas as being contaminated—and the surveyor's *a priori* expectation of the likelihood of contamination present. For example, if the surveyor believes that the potential for contamination is very low, as in an unaffected area, a relatively large signal may be required for the surveyor to conclude that contamination is present. NUREG/CR-6364, "Human Performance in Radiological Survey Scanning," provides a complete discussion of the human factors as they relate to the performance of scan surveys.

Scanning sensitivities are often empirically determined, depending on the experience of the surveyor. In fact, Lee and Tritch (DOE/CH-9501 1994) state that due to the many factors affecting scan sensitivity, the scan MDC using a particular instrument and survey technique would best be determined experimentally. While empirically determined scan MDCs provide one technique, the resources necessary to implement this option may be burdensome. The approach described in this report to determine the scan sensitivity involves several steps, resulting in an expression for scan MDCs in terms of measurable surface activities and soil concentrations. An overview of the process used to determine scan MDCs is given below.

Signal detection theory provides a framework for the task of deciding whether the audible output of the survey meter during scanning was due to background or signal plus background levels. An index of sensitivity (d') that represents the distance between the means of the background and background plus signal, in units of their common standard deviation, can be calculated for various decision errors—Type I error (α), and Type II error (β). As an example, for a correct detection or true positive rate of 95% ($1-\beta$) and a false positive rate (α) of 5%, d' is 3.29 (similar to the static MDC in Section 3 for the same decision error rates). The index of sensitivity is independent of human factors, and therefore, the ability of an ideal observer (theoretical construct), may be used to determine the minimum d' that can be achieved for particular decision errors. The ideal observer makes optimal use of the available information to maximize the percent correct

responses, providing an effective upper bound against which to compare actual surveyors. Computer simulations and field experimentation can then be performed to evaluate the surveyor efficiency (p) relative to the ideal observer. The resulting expression for the ideal observer's minimum detectable count rate (MDCR), in counts per minute, can be written

$$MDCR = d' * \sqrt{b_i} * (60/i) = s_i * (60/i)$$

where

MDCR = minimum detectable (net) count rate in counts per minute, can be written

b_i = background counts in the observation interval,

s_i = minimum detectable number of net source counts in the observation interval, and

i = observational interval (in seconds), based on the scan speed and areal extent of the contamination.

Scan MDCs are determined from the MDCR by applying conversion factors to obtain results in terms of measurable surface activities and soil concentrations. The theoretical framework for assessing human performance during radiological scans is more fully developed in the companion document NUREG/CR-6364. As an example, the scan MDC for a structure surface can be expressed as

$$Scan\ MDC = \frac{MDCR}{\sqrt{p} \epsilon_i \epsilon_s \frac{probe\ area}{100\ cm^2}} \quad (6-2)$$

6.2 Review of Scanning Sensitivity Expressions and Results

One common expression for scanning sensitivity is based on the surveyor being able to detect three times the background level for low count rates (NUREG/CR-5849). However, experience shows that at background count rates of thousands of counts per minute, an increase of 25-50% is readily detected (DOE 1992). This reduction in the detectable level above background reflects the expected relationship of detectability as a function of the square root of the background rate (refer to static MDC expression in Section 3).

The specification of detectable levels is complicated by the difficulty of defining "detectable" as applied to the performance of the surveyor. For example, guidance on scanning capabilities is given in draft ANSI Standard 13.12, "Control of Radioactive Surface Contamination on Materials, Equipment, and Facilities To Be Released for Uncontrolled Use." This document states that the scanning speed shall be slow enough to ensure that a small-diameter source is

detected with a 67% probability. However, the specification of scan MDC requires a policy regarding false positives as well; note that the familiar static MDC equations typically use a false positive rate of 5%. In theory, any correct detection rate can be achieved for any source intensity if the number of false positives permitted is unlimited.

A few attempts to quantify scanning sensitivity experimentally have been reported. Scanning MDCs have been evaluated for both alpha and beta instrumentation under varying background conditions using a semi-empirical approach (Goles et al. 1991). MDCs were defined as that activity that could be detected 67% of the time under standard survey conditions. The instruments evaluated were, for alpha detection, a 50-cm² portable alpha monitor, a 100-cm² large-area scintillation monitor, and a 100-cm² gas proportional counter; for beta/gamma detection, a pancake GM probe, a 100-cm² large-area scintillation monitor, and a 100-cm² gas proportional counter. The test procedure involved maintaining a scan rate of 5 cm/s, with a scan height held at 0.64 cm. Alpha sources were 2.54-cm-diameter, electroplated sources; beta/gamma sources consisted of point source geometries and uniformly dispersed geometries. The MDC for alpha activity was defined as the amount of activity that produces one count as the detector passes over the surface (alpha background was considered to be zero) and the MDC for beta/gamma activity was determined for different background activities (e.g., 50, 250, and 500 cpm), based on whether it could be detected 67% of the time. For the most part, the researchers concluded that detectors were more sensitive to point sources than to areal sources. The reported scanning sensitivities for the GM detectors demonstrated that activities producing net instrument responses of 305, 310, and 450 cpm could be statistically recognized 67% of the time in 50-, 250-, and 500-cpm background fields, respectively. (Goles et al. 1991, p. 4d) cautioned that the "data are highly idealized, and that the performance of these instruments may differ considerably under field conditions."

Sommers (1975) obtained experimental data to check the validity of the theoretical calculations of source detection frequency. Calibrated sources were moved past the detector windows to determine source detection frequencies for various velocities (ranging from 2.4 to 15 cm/s), and source-detector distances in a background of 120 cpm. The experimental results are averages over 100 observations per datum point from two or more experienced surveyors. The effects of varying instrument time constants, probe velocity, and background activities on source detection frequencies (in percent) were plotted. The researcher concluded that source detection frequencies were strongly dependent on source strength, survey velocity, background activity, detector sensitivity, and the time constant of the survey meter. At scanning speeds of 10 to 15 cm/s, a source strength of 10,000 to 15,000 betas/min was required to provide a detection frequency of 90%. It was also determined that "with small diameter sources emitting 5,000 betas/min, source detection frequency at 120 counts/min background is about 80% using the speaker outputs, regardless of the survey velocities between 3.5 and 15 cm/s" (Sommers 1975, p. 760).

In LA-10729, Olsher et al. determined the scanning sensitivity of alpha detection instrumentation by measuring the hot spot detection frequency under realistic survey conditions. The procedure

involved more than 40 surveyors with varying levels of experience, who were asked to survey five stations, each consisting of a 4-foot \times 4-foot section of masonite that was painted with a Th-232-based paint. The thorium-based paint, which was the same color as the original paint and thus hid the hot spots, was applied to nine locations at each station. The alpha activity levels ranged from 64 to 672 dpm. The surveyors were instructed to survey each of the five stations and to record their results on a survey grid map. The detection frequency and false positive frequency were determined for each survey group. The alpha source activity for a 50% detection frequency ranged from 392 to 913 dpm for the ZnS scintillation detectors evaluated. One interesting result of this evaluation was that less-experienced surveyors had a higher detection probability than did experienced surveyors. The authors attributed this to the fact that the inexperienced surveyors took approximately twice as long to complete the scan survey.

Lastly, in a radiation detection experiment performed by 25 health physics technicians, Thelin obtained experimental data to evaluate the scan MDC for a portable scintillation detector (Thelin 1994). Eight sources were randomly placed against the inner surface of a box with approximate dimensions 46 \times 36 \times 30 cm. The source levels ranged from 236 to 1516 net cpm. The technicians were asked to scan the outside of the box and to identify locations that have higher count rates than the box background. The number of sources identified by each technician was evaluated and a hyperbolic function was fit to the experimental data. Thelin reports that at a background count rate of 482 ± 52 cpm at 2 sigma, the technicians were able to locate and identify source levels of 700 cpm approximately 90% of the time.

6.3 Signal Detection Theory

Signal detection theory provides a means for characterizing the performance of surveyors performing scans. The theory relies on the statistical decision techniques derived in Section 3 and applies to the detection of signals in background noise by surveyors. Personnel conducting radiological surveys for residual contamination at decommissioning sites must interpret the audible output of a portable survey instrument to determine when the signal ("clicks") exceeds the background level by a margin sufficient to conclude that contamination is present. It is difficult to detect low levels of contamination because both the signal and the background vary widely.

In abstract terms, the task of personnel conducting radiological scan surveys can be briefly characterized as follows. The condition of the surface being scanned is represented to the surveyors by samples from random processes (Poisson distributed counts). Furthermore, the samples are limited in size (i.e., time constraint depending on scan speed) for practical reasons. On the basis of the samples, the surveyors must decide whether they have sampled the distribution of activity associated with a contaminated surface or an uncontaminated surface (background only). The concepts and methods of signal detection theory are well suited to the analysis of performance on such tasks, and require the specification of the acceptable Type I and Type II error rates. NUREG/CR-6364 describes signal detection theory in greater detail.

The information available to the observer can arise from either noise alone or from signal-plus-noise and can be represented by two (typically overlapping) probability density distributions (Figure 6.1). The task of the observer is to indicate whether an increase in survey instrument output arose from a “noise alone” or a “noise plus signal” event. To make this decision, a criterion must be established at some point along the continuum—e.g., once the criterion point is set, any measurement greater (to the right) than the criterion will be interpreted as contamination. If the underlying distributions can be assumed to be normal and of equal variance, an index of sensitivity (d') can be calculated which represents the distance between the means of the distributions in units of their common standard deviation. The index is calculated by transforming the true positive and false positive rates to standard deviation units, i.e., z-scores (Egan 1975, p.61) and taking the difference:

$$d' = z(\text{false positive}) - z(\text{true positive}) \quad (6-3)$$

Values of d' associated with various true positive and false positive rates are provided in Table 6.1. The d' measure is independent of the criterion adopted by the surveyor, thus allowing meaningful comparisons of sensitivity under conditions in which surveyors' criteria may be different. As stated above, surveyors' criteria may vary for a number of reasons. The relative operating characteristic (ROC) relates the probability of a correct detection to that of a false positive as the response criterion is varied (Figure 6.2). It is conventional in signal detection theory analysis to describe performance in terms of the true positive rate ($1-\beta$) and the false positive rate (α). The remaining two response conjunctions, true negatives (or correct rejections) and false negatives (“misses”) are simply the complements of the preceding quantities.

6.4 Human Factors and Two Stages of Scanning

According to statistical decision theory, the *a priori* probabilities of the events and the values and costs associated with the outcomes will influence the placement of the criterion, which is a human factors effect. Thus the detection of a signal in a noise background is determined not only by the magnitude of the signal relative to the background (d'), but also by the willingness of the surveyor to report that a signal is present, i.e., the criterion for responding “yes.” The criterion depends on two factors: response value/cost and signal probability. If, for example, a Type I error (false positive) entails a significant cost, the observer will position the criterion more conservatively (e.g., criterion C in Figure 6.1); if it is expected that signals will greatly outnumber non-signals, a more liberal placement of the criterion will yield optimal results (e.g., criterion A in Figure 6.1), but at the cost of significant false positives. It is postulated that, in the context of scanning, the Type I and Type II error rates are embodied in the criterion established by the observer for deciding based on instrument response that contamination is present.

The surveyor's decision itself is influenced by a variety of factors, including the relative costs of “misses” and “false positives,” and the surveyor's assumptions regarding the likelihood of

contamination being present. The principle implication of the signal detection theory perspective for scanning performance is that, in view of the nature of the task, one must consider false positive rate as well as correct detection rate in order to meaningfully characterize human performance. The rewards or penalties associated with various outcomes influence subjects' responses. In the context of scanning surveys, these factors may affect performance significantly. Surveyors are typically motivated to detect all instances of possible contamination, i.e., to maximize the correct detection rate. However, there are costs associated with incorrectly identifying areas as being contaminated (e.g., making follow-up static measurements or collecting and analyzing samples). The placement of the criterion reflects a balance between these two influences. Observers' estimates of the likelihood/frequency of signals will also influence their willingness to decide that a signal is present. Other things being equal, then, a surveyor will adopt a less-strict criterion when examining areas in which contamination may be expected. Similarly, surveyors' criteria may be more strict when examining areas in which they don't expect contamination to be present. The nature of this decision process is considered in more detail below.

In practice, surveyors do not make decisions on the basis of a single indication. Rather, upon noting an increased number of counts, they pause briefly and then decide whether to move on or take further measurements. Thus, scanning consists of two components: continuous monitoring and stationary sampling. In the first component, characterized by continuous movement of the probe, the surveyor has only a brief "look" at potential sources, determined by the scan speed. The surveyor's criterion (i.e., willingness to decide that a signal is present) at this stage is likely to be liberal, in that the surveyor should respond positively on scant evidence, since the only "cost" of a false positive is a little time. The second component occurs only after a positive response was made at the first stage. It is marked by the surveyor interrupting his scanning and holding the probe stationary for a period of time, while comparing the instrument output signal during that time to the background counting rate. Owing to the longer observation interval, sensitivity is relatively high. For this decision the criterion should be more strict, since the cost of a "yes" decision is to spend considerably more time taking a static measurement or sample. If the observation interval is sufficiently long, an acceptable rate of source detection can be maintained despite application of the more stringent criterion. For example, the solid line in Figure 6.2 represents performance for a 4-second observation. Under these conditions, roughly 95% correct detections can be achieved with only 10% false positives.

Owing to the fact that scanning can be divided into two stages, it is necessary to consider the surveyor's scan sensitivity for each of the stages. Typically, the MDCR associated with the first scanning stage will be greater due to the brief observation intervals of continuous monitoring—provided that the length of the pause during the second stage is significantly longer. Typically, observation intervals during the first stage are on the order of 1 or 2 seconds, while the second stage pause may be several seconds long. The greater value of MDCR from each of the scan stages is used to determine the scan sensitivity for the surveyor.

6.5 The Ideal Observer Paradigm

In addition to allowing surveyors' sensitivity to be evaluated independently from their decision criteria, signal detection theory also allows their performance to be compared to that of an ideal observer. In this section, an ideal observer approach to detection in the context of radiological scans is outlined, and the results of relevant laboratory findings are summarized.

If the nature of the distributions underlying a detection decision can be specified, it is possible to examine the performance expected of an ideal observer, i.e., one that makes optimal use of the available information to achieve a specified goal (e.g., to maximize the percent correct responses). This is of interest in the present context because it allows the basic relationships among important parameters (e.g., background rate and length of observation) to be anticipated, and it provides a standard of performance (actually an upper bound) against which to compare performance of actual surveyors.

The audio output of a survey instrument represents randomly occurring events. It will be assumed that the surveyor is a "counting" observer, i.e., one that makes a decision about the presence or absence of contamination based on the number of counts occurring in a given period of time. This number will have a Poisson distribution, and the mean of the distribution will be greater in the presence of contamination than when only background activity is present. When the intensity of activity associated with contamination is low, as it often is during final status surveys, these distributions will overlap. The ideal observer decides that contamination is present if the number of counts is greater than x , where the criterion value x is chosen to maximize percent correct. NUREG/CR-6364 describes the process by which the performance expected for an ideal observer (in terms of correct detection and false positive rates) can be determined from tabled values of the cumulative Poisson distribution.

If acceptable performance (in terms of true and false positive rates) can be specified, the source levels required to support such performance for the ideal observer can be estimated. Section 6.7 provides the calculation approach for determining the MDCR for the ideal observer. It can be shown (Egan 1975) that the MDCR would be expected to be proportional to the square root of the number of background counts. Thus, the minimum detectable net source is a multiple of the background level at count rates typical for GM detectors, and a fraction of the background level at count rates typical for gas proportional and NaI scintillation detectors.

6.6 Actual Surveyor Performance - Field Tests and Computer Simulations

The performance of surveyors conducting scans was examined under field conditions and using computer simulations. As described in the previous section, signal detection theory offers a means of understanding the constraints on human performance in such tasks. This section describes the methods and results of field studies designed to assess the performance of surveyors

working under conditions that were reasonably close to those encountered in actual surveys but that nevertheless allowed performance measures to be collected. Laboratory studies using simulated sources and backgrounds are summarized—complete descriptions of the methodology and analysis of results are provided in NUREG/CR-6364. These studies quantified the abilities of surveyors under more controlled conditions.

6.6.1 Field Tests of Surveyor Performance

Scan surveys were conducted under controlled conditions to examine the abilities of surveyors to detect typical source configurations in circumstances that approximated those encountered in the field. Both indoor and outdoor field scan tests were conducted using standard survey instruments for scanning.

6.6.1.1 General Methodology of Field Tests

Experiments were designed and analyzed in accord with the human factors considerations developed previously. Specifically, the surveyors' behavior during the scanning surveys was recorded in a way that allowed both components (continuous and stationary) of the scanning activity to be examined, and an analysis was used which allowed both true positive and false positive rates to be estimated. As a result, it was possible to describe the scanning process (rather than just the result), and to make meaningful performance comparisons among surveyors and among conditions.

The true positive rates for the continuous and the stationary components of the scanning task were determined by dividing the number of sources to which one or more positive responses were made by the number of radioactive source configurations. For the continuous scanning component, a pause in the movement of the probe was considered a positive response. A response was considered to have been associated with a source if it fell within any of the areas of elevated activity as mapped before the start of the field trials. (It should be emphasized that positive responses occurred simply by the surveyor pausing at these source locations, even if the surveyor subsequently concluded that the response did not represent a signal above background.) For the stationary component, a positive response was the identification of a location as a source judged to be in excess of background by the surveyor. The number of false positives for the continuous task was computed as the total number of times the surveyor paused minus the number of pauses associated with sources. An estimate of the number of opportunities for a false positive was required in order to compute the false positive rate (refer to NUREG/CR-6364).

The experiments employed actual radioactive sources and scanning instrumentation. Radioactive sources were positioned so that they could not be detected visually by the surveyors. The surveyors were given written instructions (see example, Figure 6.3) and a scale map of the test area to be scanned, and then instructed to perform a 100% scan of the test area at a specified scan rate. Surveyors marked on the map the areas they judged as containing residual activity in excess

of background along with the actual meter reading (in cpm) for those areas. While the surveys were being conducted, observers recorded on a similar map any locations at which the surveyor briefly paused.

The indoor experiments consisted of performing scans for beta activity on an interior wall at a height of 0.5 to 2 m with a GM detector (20 cm² probe area) and a gas proportional detector (126 cm² probe area). The length of the wall section surveyed was 5 m, resulting in a test area of 7.5 m². Scale maps of the indoor test area for the GM and gas proportional detector scans are shown in Figures 6.4 and 6.5. In the outdoor experiment, an area measuring 20 m × 30 m was surveyed. Figure 6.6 shows the scale map of the outdoor field test area. The scanning technique for the outdoor field test consisted of swinging the NaI detector from side to side, keeping the detector just above the surface of the ground at its lowest point. Surveyors covered 100% of the test area using lanes 1 m wide at a scan rate of 0.5 m/s. Additional detail concerning the field tests methodology is provided in NUREG/CR-6364.

6.6.1.2 Field Test Results

The field test results are described in NUREG/CR-6364; a few key points are discussed in this section. The analysis of the ideal observer demonstrated that the time for which the activity is sampled determines the information that is available to the surveyor. Thus, if the probe is moved too quickly, the distributions of activity on which the surveyor's decision is based will not be sufficiently distinct to support acceptable performance. This effect may have been the reason for some relatively intense sources going undetected in the outdoor survey. Although the movement of the probes was not directly measured in any of the field tests, differences in technique among surveyors were noted by the observers and probably contributed to apparent differences in sensitivity.

Similarly, surveyors sometimes failed to correctly identify sources at locations they had paused over—this may have been due to the probe being held stationary for too short a time to support a sufficiently high correct detection rate given the strict criterion for a final positive response.

The importance of the surveyor's criterion for pausing the probe was evident from the analysis of the ideal observer. The operating point for the first (continuous) component established the upper bound for correct detection rate, reflecting the need for the criterion to be quite liberal at the first scan stage. The field tests confirmed that surveyors generally do adopt liberal criteria (i.e., they paused often), but the data indicated that there was much variation among surveyors in this regard—correct detections varied greatly with changes in this criterion, especially for difficult-to-detect sources (e.g., the indoor GM survey).

Equally important in determining the minimum detectable concentration is the surveyor's criterion for identifying areas as contaminated. The field tests revealed considerable variation among surveyors—even between surveyors with roughly equal sensitivity. The extent to which

surveyor's performance in this case is subject to the assumed likelihood of a source being present, or the frequency of sources being found as the survey progresses, was also unknown.

To summarize, the important points from the field tests are (1) the sensitivity can vary considerably among surveyors, (2) the surveyor's choice of a criterion for a positive response is quite important in determining success in identifying sources—both to the decision to momentarily pause moving the probe and to the final decision regarding the presence of contamination, and (3) although a surveyor's training, experience, and scanning technique may afford adequate sensitivity to detect a given source level, detection performance may not be optimal unless *both* of these decisions are based on appropriate criteria that do not vary significantly over the course of the survey.

6.6.2 Computer Simulation Tests of Surveyor Performance

This section gives a general overview of the computer simulation tests performed to evaluate scan sensitivity—NUREG/CR-6364 provides greater detail of the procedures and results.

A computer simulation of the audio output of a survey device was developed, which allowed audio signals representing various combinations of source and background activity levels to be easily produced. Programming was added to implement a variety of psycho-physical procedures, a user interface to collect surveyor responses, and various scoring and data recording routines. In the simulation tests, three different psycho-physical procedures were used in conjunction with the survey simulation. The procedures addressed different aspects of scanning survey performance.

6.6.2.1 Adaptive Procedure

An *adaptive* procedure was used to determine the source intensity needed to support an arbitrarily chosen level of performance (75% correct) under various conditions. The objective was to determine whether the square root relationship predicted on the basis of the analysis of the ideal observer could be used to predict scanning performance. Since background rates encountered in field surveys can vary over a wide range depending on type of equipment used and type of location to be surveyed, a range of background rates was simulated in the experiments. Because detectability (for the ideal observer) is also determined by the length of the observation, various observation intervals were simulated as well.

Results were evaluated for net source levels corresponding to 75% correct performance for detection in backgrounds of 60, 120, 240, 1,000, 3,000, and 6,000 cpm. Similar to the values for lower background rates, the values for 3,000 and 6,000 cpm define a line with a slope of 0.5 on log-log axes; that is, the 'square root of background' relationship apparently holds. This indicates not only that the 'square root relationship' adequately describes performance at high as well as low background rates, but also that surveyor efficiency does not vary greatly over this range.

The results of the adaptive experiment indicate that if a given source level allows acceptable performance for a certain background rate and probe speed, it is possible to estimate the source level expected to yield equal detectability for other backgrounds and speeds. It should also be noted that, given the high degree of variability in actual performance (within and between individuals), this prediction is of *average* performance.

6.6.2.2 Confidence Ratings Procedure

A detection procedure employing *confidence ratings* was used to determine not only the true and false positive rates associated with a given condition but also the operating characteristic for each surveyor. Results from this procedure allowed a number of aspects of performance to be considered. The data allowed the calculation of independent measures of sensitivity and criterion. The objective was to determine the relationship of actual to ideal performance and to examine differences among surveyors. On the basis of the ROCs derived from the confidence ratings, it was also possible to determine whether a simple signal detection theory model could be used to predict changes in performance associated with changes in criteria.

The surveyors' actual performance as compared with what is ideally possible (given the statistics of the distributions of background and source counts) is an indication of the efficiency of the surveyors. This efficiency can be modeled by assuming that the surveyor, like the survey instrument, does not necessarily register every event. By adjusting the proportion of counts that the ideal observer registers, it is possible to roughly equate the ideal and actual performance. The proportion at which the two most closely coincide can be taken as the efficiency of the surveyor. The efficiencies established by this method for the four surveyors who completed the confidence rating experiment were between 0.5 and 0.75.

6.6.2.3 Continuous Monitoring Procedure

In the continuous *monitoring* procedure, observation intervals were not defined for the surveyor and no feedback was given as to the correctness of responses. The objective was to examine performance under circumstances closer to those characteristic of actual survey scanning. For a given background rate and observation interval length (simulated probe speed), sources were presented at random intervals during data collection sessions. The surveyors' task was to respond (by clicking a button on the computer display) whenever they detected evidence of a source. This was equivalent to the decision to momentarily halt the movement of the probe. Surveyors were then allowed to listen to the simulation for as long as they wished before making a second, yes/no decision regarding whether a source was being simulated. Thus, from the surveyor's point of view, the simulation was a reasonably close approximation of the actual task.

Using the methods discussed in NUREG/CR-6364, an index of detectability (d') was computed for the conditions simulated. Comparison of these results with the expected performance of the ideal observer and with the performance of the actual surveyor in defined-interval detection

indicated the “efficiency” of the surveyor under conditions that approximate those of actual survey activity.

Surveyors adopted criteria that allowed them to respond during or immediately after the presentation of 90% or more of the simulated sources. That is, they seemed to respond as they would in the field, pausing often as a means of minimizing the number of sources missed. The proportion of background intervals in which one or more responses were recorded ranged from 0.58 to 0.98. Pauses typically lasted roughly 4 to 5 seconds, although many longer pauses (8 seconds or more) were recorded. Examination of a portion of the yes/no decisions made after the pauses indicated that very few sources were missed at this stage, but the false positive rate was also relatively high (roughly 0.25). As expected, performance in these undefined interval tasks was poorer than that in the defined interval situation for the same background and source intensities.

6.6.2.4 General Discussion

Taken together, the results of the simulation studies indicate the extent to which human limitations and the nature of the scanning task reduce the efficiency of the surveyor relative to an ideal observer. The ideal observer attempting to detect 180 cpm (gross) in a background of 60 cpm (i.e., a source three times background), in a 4-second observation interval, will be capable of correctly detecting the source roughly 91% of the time with about 5% false alarms (determined from tabulated values of the cumulative Poisson distribution). This corresponds to a d' value of roughly 3. In the defined interval rating task, using the same background and source values, a typical surveyor detected about 90% of the sources with a false positive rate of 14% for a d' value of about 2.4. In the undefined interval procedure, under the same conditions, the performance of the same surveyor yielded a d' value of 1.8. This demonstrates that (1) even under ideal circumstances (i.e., with defined observation intervals) humans do not behave as perfect counting devices (i.e., they are less efficient than the ideal observer), and (2) in scanning, where observation intervals are not defined, the efficiency of the surveyor (relative to the ideal observer) declines further.

6.7 Estimation of Scan Minimum Detectable Count Rates (MDCRs)

The changes in detectability as a function of background level and observation interval (as determined in simulation studies using adaptive level adjustment) were consistent with theoretical predictions, i.e., the number of source counts required to yield a constant level of performance was proportional to the square root of the number of background counts in the observation. Therefore, if performance is known to be acceptable for a given background/source condition and observation interval, it is possible to estimate source levels expected to support similar performance under other conditions.

6.7.1 Determination of MDCR and Use of Surveyor Efficiency

If a value is assumed for the surveyor efficiency, the number of source counts required to yield a particular level of performance (specified in terms of d') can be estimated. The surveyors' actual performance as compared with what is ideally possible (given the statistics of the distributions of background and source counts) is an indication of surveyor efficiency. This efficiency can be modeled by assuming that the surveyor, like the survey instrument, does not register every event. By adjusting the proportion of counts that the ideal observer registers, it is possible to roughly equate the ideal and actual performance. The proportion at which the two most closely coincide can be taken as the efficiency of the surveyor. Specifically, the surveyor efficiency is used to adjust both the background and source distributions, effectively degrading the counting information available to the surveyor. On the basis of the results of the confidence rating experiment, this efficiency was estimated to be between 0.5 and 0.75. Interestingly, in the limited study of extended periods of monitoring, there was no evidence of the further decrease in performance that might have been expected owing to either a criterion shift or a loss of sensitivity. It cannot be concluded, however, that such decrements would not occur with other observers under other conditions, and it is probably advisable to assume an efficiency value at the lower end of the observed range (i.e., 0.5) when making MDC estimates.

Egan (1975, p. 182) shows that detectability for Poisson distributions can be expressed as

$$D \approx \frac{s_i}{\sqrt{b_i}} \quad (6-4)$$

where b_i is the average number of background counts in an interval. For background rates, b , in cpm and observation interval length, i , in seconds, $b_i = b(i/60)$. The detectability index (D) is asymptotically equal to d' . The minimum detectable number of net source counts in the interval is given by s_i . Therefore, for an ideal observer, the number of source counts required for a specified level of performance can be arrived at by multiplying the square root of the number of background counts by the detectability value associated with the desired performance (as reflected in d'); i.e.,

$$s_i = d' \sqrt{b_i} \quad (6-5)$$

where the value of d' is selected from Table 6.1 based on the required true positive and false positive rates.

For example, suppose that one wished to estimate the minimum count rate that is detectable by scanning in a background of 1500 cpm. Note that the minimum detectable count rate must be considered for both scan stages—and the more conservative value is selected as the minimum

count rate that is detectable. It will be assumed that a typical source remains under the probe for 1 second during the first stage, therefore, the average number of background counts in the observation interval is 25 ($b_i = 1500 * (1/60)$). Furthermore, as explained earlier, it can be assumed that at the first scanning stage a high rate (e.g., 95%) of correct detections is required, and that a correspondingly high rate of false positives (e.g., 60%) will be tolerated. From Table 6.1, the value of d' representing this performance goal is 1.38. The net source counts needed to support the specified level of performance (assuming an ideal observer) will be estimated by multiplying 5 (the square root of 25) by 1.38. Thus, the net source counts per interval, s_i , needed to yield better than 95% detections with about 60% false positives is 6.9. The minimum detectable source count rate, in cpm, may be calculated by

$$MDCR = s_i * (60 / i) \tag{6-6}$$

which, for this example, is equivalent to 414 cpm (1914 cpm gross). Table 6.2 provides the scan sensitivity for the ideal observer (MDCR) at the first scanning stage for various background levels, based on an index of sensitivity (d') of 1.38 and a 2-second observation interval. The MDCR for the second scanning stage must now be considered.

The minimum number of source counts required to support a given level of performance for the final detection decision (second scan stage) can be estimated using the same method. As explained earlier, the performance goal at this stage will be more demanding. The required rate of true positives remains high (e.g., 95%), but fewer false positives (e.g., 20%) can be tolerated, so that d' (from Table 6.1) is now 2.48. It will be assumed that the surveyor typically stops the probe over a suspect location for at least 4 seconds before making a decision, so that the average number of background counts in an observation interval is 100 ($b_i = 1,500 * (4/60)$). Therefore, the minimum detectable number of net source counts, s_i , needed will be estimated by multiplying 10 (the square root of 100) by 2.48 (the d' value); so s_i equals 24.8. The MDCR is calculated by $24.8 * (60/4)$ and equals 372 cpm. Thus, the MDCR is greater at the first stage (414 vs. 372 cpm), and will be used for purposes of estimating the scan MDC, which requires consideration of the surveyor efficiency.

For a less-than-ideal observer, Egan (1975, p. 187) shows that detectability is reduced by the efficiency of the surveyor, p , and becomes

$$D \approx \frac{s_i p}{\sqrt{b_i p}} \approx \frac{s_i \sqrt{p}}{\sqrt{b_i}} \tag{6-7}$$

The minimum detectable net source counts in the observation interval for the less-than-ideal surveyor (p), again using d' to reflect the desired performance, may be written

$$S_{\text{surveyor}, i} = \frac{d' \sqrt{b_i}}{\sqrt{P}} \quad (6-8)$$

To continue with the above example, the minimum source counts needed by a surveyor, $S_{\text{surveyor}, i}$, with an efficiency of 0.5, is estimated by dividing 6.9 by $\sqrt{0.5}$ (equals 9.8 counts in 1-second observation interval). Thus the required number of net source counts for the surveyor, $\text{MDCR}_{\text{surveyor}}$, is 585 cpm (2,085 cpm gross). Remember, based on the limited research conducted in this study, it is advisable to assume a surveyor efficiency value at the lower end of the observed range (i.e., 0.5) when making scan MDC estimates. Note that the term MDCR (without subscript) refers to the performance of the ideal observer, and $\text{MDCR}_{\text{surveyor}}$ related to the performance of the surveyor.

It should be noted that the detectable count rates estimated as described above will not necessarily be similar (414 vs. 372 net cpm) for the first and second stages of the detection model. (The pause length at which the detectable net source is equal for the two stages depends on the choice of d' for each stage.) When attempting to estimate the minimum detectable count rate for given performance requirements, one should choose the greater of the two MDCR values at each scan stage. Typically, the value associated with the first (scanning) stage will be greater, owing to the relatively brief intervals assumed. It should be noted, however, that if the length of the pause (i.e., the interval assumed for the second stage) is not significantly longer than the interval assumed for the first stage, the MDCR value associated with the second stage will be greater.

6.7.2 Review of Assumptions and Results

As a means of summarizing the development of the method for estimating MDCR, each of the key assumptions and the relevant experimental results will be briefly reviewed below.

The central assumption in the estimation of minimum detectable count rate described in this report is that the minimum detectable increment in the number of counts in an observation varies as a function of the square root of the number of background counts in an observation. This is based on a signal detection theory model of a Poisson (or "counting") observer. The results of the adaptive simulation experiments indicated that this relationship adequately represents observers' performance over a wide range of background rates. It should be noted, however, that for low background rates there was considerable variability in these results both within and between observers.

It was assumed that observers' performance could be related to that expected of an ideal observer by an efficiency factor which represents the probability of a count being recorded by the observer's decision process, thus reducing the effective number of background and source counts in the observation. The results of the defined-interval confidence rating experiment indicate that

this factor is no greater than 0.75. The monitoring (undefined interval) results, along with human factors literature, suggest that a value of 0.5 is more appropriate in estimating minimum levels detectable in the field.

The use of d' to convert performance requirements (desired detection rate and permissible false positive rate) into an index of detectability implicitly assumes that the distributions underlying the observers' performance are normal. As mentioned earlier, the fact that the ROCs resulting from the confidence rating experiments were not markedly asymmetrical indicates that the assumption of normality is acceptable.

Finally, it was assumed that surveyors would employ a lenient criterion for pausing the probe (i.e., pausing often) and a more strict criterion when judging the activity observed during the pause. The results of the field experiments were consistent with this assumption and provided a basis for the true and false positive rates assumed in the sample calculations in the previous section. However, as with the other results, there was considerable variation in surveyors' performance in the field studies. The values used in the examples were typical of the best-performing surveyors. This brings up the point that, although a surveyor efficiency factor was used to adjust estimates calculated in the previous section, the estimates may still represent "ideal" performance with respect to the criteria adopted by the hypothetical surveyor. It is assumed that the surveyor "chooses" and is able to maintain criteria for both decision stages that will allow a desired overall level of performance to be achieved. Of course, surveyors do not consciously set the precise parameters of their behavior; nor are they necessarily aware of changes in these values as a survey progresses. It should also be recognized that estimates produced as illustrated in this document reflect performance typical of a relatively small number of surveyors.

In addition to providing a basis for estimates of MDCR, the model of survey activity described in the previous section implies an optimal relationship between the lengths of the observations associated with the first and second detection stages, deviation from which will result in poorer overall performance. Experiments in which the movements of the probe are tracked and timed would reveal whether surveyors' actual performance approximates the predicted relationship. Because time limitations (explicit or implicit) are necessarily a part of the survey task, surveyors' relative allocation of time to scanning and pausing when the total time available is limited will have a great influence on their effectiveness.

6.8 Scan MDCs for Structure Surfaces and Land Areas

The survey design for determining the number of data points for areas of elevated activity (as in the MARSSIM guidance) depends on the scan MDC for the selected instrumentation. In general, alpha or beta scans are performed on structure surfaces to satisfy the elevated activity measurements survey design, while gamma scans are performed for land areas. Because of their low background levels, the determination of scan MDCs for alpha contaminants is not generally applicable using the approach described in Section 6—rather, the reader is referred to the

MARSSIM manual for an appropriate methodology for determining alpha scan MDCs for building surfaces. In any case, the data requirements for assessing potential elevated areas of direct radiation depend on the scan MDC of the survey instrument (e.g., floor monitor, GM detector, NaI scintillation detector).

6.8.1 Scan MDCs for Building/Structure Surfaces

The scan MDC is determined from the minimum detectable count rate (MDCR) by applying conversion factors that account for detector and surface characteristics and surveyor efficiency. As discussed above, the MDCR accounts for the background level, performance criteria (d'), and observation interval. The observation interval during scanning is the actual time that the detector can respond to the contamination source—it depends on the scan speed, detector size in direction of scan, and size of the hot spot. In this context, the size of the hot spot relates to the area of detection defined by the detector-to-source geometry (for instance, a 2-mm² point source may produce an effective hot spot area of over 100 cm²). Therefore, the greater the contamination source effective area, and slower the scan rate, the greater the observation interval. Because the actual areal dimensions of potential hot spots in the field cannot be known *a priori*, it becomes necessary to postulate a certain hot spot area (e.g., perhaps 50 to 200 cm²), and then to select a scan rate that provides a reasonable observation interval. Finally, the scan MDC for structure surfaces may be calculated as follows:

$$\text{Scan MDC} = \frac{\text{MDCR}}{\sqrt{p} \epsilon_i \epsilon_s \frac{\text{probe area}}{100 \text{ cm}^2}} \quad (6-9)$$

where

ϵ_i = the instrument efficiency, and
 ϵ_s = the surface efficiency (refer to Section 5).

As an example, the scan MDC (in dpm/100 cm²) for Tc-99 on a concrete surface may be determined for a background level of 300 cpm and a 2-second observation interval using a hand-held gas proportional detector (126 cm² probe area). For a specified level of performance at the first scanning stage of 95% true positive rate and 60% false positive rate (and assuming the second stage pause is sufficiently long to ensure that the first stage is more limiting), d' equals 1.38 (Table 6.1) and the MDCR is 130 cpm (Table 6.2). Using a surveyor efficiency of 0.5, and assuming instrument and surface efficiencies of 0.36 and 0.54, respectively, the scan MDC is calculated as follows:

$$\text{Scan MDC} = \frac{130}{\sqrt{0.5} (0.36) (0.54) (1.26)} = 750 \text{ dpm}/100 \text{ cm}^2 \quad (6-10)$$

The scan MDC above may be compared to the static MDC (1-minute count) for the same detector of approximately 340 dpm/100 cm² using Equation 3-9.

The scan MDC in the above example may be calculated using a faster scan rate, such that yields only a 1-second observation interval. Assuming other parameters in the example remain constant, the calculation steps are

- (1) $b_i = (300 \text{ cpm}) * (1 \text{ sec}) * (1 \text{ min}/60 \text{ sec}) = 5 \text{ counts}$
- (2) $\text{MDCR} = (1.38) * (\sqrt{5}) * (60 \text{ sec}/1 \text{ min}) = 185 \text{ cpm}$
- (3) Calculate scan MDC:

$$\text{Scan MDC} = \frac{185}{\sqrt{0.5} (0.36) (0.54) (1.26)} = 1,070 \text{ dpm}/100 \text{ cm}^2 \quad (6-11)$$

The scan MDC may be calculated for a higher background level (400 cpm) and a 1-second observation interval. Assuming other parameters in the example remain constant, the calculation steps are

- (1) $b_i = (400 \text{ cpm}) * (1 \text{ sec}) * (1 \text{ min}/60 \text{ sec}) = 6.7 \text{ counts}$
- (2) $\text{MDCR} = (1.38) * (\sqrt{6.7}) * (60 \text{ sec}/1 \text{ min}) = 214 \text{ cpm}$
- (3) Calculate scan MDC:

$$\text{Scan MDC} = \frac{214}{\sqrt{0.5} (0.36) (0.54) (1.26)} = 1,230 \text{ dpm}/100 \text{ cm}^2 \quad (6-12)$$

Now consider an example to determine the scan MDC for a GM detector (20 cm²) that is used to scan a concrete wall potentially contaminated with Tc-99—in a background of 60 cpm and with a 2-second observation interval. Using the same level of performance, i.e., 95% correct detection rate and 60% false positive rate at the first scan stage, Table 6.2 provides an MDCR of 60 cpm.

Assuming instrument and surface efficiencies of 0.19 and 0.52, respectively, the scan MDC is calculated as follows:

$$\text{Scan MDC} = \frac{60}{\sqrt{0.5} (0.19) (0.52) (0.20)} = 4,300 \text{ dpm}/100 \text{ cm}^2 \quad (6-13)$$

Finally, an example for determining the scan MDC for a floor monitor is provided. The scan MDC for a large-area (573 cm²), gas proportional floor monitor may be calculated once a hot-spot area has been postulated. The hot-spot area is necessary not only for the observation interval determination, but also to calculate an appropriate probe area correction. That is, it is typical for the postulated hot-spot size to be less than the floor monitor probe area and, therefore, applying the standard probe area correction of 573 cm² /100 cm² (equals 5.73) is likely not appropriate. For example, assume that the floor monitor is used to scan a concrete floor for SrY-90 contamination, and the modeled hot-spot area is 100 cm² (probe correction factor is unity). Detector parameters include a background level of 1,200 cpm, instrument and surface efficiencies of 0.58 and 0.65, respectively, and a scan rate that yields a 1-second observation interval. The scan MDC is determined for the same level of performance (*d'* equals 1.38)

- (1) $b_i = (1,200 \text{ cpm}) * (1 \text{ sec}) * (1 \text{ min} / 60 \text{ sec}) = 20 \text{ counts}$
- (2) $\text{MDCR} = (1.38) * (\sqrt{20}) * (60 \text{ sec} / 1 \text{ min}) = 370 \text{ cpm}$
- (3) Calculate scan MDC as follows:

$$\text{Scan MDC} = \frac{370}{\sqrt{0.5} (0.58) (0.65) (1)} = 1,390 \text{ dpm}/100 \text{ cm}^2 \quad (6-14)$$

6.8.2 Scan MDCs for Land Areas

In addition to the MDCR and detector characteristics, the scan MDC (in pCi/g) for land areas is based on areal extent of the hot spot, depth of the hot spot, and the radionuclide (i.e., energy and yield of gamma emissions). If one assumes constant parameters for each of the above variables, with the exception of the specific radionuclide in question, the scan MDC may be reduced to a function of the radionuclide alone. It is generally assumed that NaI scintillation detectors are used for scanning land areas.

An overview of the approach used to determine scan MDCs for land areas follows. The NaI scintillation detector background level and scan rate (observation interval) are postulated, and the MDCR for the ideal observer, for a given level of performance, is obtained. A surveyor efficiency is selected, and then it is necessary to relate the surveyor MDCR ($\text{MDCR}_{\text{surveyor}}$) to a radionuclide

concentration in soil (in pCi/g). This correlation requires two steps—first, the relationship between the detector's net count rate to net exposure rate (cpm/ μ R/h) is established; and second, the relationship between the radionuclide contamination and exposure rate is determined.

For a particular gamma energy, the relationship of NaI scintillation detector count rate and exposure rate may be determined analytically (in cpm per μ R/h). The approach was to determine the gamma fluence rate necessary to yield a fixed exposure rate (1 μ R/h) as a function of gamma energy. The NaI scintillation detector response (cpm) was then related to the fluence rate at specific energies, considering the detector's efficiency (probability of interaction) at each energy. It was then possible to obtain NaI scintillation detector versus exposure rate for varying gamma energies (Table 6.3). An example using a 2" \times 2" NaI scintillation detector is provided for clarity. Assume that the cpm per μ R/h is needed for a gamma energy (E_γ) of 400 keV. The relative fluence rate to exposure rate (value has no particular units associated) may be calculated as follows:

$$\text{Fluence rate} \approx \frac{1 \mu\text{R/h}}{(E_\gamma) (\mu_{en}/\rho)_{air}} \approx \frac{1}{(400) (0.0296)} = 0.0844 \quad (6-15)$$

where (μ_{en}/ρ) is the energy absorption coefficient for air and the value used is for 400 keV.

Next, assuming that the primary gamma interaction producing the detector response occurs through the end of the detector (as opposed to the sides), the probability of interaction (P) for a 400 keV gamma may be calculated as follows:

$$P = 1 - e^{-(\mu/\rho)_{NaI} (x) (\rho_{NaI})} = 1 - e^{(0.117 \text{ cm}^2/\text{g})(5.1 \text{ cm}) (3.67 \text{ g/cm}^3)} = 0.89 \quad (6-16)$$

where

$(\mu/\rho)_{NaI}$ = the absorption coefficient for NaI (0.117 cm^2/g at 400 keV),

x = the thickness of the NaI (5.1 cm), and

ρ_{NaI} = the density of NaI (3.67 g/cm^3).

Therefore, the relative detector response for this energy is determined by multiplying the relative fluence to exposure rate (0.0844) by the probability of interaction (0.89)—equals 0.0750.

The manufacturer provides a value of 900 cpm per $\mu\text{R/h}$ for this detector for Cs-137. Using the same methodology described above for the Cs-137 gamma (662 keV), the relative detector response was 0.0396. Finally, the cpm per $\mu\text{R/h}$ for 400 keV for this detector is obtained by taking the ratio of the relative detector response at each energy

$$\text{cpm}/\mu\text{R/h, 400 keV} = (900) * \frac{0.0750}{0.0396} = 1,700 \text{ cpm}/\mu\text{R/h} \quad (6-17)$$

Therefore, once the relationship between the NaI scintillation detector response (cpm) and the exposure rate is known (Table 6.3), the $\text{MDCR}_{\text{surveyor}}$ (in cpm) of the NaI scintillation detector can be related to the minimum detectable net exposure rate. The minimum detectable exposure rate is used to determine the minimum detectable radionuclide concentration (i.e., the scan MDC) by modeling a specified hot spot.

Modeling (i.e., using Microshield™) of the hot spot (soil concentration) is used to determine the net exposure rate produced by a radionuclide concentration at a distance 10 cm above the source. This position is selected because it relates to the average height of the NaI scintillation detector above the ground during scanning. The following factors are considered in the modeling:

- radionuclide of interest (considering all gamma emitters for decay chains)
- concentration of radionuclide of interest
- areal dimensions of hot spot
- depth of hot spot
- location of dose point (NaI scintillation detector height above the surface)
- density of soil

Modeling analyses were conducted by selecting a radionuclide (or radioactive material decay chain) and then varying the concentration of the contamination. The other factors were held constant—the areal dimension of the cylindrical hot spot was 0.25 m^2 (radius of 28 cm), the depth of the hot spot was 15 cm, the dose point was 10 cm above the surface, and the density of soil was 1.6 g/cm^3 . The objective was to determine the radionuclide concentration that was correlated to the minimum detectable net exposure rate.

As an example, the scan MDC for Cs-137 using a $1.5'' \times 1.25''$ NaI scintillation detector is considered in detail. Assume that the background level is 4,000 cpm and that the desired level of performance, 95% correct detections and 60% false positive rate, results in a d' of 1.38. The scan rate of 0.5 m/s provides an observation interval of 1-sec (based on hot spot diameter of about 56 cm). The $\text{MDCR}_{\text{surveyor}}$ may be calculated assuming a surveyor efficiency (p) of 0.5 as follows:

- (1) $b_i = (4,000 \text{ cpm}) * (1 \text{ sec}) * (1 \text{ min}/60 \text{ sec}) = 66.7 \text{ counts}$
- (2) $\text{MDCR} = (1.38) * (\sqrt{66.7}) * (60 \text{ sec}/1 \text{ min}) = 680 \text{ cpm}$
- (3) $\text{MDCR}_{\text{surveyor}} = 680/\sqrt{0.5} = 960 \text{ cpm}$

The corresponding minimum detectable exposure rate is determined for this detector and radionuclide. The manufacturer of this particular 1.5" x 1.25" NaI scintillation detector quotes a count rate to exposure rate ratio for Cs-137 of 350 cpm/μR/h (Table 6.3), which is assumed to account for the 662-keV gamma emission from its short-lived progeny, Ba-137m. Although it is recognized that one must account for the resulting gamma energy spectrum incident on the NaI detector (both primary and scattered gamma radiation), the Microshield™ modeling code only considered primary gamma energies when evaluating the buildup from scattered photons. The NaI detector response will be greater during field applications as compared to the calculated detector response because the detector is more efficient at detecting lower energy scattered photons. This situation is anticipated to yield a conservative determination of the detector response and resulting scan MDC estimate.

The minimum detectable exposure rate is calculated

$$\begin{aligned} \text{Minimum detectable exposure rate} = \\ \frac{960 \text{ cpm}}{350 \text{ cpm}/\mu\text{R}/\text{h}} = 2.73 \mu\text{R}/\text{h} \end{aligned} \tag{6-18}$$

Both Cs-137 and its short-lived progeny, Ba-137m, were chosen from the Microshield™ library. The source activity and other modeling parameters were entered into the modeling code. The source activity was selected on the basis of an arbitrary concentration of 5 pCi/g, and converted to the appropriate units as follows:

$$\begin{aligned} (5 \text{ pCi}/\text{g}) * (1.6 \text{ g}/\text{cm}^3) * (1 \mu\text{Ci}/10^6 \text{ pCi}) \\ = 8E-6 \mu\text{Ci}/\text{cm}^3 \end{aligned} \tag{6-19}$$

The modeling code performed the appropriate calculations and determined an exposure rate of 1.307 μR/h (which accounts for buildup). Finally, the radionuclide concentrations of Cs-137 and Ba-137m (scan MDC) necessary to yield the minimum detectable exposure rate (2.73 μR/h) may be calculated as follows:

$$\text{Scan MDC} = (5 \text{ pCi/g}) * \frac{2.73 \text{ } \mu\text{R/h}}{1.307 \text{ } \mu\text{R/h}} = 10.4 \text{ pCi/g} \quad (6-20)$$

It must be emphasized that while a single scan MDC value can be calculated for a given radionuclide—other scan MDC values may be equally justifiable depending on the values chosen for the various factors, including the MDCR (background level, acceptable performance criteria, observation interval), surveyor efficiency, detector parameters and the modeling conditions of the contamination.

Determination of the scan MDC for radioactive materials—like uranium and thorium—must consider the gamma radiation emitted from the entire decay series. The following example considers the scan MDC for 3% enriched uranium using the same 1.5" × 1.25" NaI scintillation detector as in the previous example. It is assumed that the only variable change from the previous example is that 3% enriched uranium is modeled instead of Cs-137. Thus, the background level is 4,000 cpm, d' is 1.38, the observation interval is 1-second and the $\text{MDCR}_{\text{surveyor}}$ is 960 cpm, assuming a surveyor efficiency of 0.5.

Before the corresponding minimum detectable exposure rate can be determined for the detector and radioactive material decay series, it is necessary to run Microshield™ and determine the count rate to exposure rate ratio (in cpm/μR/h) by considering each of the gamma emissions and their contribution to the total exposure rate. The first step is to determine the source term for 3% enriched uranium. Realizing that, by weight, the ratio of U-235 to total uranium is 3%, and assuming an activity ratio of U-234-to-U-235 of 22—the activity fractions of 3% enriched uranium are 0.179, 0.036, and 0.785, respectively for U-238, U-235, and U-234. The short-lived progeny of U-238, Th-234 and Pa-234m, will also be present at the same activity fraction as U-238 (0.179) and Th-231, the progeny of U-235, will also be present at an activity concentration of 0.036. There are no short-lived progeny in the decay series immediately following U-234.

The source activity was selected based on an arbitrary concentration of 50 pCi/g for total uranium, divided between the uranium isotopes according to their activity fractions and converted to appropriate units for the modeling code. Therefore, the source term entered from the Microshield™ library was as follows:

- U-238 1.43E-5 μCi/cm³
- Th-234 1.43E-5 μCi/cm³
- Pa-234m 1.43E-5 μCi/cm³
- U-234 6.28E-5 μCi/cm³
- U-235 2.88E-6 μCi/cm³
- Th-231 2.88E-6 μCi/cm³

HUMAN PERFORMANCE AND SCANNING SENSITIVITY

The modeling code performed the appropriate calculations and determined the total exposure rate, with buildup, of 0.1747 $\mu\text{R}/\text{h}$. Additionally, Microshield™ provided the exposure rate for a number of gamma energies associated with the input source term. These data were used to weight the $\text{cpm}/\mu\text{R}/\text{h}$ value at each energy by the fractional exposure rate to estimate an overall $\text{cpm}/\mu\text{R}/\text{h}$ value specific to the source term. Specifically,

Energy (keV) (from Microshield™)	Exposure Rate ($\mu\text{R}/\text{h}$)	$\text{cpm}/\mu\text{R}/\text{h}$ (from Table 6.3)	$\text{cpm}/\mu\text{R}/\text{h}$ (weighted)
30	9.86E-4	2320	13.1
50	3.30E-4	5320	10.1
60	3.63E-3	5830	121
80	3.95E-3	5410	122
100	2.01E-2	4420	508
150	1.49E-2	2710	230
200	8.83E-2	1890	955
800	6.38E-3	270	9.86
1,000	3.62E-2	200	41.5

Total weighted $\text{cpm}/\mu\text{R}/\text{h}$ **2,010**

It is interesting to note that about 85% of the NaI scintillation detector's response to 3% enriched uranium is from gamma energies in the 100 to 200 keV range.

Finally, the minimum detectable exposure rate can be calculated using the $\text{cpm}/\mu\text{R}/\text{h}$ value, as follows:

$$\text{Minimum detectable exposure rate} = \frac{960 \text{ cpm}}{2,010 \text{ cpm}/\mu\text{R}/\text{h}} = 0.478 \mu\text{R}/\text{h} \quad (6-21)$$

Lastly, the scan MDC for 3% enriched uranium for the conditions stated in this example may be calculated as follows:

$$\text{Scan MDC} = (50 \text{ pCi/g}) * \frac{0.478 \mu\text{R}/\text{h}}{0.1747 \mu\text{R}/\text{h}} = 137 \text{ pCi/g} \quad (6-22)$$

Table 6.4 provides scan MDCs for common radionuclides and radioactive materials in soil. It is important to note that the variables used in the above examples to determine the scan MDCs for

HUMAN PERFORMANCE AND SCANNING SENSITIVITY

the 1.25" × 1.5" NaI scintillation detector—i.e., the $MDCR_{\text{surveyor}}$ detector parameters (e.g., cpm/ μ R/h), and the hot-spot conditions—have all been held constant to facilitate the calculation of scan MDCs provided in Table 6.4. The benefit of this approach is that generally applicable scan MDCs are provided for different radioactive contaminants. Additionally, the relative detectability of different contaminants is evident because the only variable in Table 6.4 is the nature of the contaminant.

Table 6.1 Values of d' for Selected True Positive and False Positive Proportions

False Positive Proportion	True Positive Proportion							
	0.60	0.65	0.70	0.75	0.80	0.85	0.90	0.95
0.05	1.90	2.02	2.16	2.32	2.48	2.68	2.92	3.28
0.10	1.54	1.66	1.80	1.96	2.12	2.32	2.56	2.92
0.15	1.30	1.42	1.56	1.72	1.88	2.08	2.32	2.68
0.20	1.10	1.22	1.36	1.52	1.68	1.88	2.12	2.48
0.25	0.93	1.06	1.20	1.35	1.52	1.72	1.96	2.32
0.30	0.78	0.91	1.05	1.20	1.36	1.56	1.80	2.16
0.35	0.64	0.77	0.91	1.06	1.22	1.42	1.66	2.02
0.40	0.51	0.64	0.78	0.93	1.10	1.30	1.54	1.90
0.45	0.38	0.52	0.66	0.80	0.97	1.17	1.41	1.77
0.50	0.26	0.38	0.52	0.68	0.84	1.04	1.28	1.64
0.55	0.12	0.26	0.40	0.54	0.71	0.91	1.15	1.51
0.60	0.00	0.13	0.27	0.42	0.58	0.82	1.02	1.38

Table 6.2 Scanning Sensitivity (MDCR) of the Ideal Observer for Various Background Levels^a

Background (cpm)	MDCR (net cpm)	Scan Sensitivity (gross cpm)
45	50	95
60	60	120
260	120	380
300	130	430
350	140	490
400	150	550
1,000	240	1,240
3,000	410	3,410
4,000	480	4,480

^aThe sensitivity of the ideal observer during the first scanning stage is based on an index of sensitivity (d') of 1.38 and a 2-second observation interval.

Table 6.3 NaI Scintillation Detector Count Rate Versus Exposure Rate (cpm per μ R/h)

Gamma Energy (keV)	cpm per μ R/h ^a	
	2" x 2" NaI Detector ^b	1.25" x 1.50" NaI Detector
20	2,200	990
30	5,160	2,320
40	8,880	3,990
50	11,800	5,320
60	13,000	5,830
80	12,000	5,410
100	9,840	4,420
150	6,040	2,710
200	4,230	1,890
300	2,520	1,070
400	1,700	700
500	1,270	510
600	1,010	390
662	900	350
800	710	270
1,000	540	200
1,500	350	130
2,000	260	100
3,000	180	70

^aBased on normalizing detector response to the cpm per μ R/h value provided by manufacturer for Cs-137. The calculational approach is described in the text.

^bDetector used was Ludlum Model 44-10; manufacturer provided 900 cpm per μ R/h for Cs-137.

^cDetector used was Victoreen Model 489-55; manufacturer provided 350 cpm per μ R/h for Cs-137.

Table 6.4 NaI Scintillation Detector Scan MDCs for Common Radiological Contaminants^a

Radionuclide/Radioactive Material	1.25" × 1.5" NaI Detector		2" × 2" NaI Detector	
	Scan MDC (pCi/g)	Weighted cpm/μR/h	Scan MDC (pCi/g)	Weighted cpm/μR/h
Am-241	44.6	5,830	31.5	13,000
Co-60	5.8	160	3.4	430
Cs-137	10.4	350	6.4	900
Th-230	3,000	4,300	2,120	9,580
Ra-226 (In equilibrium with progeny)	4.5	300	2.8	760
Th-232 decay series (Sum of all radionuclides in thorium decay series, in equilibrium)	28.3	340	18.3	830
Th-232 alone ^b (In equilibrium with progeny in decay series)	2.8	340	1.8	830
Depleted Uranium ^c (0.34% U-235)	80.5	1,680	56.0	3,790
Processed Natural Uranium ^c	115	1,770	80.0	3,990
3% Enriched Uranium ^c	137	2,010	95.7	4,520
20% Enriched Uranium ^c	152	2,210	107	4,940
50% Enriched Uranium ^c	168	2,240	118	5,010
75% Enriched Uranium ^c	188	2,250	132	5,030

^aRefer to text for complete explanation of factors used to calculate scan MDCs. For example, the background level for the 1.25" × 1.5" NaI detector was assumed to be 4,000 cpm and 10,000 cpm for the 2" × 2" NaI detector. The observation interval was 1 second and the level of performance was selected to yield d' of 1.38.

^bNote that the scan MDCs for Th-232 were determined by dividing scan MDC for entire Th-232 series by 10 to account for individual progeny (e.g., Th-232, Ra-228, Ac-228, etc.).

^cScan MDC for uranium includes sum of U-238, U-235, and U-234.

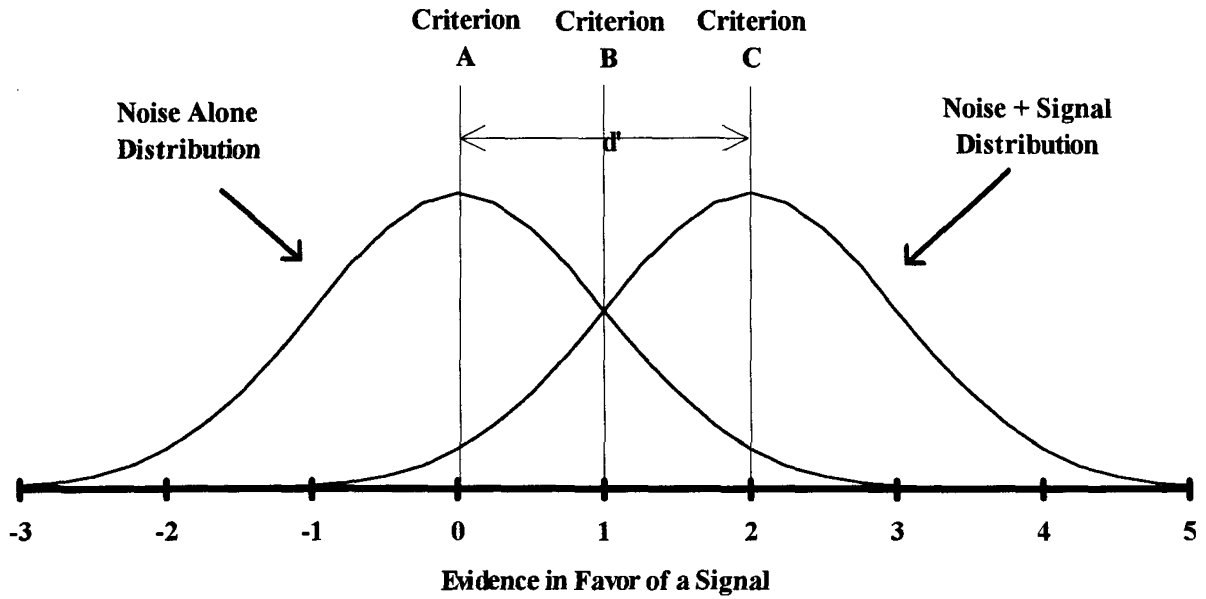


Figure 6.1: Signal Detection Theory Measures of Sensitivity (d') and Criterion Shown Relative to Assumed Underlying Distributions

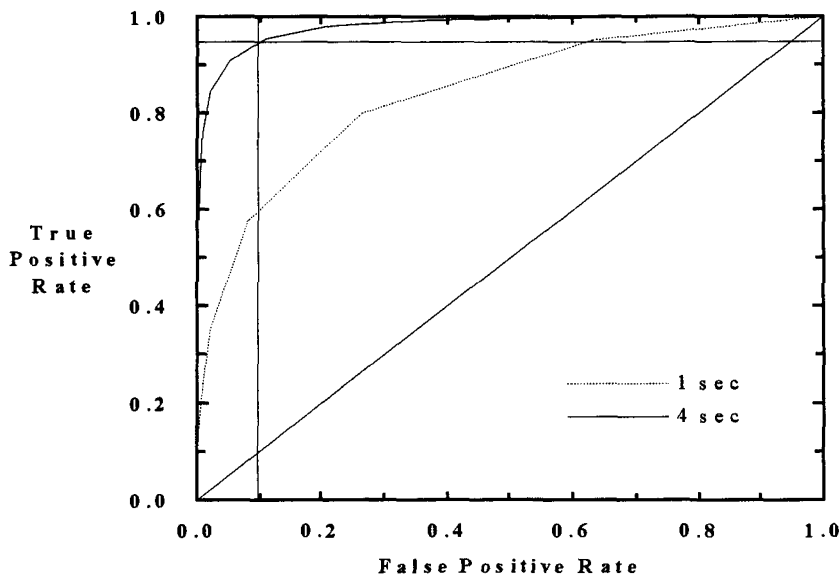


Figure 6.2: Relative Operating Characteristic (Ideal Observer) for Detection of 120 cpm (Net) in a Background of 60 cpm; Observation Intervals of 1 Second and 4 Seconds

Field Determination of Scanning Sensitivity Survey Instructions

Introduction

Sections of the cardboard are covering radioactive sources that were fastened to the back-side of the cardboard in contact with the wall. Sixteen radioactive sources were randomly positioned on the cardboard in nine discrete configurations. The radioactive sources included C-14, Co-60, Sr-90, Tc-99, Cs-137, and uranium. The radioactive source configurations were prepared to provide varying radiation levels and geometries. The radioactive sources were purposely chosen to emit levels of radiation that are barely discernible above background. Your task is to identify the locations of the areas of direct radiation and record count rate (in cpm) on the provided survey map. You will need a pen and a clipboard to record the results of your survey. Expect to spend 45 to 60 minutes on this exercise.

Specific Tasks

1. Prior to initiating the scan survey, determine the background radiation level of the GM detector the section of cardboard on the wall denoted "Background Check". At this time it is also necessary to compare the cardboard wall with the provided survey map, to ensure that you will record the results on the proper locations on the map.
2. Record the background value of your survey map. Observers will also be recording the results of your scan survey.
3. Put on the headphones and get adjusted to the background counting rate again.
4. Scan the cardboard at a rate of approximately 1 detector width per second (about 5 cm per second with the GM detector), 1 grid section at a time. Instructors will be available to ensure you are scanning at the desired rate. You should keep the detector in contact with the surface during the scan.
5. Listen carefully for an increased click rate above the background count rate.
6. When you think that you have identified an area of elevated direct radiation or "hit", stop and immediately mark that point on your map. Observers will record the number of pauses, even if you can immediately determine that the location was really just a variation of background clicks.
7. Use the following notation when recording the results:

Record actual cpm on map for hits.

Figure 6.3 Instructions Given to Field Survey Test Participants for Indoor GM Scans

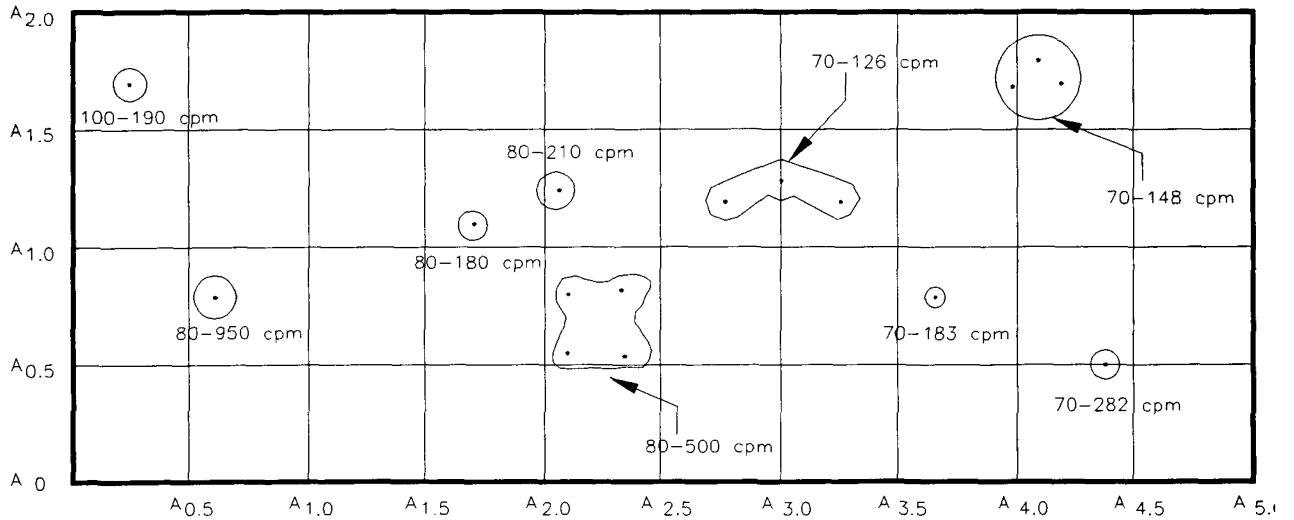


Figure 6.4: Scale Map of the Wall Showing Location, Extent, and Radiation Levels of Hidden Sources for GM Scans

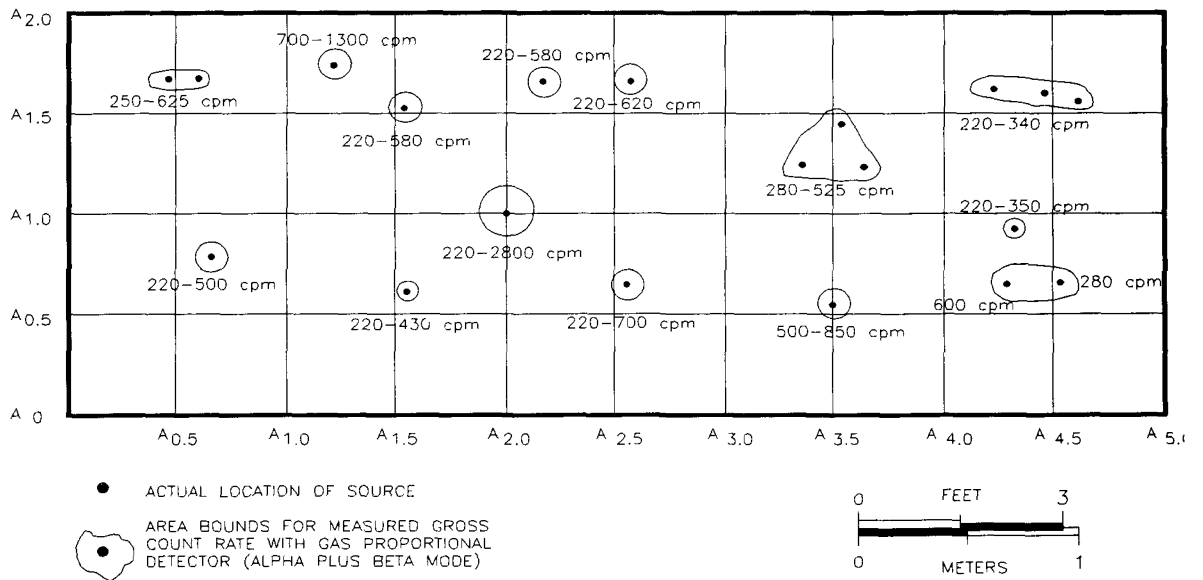


Figure 6.5: Scale Map of the Wall Showing Location, Extent, and Radiation Levels of Hidden Sources for Gas Proportional Scans

HUMAN PERFORMANCE AND SCANNING SENSITIVITY

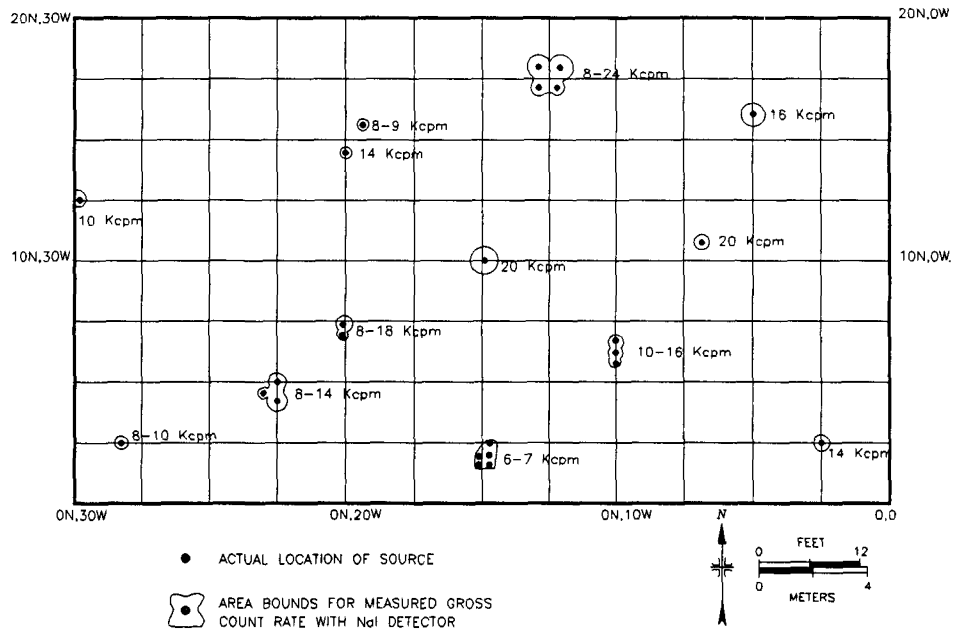


Figure 6.6: Scale Map of the Outdoor Scan Test Area Showing Location Extent, and Radiation Levels of Hidden Sources for NaI Scans

7 IN SITU GAMMA SPECTROMETRY AND EXPOSURE RATE MEASUREMENTS

The use of spectrometric techniques to assess radioactivity may produce a significant increase in sensitivity as compared to radiation measurements that rely on gross instrument counts. Spectrometry allows a specific radionuclide to be measured, relying on characteristic energies of the radionuclide of concern to discriminate from all sources present. *In situ* gamma spectrometry refers to the assessment of the ambient gamma ray flux that is collected in the field (i.e., *in situ*), and analyzed to identify and quantify the radionuclides present.

The Environmental Measurements Laboratory (EML) has performed detailed and quantitative evaluations of portable gamma spectrometry systems. The reader is referred to "Measurement Methods for Radiological Surveys in Support of New Decommissioning Criteria (Draft Report for Comment)" (NUREG-1506) for detailed guidance on how to employ *in situ* gamma spectrometry during survey activities. That report gives examples of minimum detectable concentrations using a typical 25% relative efficiency p-type germanium detector and a 10-minute count time at typical background radiation levels. Using these assumptions, the minimum detectable concentrations (MDCs) for Co-60, Cs-137, Eu-152, Ra-226 (based on measurement of progeny) and Ac-228 (to infer Th-232) are all approximately 0.05 pCi/g. It is necessary to use a more efficient detector, such as a 75% relative efficiency n-type germanium detector, to measure the radionuclides that are more difficult to detect. For example, using the 75% relative efficiency n-type germanium detector for a 10-minute count time, results in an MDC of 0.5 pCi/g for Am-241, and 2 pCi/g for U-238 (based on measurement of short-lived Th-234 progeny) and Ra-226 (based on measurement of the 186 keV gamma energy line). These typical MDCs scale as the square root of the count time; that is, quadrupling the count time results in a factor of two increase in the sensitivity of the *in situ* measurement.

7.1 In Situ Gamma Spectrometry Measurements in Outdoor Test Area

In situ gamma spectrometry measurements were performed within the outdoor test area (this same area was also used to evaluate the scan sensitivity of surveyors) to determine the spectrometer's ability to identify and locate the sources. It should be understood that this particular exercise was intended to evaluate the scanning capabilities of the *in situ* gamma spectrometer, not its ability to determine radionuclide concentrations in soil, which requires detailed detector calibration and modeling of the contaminant distribution in the soil.

As stated in Section 6, 25 gamma-emitting sources were buried in the test area, including 12 Co-60 sources and 5 Cs-137 sources. Measurements were made at nine grid locations in the test area, at both 0.5 meter and 1 meter above the ground (Figure 7.1). A background measurement at 1 meter above the ground was performed in an adjacent area unaffected by the test area sources. ESSAP used a 13% relative efficiency p-type germanium detector and a 30-minute count time at each measurement location. The net counts collected in both the Co-60 and Cs-137 peak regions were determined and are given in Table 7.1. The Co-60 data were presented

IN SITU GAMMA SPECTROMETRY MEASUREMENTS IN OUTDOOR TEST AREA

in Figure 7.1 to allow a visual correlation between the detector response and the Co-60 source location. Cs-137 data were not evaluated in this manner because in only a few locations did levels of Cs-137 exceed background.

The results indicated that the portable gamma spectrometry system was able to identify the presence of Cs-137 and Co-60 contamination in the test area. This elementary finding warrants additional thought and should not be dismissed without consideration as to its implications on the use of *in situ* gamma spectrometry as a scanning tool. Recognizing that *in situ* gamma spectrometry is able to detect relatively low levels of gamma-emitting radionuclides is of particular value when the detector is used to verify the absence of contamination in an area. That is, if the detector's MDC can be demonstrated to be sufficiently below the contamination guidelines, then *in situ* gamma spectrometry measurements may be used to demonstrate that further survey efforts in an area are not warranted. Furthermore, using *in situ* gamma spectrometry to determine that residual radioactivity is below a specified concentration has an additional benefit in the improved documentation of the scan survey. Records of *in situ* gamma spectrometry measurements are generally more objective and less likely to be influenced by human factors than the conventional scan survey records obtained with NaI scintillation detectors or other portable field instrumentation, which require subjective interpretation of the detector response by the surveyor.

For the present experimentation, the *in situ* gamma spectrometer did identify the presence of Co-60 and Cs-137 contamination and, therefore, the data were analyzed in an effort to locate the contamination. Figure 7.1 shows the net counts in the Co-60 peak region at both 1 meter and 0.5 meter above the surface at each grid coordinate (top number is 1-meter value, bottom number is 0.5 m value). In the case of uniform contamination and a detector height of 1 meter, approximately 80% of the detector's response would be from a 5-meter radius (NUREG-1506). Because detector height above the surface affects the amount of ground being viewed, moving the detector closer to the ground results in a smaller section of the ground being viewed.

The greatest quantity of Co-60 activity was identified at grid location 15N,5W. The fact that the net counts for Co-60 increased as the detector was moved closer to the ground indicates that the source is relatively close to the sampled grid coordinate. Also, because the Co-60 result at coordinate 10N,5W has significantly less Co-60 activity than at 15N,5W, it is likely that the source is not south of grid coordinate 15N,5W.

The Co-60 results for grid coordinates 5N,5W and 15N,10W (both have 1-meter readings greater than 0.5-meter readings) indicate that Co-60 contamination is nearby, but not necessarily in the immediate vicinity of the sampled grid coordinate. Although this analysis does not direct the surveyor to the exact location of the contamination, it does provide for a focused plan for subsequent NaI scintillation scan surveys.

7.2 Exposure Rate Measurements in Outdoor Test Area

Exposure rate measurements using a pressurized ionization chamber (PIC) were performed within the outdoor test area to evaluate the PIC's sensitivity in measuring exposure rate. Measurements were performed at six grid coordinate locations, each reading at 1 meter above the surface (Figure 7.2). The background exposure rate (10.3 $\mu\text{R}/\text{h}$) was determined in an area adjacent to the test area, but unaffected by the test area sources.

The sensitivity of the PIC is directly proportional to the standard deviation of the background exposure rate. Therefore, areas exhibiting only minor background exposure rate variations will have the lowest minimum detectable exposure rates. The exposure rate measurements in the test area ranged from 10.2 to 11.1 $\mu\text{R}/\text{h}$ (Table 7.2). Figure 7.2 illustrates the correlation between the exposure rate measurements and the source locations. The larger exposure rates correspond to the larger gamma radiation levels that were obtained during characterization of the test area (refer to grid locations 15N,15W and 15N,5W). These results indicate that the PIC response was affected by the gamma-emitting sources. The minimum detectable exposure rate obtained with the PIC can be expected to be approximately 1 $\mu\text{R}/\text{h}$ above background levels, depending on the background variability.

IN SITU GAMMA SPECTROMETRY MEASUREMENTS IN OUTDOOR TEST AREA

Table 7.1 In Situ Gamma Spectrometry Data From Outdoor Test Area

Measurement Location ^a		Net Count in Peak Region	
		Cs-137 (662 keV)	Co-60 (1332 keV)
Background	1 m ^b	-4 ± 8	6 ± 14
5N, 5W	1 m	-18 ± 10	30 ± 10
5N, 5W	0.5 m	-4 ± 8	5 ± 16
10N, 5W	1 m	5 ± 7	27 ± 13
10N, 5W	0.5 m	15 ± 7	26 ± 12
15N, 5W	1 m	11 ± 8	163 ± 18
15N, 5W	0.5 m	-2 ± 7	234 ± 25
5N, 15W	1 m	-1 ± 8	38 ± 7
5N, 15W	0.5 m	4 ± 8	40 ± 13
10N, 15W	1 m	7 ± 9	9 ± 17
10N, 15W	0.5 m	8 ± 9	36 ± 15
15N, 15W	1 m	7 ± 8	40 ± 12
15N, 15W	0.5 m	-11 ± 9	18 ± 16
5N, 25W	1 m	7 ± 8	20 ± 18
5N, 25W	0.5 m	19 ± 9	23 ± 17
10N, 25W	1 m	3 ± 8	4 ± 17
10N, 25W	0.5 m	17 ± 8	36 ± 13
15N, 25W	1 m	-6 ± 8	8 ± 15
15N, 25W	0.5 m	10 ± 8	25 ± 11

^aRefer to Figure 7.1.

^bDistance refers to detector height above the surface.

IN SITU GAMMA SPECTROMETRY MEASUREMENTS IN OUTDOOR TEST AREA

Table 7.2 Exposure Rate Measurements From Outdoor Test Area

Measurement Location ^a	Exposure Rate ^b (μR/h)
Background	10.3
5N, 5W	10.8
5N, 15W	10.2
5N, 25W	10.9
15N, 5W	11.1
15N, 15W	11.0
15N, 25W	11.0

^aRefer to Figure 7.2.

^bMeasurements made at 1 meter above the surface.

IN SITU GAMMA SPECTROMETRY AND EXPOSURE RATE MEASUREMENTS

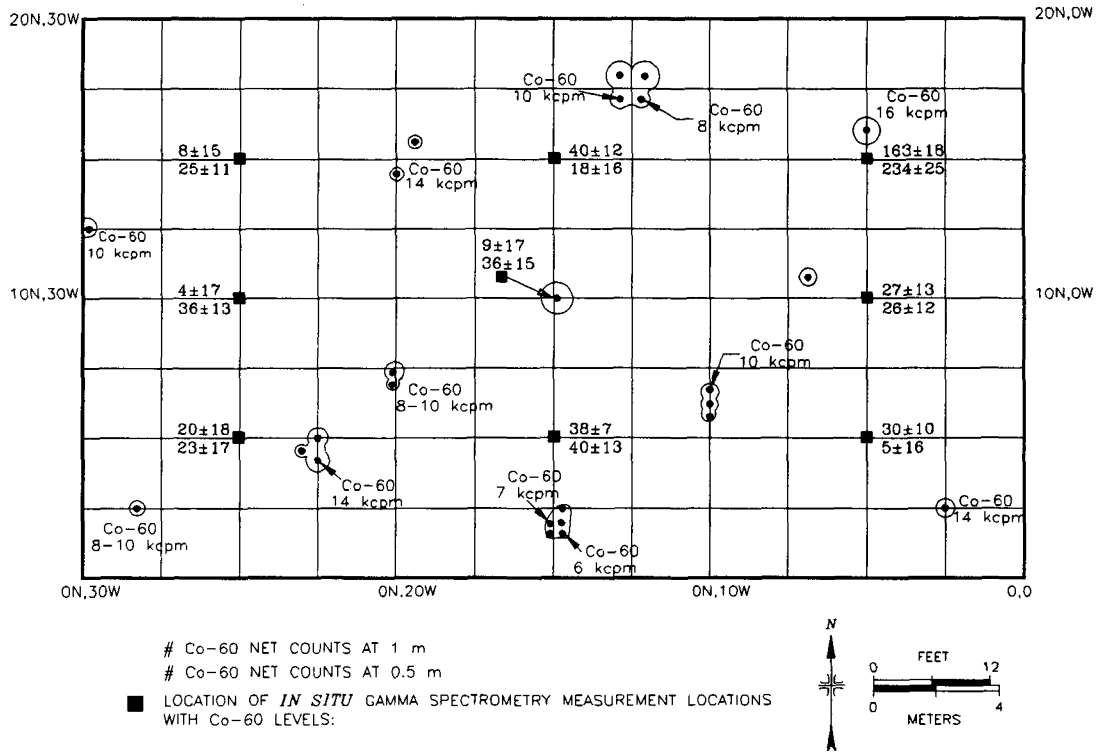


Figure 7.1: Co-60 *in situ* Gamma Spectrometry Results in Outdoor Test Area

IN SITU GAMMA SPECTROMETRY AND EXPOSURE RATE MEASUREMENTS

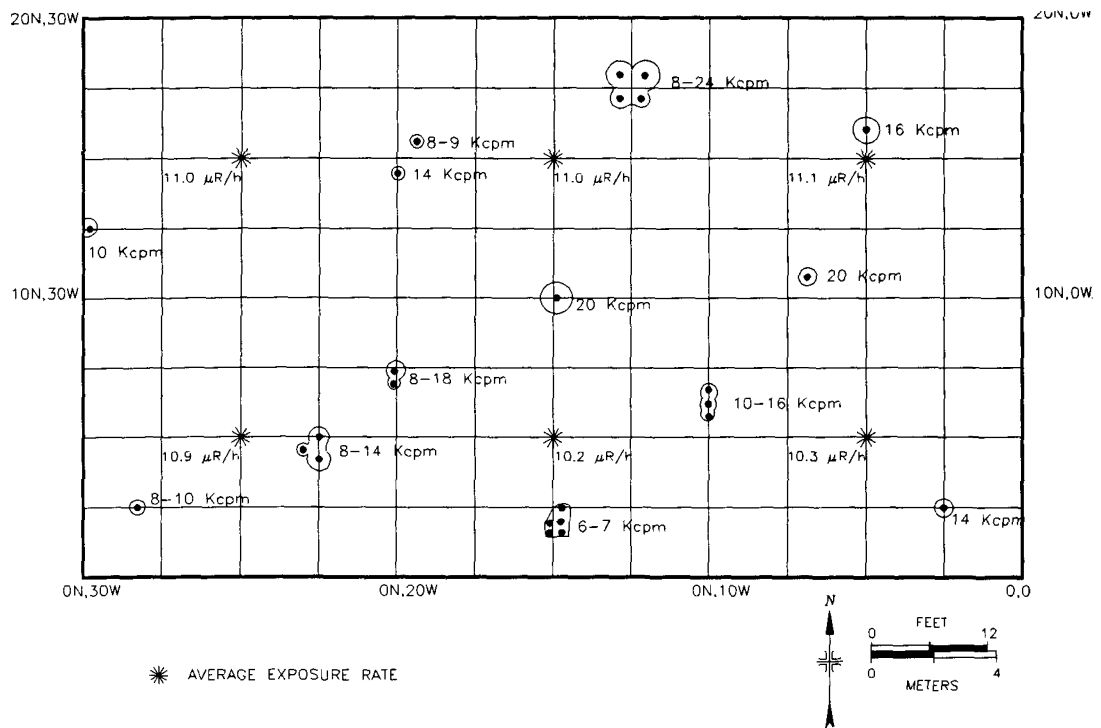


Figure 7.2: Exposure Rate Measurements in the Outdoor Test Area

8 LABORATORY INSTRUMENTATION DETECTION LIMITS

Frequently during surveys in support of decommissioning it is not feasible, or even possible, to detect the contaminants with portable field instrumentation; thus arises the need for laboratory analysis of media samples. This is especially the case for such media samples as soil, that result in significant self-absorption of the radiation from the residual radioactivity. Another common situation that necessitates the use of laboratory analyses occurs when the contaminants are difficult to detect even under ideal conditions. This includes residual radioactivity that emits only low-energy beta radiation (e.g., H-3 and Ni-63) or x-ray radiation (e.g., Fe-55).

Laboratory analyses for radionuclide identification, using spectrometric techniques, are often performed during scoping or characterization surveys. Here the principal objective is to simply determine the specific radionuclides in the contamination, without necessarily having to assess the quantity of contamination. Once the radioactive contaminants have been identified, sufficiently sensitive field survey instrumentation and techniques are selected to demonstrate compliance with the DCGLs.

8.1 Review of Analytical Minimum Detectable Concentrations

In 1993, M. H. Chew and Associates prepared a database which contains a listing of minimum detectable concentrations (MDCs) for various radionuclides, sample sizes, count times, instrument efficiencies, and background count rates. This information was compiled by surveying several government and commercial laboratories which provided their "best estimates" in response to the survey. The instrumentation used, instrument efficiencies, and sample geometries varied among laboratories, and, for the same laboratory, varied from one radionuclide to the other. These variations are given as ranges. In short, the report constitutes a survey, not a controlled study.

The listing prepared by Chew and Associates is helpful in identifying approximate MDCs to be expected for detection of specific radionuclides. However, on the basis of that information, it is not possible to make accurate predictions as to how the MDC will be affected quantitatively if sample density, sample background activity, the mixture of radionuclides, or chemical composition of soil samples are altered. These can be very significant factors in determining the MDC. For example, in some geographic locations, there may be increased concentrations of aluminum in the soil. These interfere with the nitric acid leaching procedure in radiochemical analysis for thorium or uranium; increased levels of calcium or potassium interfere with radiochemical analysis for Sr-90; increased levels of iron interferes with several radiochemical analysis procedures. Other field conditions may affect the detectability of contaminants. The effects of these conditions were quantitatively evaluated for various types of radionuclides.

8.2 Background Activities for Various Soil Types

Radionuclide concentrations in background soil samples vary for numerous reasons, such as the soil type and density, geology, geographic location, radioactive fallout patterns, and many other

LABORATORY INSTRUMENTATION DETECTION LIMITS

reasons. NUREG-1501 provides an in-depth study of the factors that are responsible for variations in the background radioactivity in soil.

During the course of performing environmental assessments of background radioactivity throughout the United States, Environmental Survey and Site Assessment Program (ESSAP) investigators at the Oak Ridge Institute for Science and Education (ORISE) stated that background radionuclide concentrations vary both on a regional basis (e.g., western U.S., southeastern U.S., coastal areas) and within a particular region. Table 8.1 gives typical U-238, Th-232, and Cs-137 concentrations found in background soil samples in the United States. These data were compiled from historical databases on background soil concentrations and are intended to give information on the variations that exist both among and within various regions. For many locations, the soil samples represent different soil types, such as silty loam, sandy loam, and clay. The radionuclide analyses performed on these samples used both alpha and gamma spectrometry.

The fallout radioactivity, Cs-137, was determined to have the greatest variability within a particular region, as compared to the terrestrial radionuclides from the uranium and thorium decay series. The large variation in fallout radioactivity may be due to the specific soil sample locations. Wooded areas tend to exhibit higher concentrations of fallout radioactivity than open field areas, likely due to the increased foliar interception in forested areas.

8.3 Effects of Soil Condition on MDC

The density and chemical composition of the soil can affect the detection sensitivity of survey instruments. Soil density and composition can also affect the MDC of laboratory instrumentation and procedures. For example, higher densities may result in an underestimation of gamma activity, particularly for low-energy gamma emitters.

Within each category of soil, detection sensitivity of the instruments may be affected by variations in (a) moisture content, (b) soil density, and (c) presence of high-Z (atomic number) materials in the sample. As part of this study, the effects of soil density and composition, moisture content, and presence of high-Z material on the gamma spectrometry analysis was evaluated. It was necessary to prepare soil standards for this evaluation.

Each germanium detector was calibrated for each counting geometry using a NIST-traceable standard (typically mixed gamma-emitting activity in liquid form). Vendors that supplied the standards can demonstrate traceability to the National Institute of Standards and Technology (NIST).

The ESSAP counting room presently prepares two standards for the 0.5-liter Marinelli soil geometry. One standard is prepared from top soil and weighs between 700 and 800 g. This standard was used to quantify soil samples that weigh in the range of 450 to 850 g. The second

LABORATORY INSTRUMENTATION DETECTION LIMITS

Marinelli standard was prepared using sand; it weighs approximately 1000 g. This standard was used to quantify soil samples that weigh between 850 and 1150 g.

For the smaller aluminum-can geometries (approximately 120-g capacity), a comparison of the counting efficiencies obtained from both the top soil and sand standards resulted in the counting efficiencies being equal within the statistical limits. For this reason, only one counting efficiency curve was used for the aluminum-can geometry.

The soil calibration standard, consisting of Am-241, Ce-139, Cs-137, and Co-60, was prepared by weighing a known quantity of the liquid standard and adding this quantity to either the top soil or sand matrix. To ensure that the soil standard has been adequately mixed, equal aliquots (soil fractions) were placed in the aluminum-can geometry and analyzed with the germanium detector. The radionuclide concentration of each soil fraction was determined. The radionuclide concentrations of the soil fractions were evaluated to determine if they were statistically equal and, thus, to conclude that the soil standard was homogeneous. Once homogeneity was demonstrated, the standard was used to calibrate the germanium detectors for the various soil counting geometries.

8.3.1 Effects of Soil Moisture on MDC

The moisture content of the soil can vary significantly, depending on geographic location, time after rainfall, etc., and can have significant impact on detection of radionuclides with beta and low-energy gamma emissions. Therefore, a relatively wide range of moisture contents was examined in this study.

Water content can be measured accurately in the laboratory and can be changed by homogenizing known quantities of water in the soil. A calibrated counting geometry with a known weight was obtained. The initial weight was 112.9 g. At first, 5.9% moisture was added to the initial weight. This amount of water was not great enough to evenly disburse throughout the soil. To evenly disburse the water, 95% ETOH was used. A visual check was used to determine if the soil was saturated. The soil was allowed to air dry to the desired weight of 119 g. Among the problems discovered while working with smaller moisture contents were soil loss by airflow because of the small particle size and not being able to return all of the soil into the container after the water was added. These soil loss problems were controlled by increasing the amount of water added and then allowing the soil to dry to the next desired weight. At this point, 20% moisture was added for a test weight of 125.6 g. Due to the increased volume of water added, 8.7 g of dry soil could not be returned to the container. The moisture added was sufficient to saturate the soil thoroughly. After the addition of water, the soil was allowed to absorb the moisture for approximately 1 hour. The next percent moisture was obtained by simply allowing the soil to air dry. The subsequent moisture percentage to be tested was 15% at a weight of 118.3 g. The 10.5% moisture was obtained in the same manner as above for a test weight of 112.25 g. At this point, it was necessary to increase the moisture content. A moisture content of 35.5% was

LABORATORY INSTRUMENTATION DETECTION LIMITS

obtained for a total weight of 152.70 g. This amount was then allowed to air dry to 31% moisture for a total weight of 145.03 g. At this moisture content, the soil was barely able to absorb all the water added. Finally, water was added to the point of total saturation. The maximum amount of water that could be added to the container geometry was 38.5%, for a final weight of 162.7 g.

Because the addition of water to the soil standard diluted the radionuclide concentration, it was necessary to account for the dilution factor. This was done by increasing the measured concentration by a degree equal to the weight percent of the water added to the standard. This concentration corrected for dilution was compared to the measured concentration (Table 8.2). The results indicate that lower concentrations obtained from the increasing moisture content are largely due to the dilution effect. That is, the radionuclide concentration in soil is lower as a result of the contaminated soil being replaced by water.

8.3.2 Effects of Soil Density on MDC

As stated previously, soil density can affect the MDC of laboratory instrumentation and procedures. Higher density samples, relative to the calibration soil standard, can result in an underestimation of gamma activity, particularly for low-energy gamma emitters.

The gamma efficiency for a particular geometry is decreased as the soil density is increased. Figure 8.1 illustrates this effect for three soil calibration geometries with densities of 1.1, 1.54, and 2.02 g/ml. The greatest gamma efficiency deviation in the three samples occurs at the low-energy range.

8.3.3 Effects of High-Z Materials on MDC

Gamma spectrometry analyses to determine the radionuclide concentration in soil samples commonly involves the use of a calibration standard traceable to NIST. The calibration standards used for the analysis of soils should consist of a material similar in composition to that of soil, e.g., a silica-based material. Efficiencies at each gamma energy are then established for each radionuclide energy that is present in the calibration standard. An efficiency versus energy curve is generated from each of the individual efficiency data points. This efficiency curve is then used to assess the radionuclide concentrations in media that may be considered similar in composition to that of soil.

A potential deviation from the calibrated geometry described above occurs when a sample contains a measurable quantity of high-Z material, such as metals. The presence of high-Z materials produces attenuation of the gamma radiation (especially the low-energy gamma emissions) in the sample that may not be accounted for in the calibration standard. If no correction is made to account for the absorption of the gamma radiation, use of the standard efficiency curve will underestimate the true radionuclide concentration in the sample. The

LABORATORY INSTRUMENTATION DETECTION LIMITS

magnitude of these effects was evaluated by mixing in measurable quantities of metal fines and powder. Specifically, the metals studied were iron, lead, and zirconium, which were mixed in the calibration standards at 1, 5, and 10 weight percents. Table 8.3 presents the results of this experiment. Because the addition of material (i.e., high-Z material) to the soil standard dilutes radionuclide concentration, it is necessary to account for the dilution factor. This was done by increasing the measured concentration by a degree equal to the weight percent of material added to the standard. For example, the measured radionuclide concentration for the sample containing 5% lead was increased proportionately. The results indicate that in general, the high-Z material effects are most pronounced at the lower gamma energies. Furthermore, the zirconium produces the most significant attenuation losses, followed by lead and then iron.

In summary, using a typical low-Z soil calibration standard to assay a high-Z material sample will likely result in an underestimation of the radionuclide concentration in that sample. This is because low-energy gamma radiation is attenuated more in the high-Z material sample than it is in the calibration standard. Sample attenuation concerns may be addressed by application of the direct ratio method of gamma radiation counting. The direct ratio method works by comparing the gamma photopeak energy of interest in the sample to the gamma photopeak in a suitable calibration standard, with both photopeaks corrected for the relative amount of attenuation present in the sample and calibration standard. Additional details for applying this technique can be found in Abelquist et al. (1996).

**Table 8.1 Typical Radionuclide Concentrations
Found in Background Soil Samples in the United States**

Location	Radionuclide Concentration (pCi/g)		
	U-238	Th-232	Cs-137
Boston, Massachusetts	0.7 to 1.3	<0.2 to 1.5	-- ^a
Cambridge, Massachusetts	0.4 to 1.2	---	0.1 to 0.7
Cincinnati, Ohio	<0.4 to 2.5	0.3 to 1.5	0.2 to 1.5
Jacksonville, Florida	0.4 to 1.0	0.5 to 1.0	<0.1 to 0.5
Kingsport, Tennessee	<0.5 to 2.2	0.8 to 1.8	---
Platteville, Colorado	0.9 to 2.1	1.5 to 2.2	<0.1 to 0.2
San Diego, California	1.0 to 1.6	0.7 to 1.6	<0.1 to 0.4

^aRadionuclide measurement not performed.

Table 8.2 Effects of Moisture Content on Gamma Spectrometry Analyses

Moisture ^a (%)	Radionuclide Concentration (pCi/g)											
	Am-241			Ce-139			Cs-137			Co-60		
	Meas ^b	Corr ^c	%Diff ^d	Meas ^b	Corr ^c	%Diff ^d	Meas ^b	Corr ^c	%Diff ^d	Meas ^b	Corr ^c	%Diff ^d
Dry	125.1	---	---	17.7	---	---	117.3	---	---	133.4	---	---
5%	108.4	115.2	7.92	15.5	16.4	7.39	102.3	108.7	7.32	116.1	123.4	7.51
10%	108.5	121.2	3.09	14.8	16.6	6.53	102.1	114.1	2.75	114.3	127.7	4.27
15%	103.2	121.6	2.83	14.5	17.1	3.59	96.5	113.7	3.07	110.2	129.8	2.70
20%	95.8	119.8	4.25	13.2	16.6	6.71	89.6	112.0	4.51	98.8	123.5	7.42
31%	83.1	120.5	3.68	11.2	16.2	8.75	83.6	121.1	-3.28	93.5	135.6	-1.62
35%	79.5	123.3	1.46	10.7	16.6	6.66	79.4	123.1	-4.93	90.4	140.1	-5.05
38%	73.5	119.5	4.47	9.2	15.0	15.64	69.7	113.3	3.42	79.5	129.3	3.07

^aMoisture content calculated by the following:

$$\text{Moisture Content} = \frac{\text{Wet Weight} - \text{DryWeight}}{\text{Wet Weight}}$$

^bMeasured radionuclide concentration.

^cRadionuclide concentration corrected for dilution by dividing the measured concentration by one minus the moisture content.

^dPercent difference between the measured and calculated concentrations.

Table 8.3 Effects of High-Z Content on Gamma Spectrometry Analyses

High-Z Material (%)	Radionuclide Concentration (pCi/g)											
	Am-241			Ce-139			Cs-137			Co-60		
	Meas ^a	Corr ^b	%Diff ^c	Meas ^a	Corr ^b	%Diff ^c	Meas ^a	Corr ^b	%Diff ^c	Meas ^a	Corr ^b	%Diff ^c
Lead												
No Z Material	109.8	---	---	14.6	---	---	112.8	---	---	115.8	---	---
1	108.2	109.3	0.45	13.8	14.0	4.0	109.4	110.5	2.0	111.2	112.3	3.0
5	92.9	97.8	10.9	12.6	13.2	9.2	105.9	111.5	1.2	110.0	115.8	0.01
10	79.7	88.9	19.0	11.3	12.6	13.9	101.5	113.2	-0.4	104.6	116.7	-0.8
Iron												
No Z Material	111.3	---	---	13.6	---	---	108.0	---	---	113.4	---	---
1	113.1	114.2	-2.6	13.5	13.6	-0.4	107.6	108.7	-0.6	110.3	111.4	1.8
5	97.0	102.1	8.3	13.0	13.7	-0.8	102.4	107.8	0.2	106.9	112.5	0.8
10	98.4	109.5	1.6	13.5	15.0	-10.4	102.7	114.4	-5.9	104.6	116.5	-2.7
Zirconium												
No Z Material	121.0	---	---	14.7	---	---	113.4	---	---	115.2	---	---
1	98.8	99.8	17.5	14.3	14.4	1.5	110.2	111.3	1.8	112.2	113.3	0.05
5	80.9	85.2	29.6	13.7	14.4	1.6	109.1	114.8	-1.3	107.7	113.4	0.03
10	62.7	69.6	42.5	12.3	13.7	6.5	100.4	111.6	1.6	100.2	111.3	1.8

^aMeasured radionuclide concentration.

^bRadionuclide concentration corrected for dilution by dividing the measured concentration by one minus the high Z material content.

^cPercent difference between the measured (no Z material) and calculated concentrations.

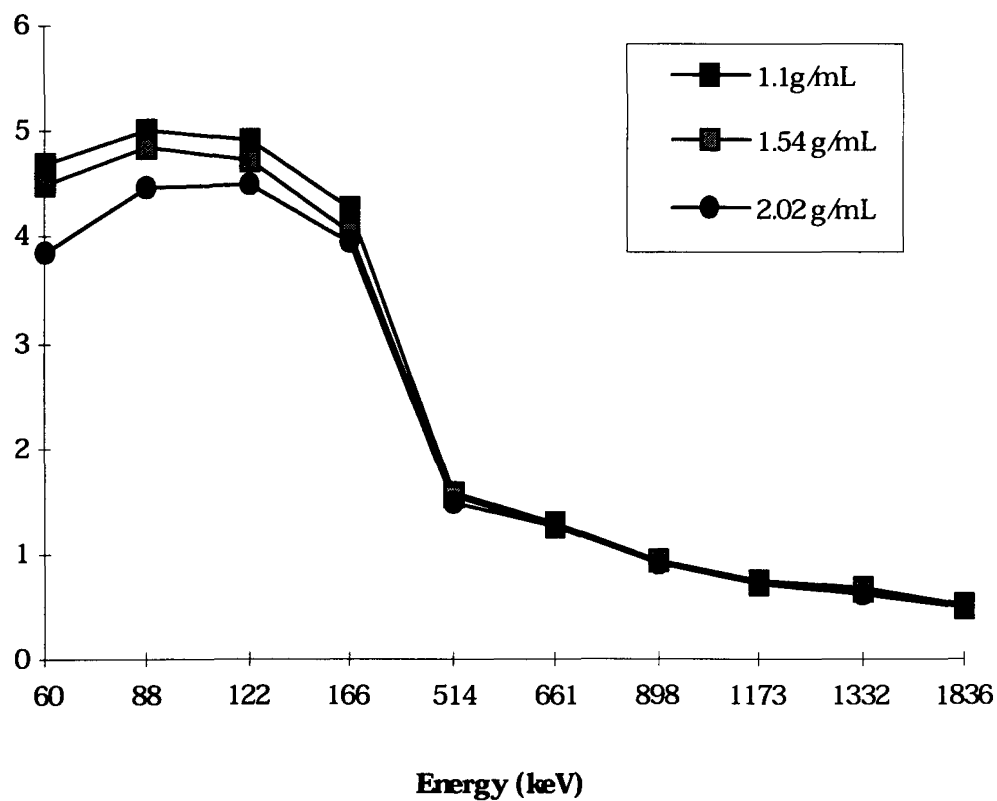


Figure 8.1: Efficiency vs. Energy for Various Densities

9 REFERENCES

- Abelquist, E.W., R.D. Condra, M.J. Laudeman. "Determination of Uranium and Thorium Concentrations in High Z Material Samples Using Direct Counting Method of Gamma Spectroscopy," *Radiation Protection Management* 13:42-49. 1996.
- Altshuler, B., and B. Pasternak. "Statistical Measures of the Lower Limit of Detection of a Radioactivity Counter," *Health Physics* 34(9):293-298. 1963.
- ANSI N13.30. "Performance Criteria for Radiobioassay." New York: American National Standards Institute, Inc. 1996.
- ANSI 13.12. "Control of Radioactive Surface Contamination on Materials, Equipment, and Facilities To Be Released for Uncontrolled Use (Draft)." New York: American National Standards Institute, Inc. December 1985.
- Brodsky, A. "Exact Calculation of Probabilities of False Positives and False Negatives for Low Background Counting," *Health Physics* 63(2):198-204. August 1992.
- Brodsky, A. "Standardizing Minimum Detectable Amount Formulations," *Health Physics* 64(4): 434-435. April 1993.
- Brodsky, A., and R.G. Gallagher. "Statistical Considerations in Practical Contamination Monitoring," *Radiation Protection Management* 8(4):64-78. July/August 1991.
- Brown, W.S., and D.S. Emmerich. "Auditory Detection of an Increment in the Rate of a Random Process," *Journal of the Acoustical Society of America* 95(5) Part 2:2941. 1994.
- Bruns, L.E. "Capability of Field Instrumentation To Measure Radionuclide Limits," *Nuclear Technology* 58:154-169. August 1982.
- Chambless, D.A., Dubose, S.S., and Sensintaffar, E.L. "Detection Limit Concepts: Foundations, Myths, and Utilization," *Health Physics* 63(3):338-340. 1992.
- Chew and Associates, Inc. "Summary of Current Capabilities With Regards to Detection of Radioactivity: A Survey of Commercial Radiochemistry Laboratories and Instrument Suppliers (Interim Report)." Washington, D.C. August 1993.
- Currie, L.A. "Limits for Qualitative Detection and Quantitative Determination," *Analytical Chemistry* 40(3):586-593. 1968.

REFERENCES

- DOE/CH-9501. "Radioactivity Measurements and Surveys: Statistical and Practical Considerations." William S. Lee and Tristan M. Tritch, Chicago: Mac Technical Services Company. November 1994.
- DOE. "Environmental Implementation Guide for Radiological Survey Procedures." (Draft) Washington, D.C.: Department of Energy. November 1992.
- DOE/EP-0100. "A Guide for Radiological Characterization and Measurements for Decommissioning of U.S. Department of Energy Surplus Facilities." Washington, D.C.: Department of Energy. August 1983.
- Egan, J.P. *Signal Detection Theory and ROC Analysis*. New York: Academic Press. 1975.
- Goles, R.W., B.L. Baumann, and M.L. Johnson. "Contamination Survey Instrument Capabilities" (PNL-SA-1984, Letter to the U.S. Department of Energy). 1991.
- Green, S., R.H. Miller, and R.A. Nelson. "Development and Use of Statistical Survey Criteria for Release of Materials at a Former Uranium Processing Facility," *Health Physics* 61(6):903-911. December 1991.
- HPSR-1/EPA 520/1-80-012. "Upgrading Environmental Radiation Data," Washington, D.C.: Health Physics Society Committee/Environmental Protection Agency. August 1980.
- ISO 7503-1. "Evaluation of Surface Contamination - Part 1: Beta Emitters and Alpha Emitters (first edition)." Geneva: International Organization for Standardization. 1988.
- ISO 8769. "Reference Sources for the Calibration of Surface Contamination Monitors." Geneva: International Organization for Standardization. 1988.
- LA-10729. "Alpha RADIAC Evaluation Project." Los Alamos, N.M.: Los Alamos National Laboratory. June 1986.
- Macmillan, N.A., and C.D. Creelman. *Detection Theory: A User's Guide*. Cambridge, England: Cambridge University Press. 1991.
- Maushart, R. "Contamination Monitoring in the Federal Republic of Germany." *Radiation Protection Management* 3(2):49-57. January 1986.
- NCRP 50. "Environmental Radiation Measurements." Bethesda, Md.: National Council on Radiation Protection and Measurements. December 27, 1976.

REFERENCES

NCRP 58. "A Handbook of Radioactivity Measurements Procedures." Bethesda, Md.: National Council on Radiation Protection and Measurements. February 1, 1985.

NCRP 112. "Calibration of Survey Instruments Used in Radiation Protection for the Assessment of Ionizing Radiation Fields and Radioactive Surface Contamination." Bethesda, Md.: National Council on Radiation Protection and Measurements. December 31, 1991.

NUREG-1500. "Working Draft Regulatory Guide on Release Criteria for Decommissioning: NRC Staff's Draft for Comment." Washington D.C.: Nuclear Regulatory Commission. August 1994.

NUREG-1501. "Background as a Residual Radioactivity Criterion for Decommissioning" (Draft Report for Comment). Washington, D.C.: Nuclear Regulatory Commission. August 1994.

NUREG-1506. "Measurement Methods for Radiological Surveys in Support of New Decommissioning Criteria" (Draft Report for Comment). Washington, D.C.: Nuclear Regulatory Commission. August 1995.

NUREG-1575. "Multiagency Radiation Survey and Site Investigation Manual (MARSSIM)." Washington, D.C.: Nuclear Regulatory Commission. December 1997.

NUREG/CR-4007. "Lower Limit of Detection: Definition and Elaboration of a Proposed Position for Radiological Effluent and Environmental Measurements." Washington, D.C.: Nuclear Regulatory Commission. 1984.

NUREG/CR-4604. "Statistical Methods for Nuclear Material Management." Washington, D.C.: Nuclear Regulatory Commission. December 1988.

NUREG/CR-5849. "Manual for Conducting Radiological Surveys in Support of License Termination" (Draft). Washington, D.C.: Nuclear Regulatory Commission. May 1992.

NUREG/CR-6062. "Performance of Portable Radiation Survey Instruments." Washington, D.C.: Nuclear Regulatory Commission. December 1993.

NUREG/CR-6364. "Human Performance in Radiological Survey Scanning." Washington, D.C.: Nuclear Regulatory Commission. December 1997.

Sommers, J.F. "Sensitivity of G-M and Ion Chamber Beta-Gamma Survey Instruments." *Health Physics* 28(6):755-761. June 1975.

REFERENCES

Strom, D.J., and P.S. Stansbury. "Minimum Detectable Activity When Background Is Counted Longer Than the Sample," *Health Physics* 63(3):360-1. September 1992.

Swinth, K.L., and J.L. Kenoyer. "Evaluation of Draft ANSI Standard N42.17 by Testing." Richland, Wash.: Pacific Northwest Laboratory. July 1984.

Thelin, L. "Radiation Detection Experiment for HP Technicians." Tuxedo, N.Y.: Cintichem Interoffice Correspondence. September 1994.

Walker, E. "Proper Selection and Application of Portable Survey Instruments for Unrestricted Release Surveys." Bechtel Environmental, Inc. Presented at 1994 International Symposium on D&D. Knoxville, TN April 24-29, 1994.

Walpole, R.E., and R.H. Myers. *Probability and Statistics for Engineers and Scientists*. New York, N.Y.: MacMillan Publishing Company. 1985.

BIBLIOGRAPHIC DATA SHEET

(See instructions on the reverse)

1. REPORT NUMBER
(Assigned by NRC, Add Vol., Supp., Rev.,
and Addendum Numbers, if any.)

NUREG-1507

3. DATE REPORT PUBLISHED

MONTH	YEAR
June	1998

4. FIN OR GRANT NUMBER

6. TYPE OF REPORT

Technical

7. PERIOD COVERED (Inclusive Dates)

8/6/97 to 1/31/98

8. PERFORMING ORGANIZATION - NAME AND ADDRESS (If NRC, provide Division, Office or Region, U.S. Nuclear Regulatory Commission, and mailing address; if contractor, provide name and mailing address.)

Oak Ridge Institute for Science and Education Oak Ridge, TN 37831-0117	Brookhaven National Laboratory Upton, NY 11973-5000	U.S. Nuclear Regulatory Commission Washington DC 20555-0001
---	--	--

9. SPONSORING ORGANIZATION - NAME AND ADDRESS (If NRC, type "Same as above"; if contractor, provide NRC Division, Office or Region, U.S. Nuclear Regulatory Commission, and mailing address.)

Division of Regulatory Applications
Office of Nuclear Regulatory Research
U.S. Nuclear Regulatory Commission
Washington, DC 20555-0001

10. SUPPLEMENTARY NOTES

G.E. Powers, NRC Project Manager

11. ABSTRACT (200 words or less)

This document describes and quantitatively evaluates the effects of various factors on the detection sensitivity of commercially available portable field instruments being used to conduct radiological surveys in support of decommissioning. The U.S. Nuclear Regulatory Commission (NRC) has amended its regulations to establish residual radioactivity criteria for decommissioning of licensed nuclear facilities. In support of that rulemaking, the Commission has prepared a Generic Environmental Impact Statement (GEIS), consistent with the National Environmental Policy Act (NEPA). The effects of this new rulemaking on the overall cost of decommissioning are among the many factors considered in the GEIS. The overall cost includes the costs of decontamination, waste disposal, and radiological surveys to demonstrate compliance with the applicable guidelines. An important factor affecting the costs of such radiological surveys is the minimum detectable concentration (MDC) of field survey instruments in relation to the residual radioactivity criteria. The purpose of this study was two-fold. First, the data were used to determine the validity of the theoretical minimum detectable concentrations (MDCs) used in the GEIS. Second, the results of the study, published herein, provide guidance to licensees for (a) selection and proper use of portable survey instruments and (b) understanding the field conditions and the extent to which the capabilities of those instruments can be limited. The types of instruments commonly used in field radiological surveys that were evaluated included, in part, gas proportional, Geiger-Mueller (GM), zinc sulfide (ZnS), and sodium iodide (NaI) detectors.

12. KEY WORDS/DESCRIPTORS (List words or phrases that will assist researchers in locating the report.)

Survey Instruments, Radiological Surveys, Decommissioning, MARSSIM, Minimum Detectable Concentration

13. AVAILABILITY STATEMENT

unlimited

14. SECURITY CLASSIFICATION

(This Page)

unclassified

(This Report)

unclassified

15. NUMBER OF PAGES

16. PRICE



Federal Recycling Program

UNITED STATES
NUCLEAR REGULATORY COMMISSION
WASHINGTON, DC 20555-0001

OFFICIAL BUSINESS